Pain Classification Using EEG Evoked by Electrical Stimulation

August 2021

Kornkanok Tripanpitak

Graduate School of Science and Engineering

CHIBA UNIVERSITY

（千葉大学審査学位論文）

Pain Classification Using EEG Evoked by Electrical Stimulation

August 2021

Kornkanok Tripanpitak

Graduate School of Science and Engineering

CHIBA UNIVERSITY

Abstract

Pain is a complex phenomenon to measure due to its composition of perceptual and affective processes, which is based on individual subjective nature. Healthcare needs a reliable pain quantification for pain scores and pain types, in which the former corresponds to the individual pain sensitivity and the latter corresponds to acute and chronic pain, resulting from the activation of nociceptive fibers, Aδ and C, respectively. Recently, many research studies on using classification using features from cortical responses through electroencephalography (EEG) to classify pain perception levels besides using commercial pain measurement devices. However, the current classification systems, including the classifier model and feature, cannot achieve high accuracy for classifying multiple pain perception levels and nociceptive fibers activations. A major problem lies in the lack of effective features.

To address this gap in research, we developed novel features with nonlinear analysis and Granger causality (GC) analysis for classifying multiple pain perception levels and activations of Aδ- and C-fibers, respectively. The goal was to provide the effective features extracted from EEG induced by electrical stimulation for pain classification that would enable the prediction of pain levels and pain nerves activations. Moreover, aiming to demonstrate the possibility of EEG-based features in an online scenario.

Several feature extraction approaches were proposed, including nonlinear analyses of Higuchi's fractal dimension, Grassberger-Procaccia correlation dimension, with functions of autocorrelation and moving variance for evaluating pain perception levels, and GC analysis for classifying nociceptive fibers activations. Furthermore, exploration of the different numbers of channels and trials for proof the concept of applying the current features for future online classification.

The novelties and contributions were: 1) Using combined nonlinear features is effective to quantify pain into a maximum of four pain levels than using single nonlinear features; 2) The use of nonlinear feature extracted from EEG in the time domain with a number of trials less than 20 is not preferable because it cannot achieve sensible accuracy, which makes it difficult for instantaneous classification of pain perception levels; 3) For classification of Aδ- and C-fibers activations, frequency-related GC has the best classification results among other GC features for the current data; 4) In a simulation of online analysis, apply detrending and dynamic time warping (DTW) to GC features extracted from EEG in the frequency domain can enhance the accuracy in the classification of nociceptive fibers activations. The obtained findings could be used further to improve the performances of the EEG-based pain classification system.

Acknowledgments

I would like to acknowledge all the people who have supported me during the period of my Ph.D. program.

First of all, I am exceptionally grateful to Yu sensei, my thesis advisor, for providing me the opportunity to do my Ph.D. at his lab and helping me to improve this work with his trust and patience. I would also be grateful to Professor Huang from Singapore University of Technology and Design for assisting in my publications. I would like to thank my review board members, Nakaguchi sensei, Shimomura sensei, Nakagawa sensei, and Orita sensei, for their comments that help me accomplish my thesis. I am thankful to Osugi san, our lab's secretary, who supports in acquiring materials for research and also aids my living life in Japan.

I am grateful to Chiba University and Japanese Ministry of Education, Culture, Sports, Science and Technology for providing MEXT scholarship for my postgraduate degree.

I would like to thank Nan for providing gratifying moments and keeping me going through life, Asst. Prof. Dr. Yutthasak and Tik for giving perspectives on academic writing and giving exceptional support at all times, Macy for providing invaluable insight about academic contents, and Pear for always pushing and encouraging me to get through all obstacles not only in research but also in my personal life.

I would also like to thank all our lab members, especially Ilker, Tapio, Siyu, Xinyao, and Adan, for their friendships and helpful ideas to improve my study.

Finally, I wish to acknowledge my friends in Thailand and Japan and colleagues at Siriraj Hospital for their friendships and motivate me to succeed in my academics. Also, I would like to thank my family for appreciating my decision to complete my Ph.D. in Japan.

List of Publications

Publications

- Tripanpitak K, He S, Sönmezışık I, Morant T, Huang SY, Yu W. Granger Causality-Based Pain Classification Using EEG Evoked by Electrical Stimulation Targeting Nociceptive Aδ and C-fibers. IEEE Access. 2021 Jan 8;9:10089-106.
- Tripanpitak K, Viriyavit W, Huang SY, Yu W. Classification of Pain Event Related Potential for Evaluation of Pain Perception Induced by Electrical Stimulation. Sensors. 2020 Jan;20(5):1491.

- He S, Tripanpitak K, Yoshida Y, Takamatsu S, Huang SY, Yu W. Gate Mechanism and Parameter Analysis of Anodal-First Waveforms for Improving Selectivity of C-Fiber Nerves. *J Pain Res*. 2021;14:1785-1807
- He S, Yoshida Y, Tripanpitak K, Takamatsu S, Huang SY, Yu W. A simulation study on selective stimulation of C-fiber nerves for chronic pain relief. IEEE Access. 2020 May 27; 8: 101648-661.

Conferences

- Tripanpitak K, Yu W. The relationship between pain-related evoked potential and pain perception level in the peripheral nervous system. In Proceedings of the 12th International Convention on Rehabilitation Engineering and Assistive Technology 2018 Jul 13 (pp. 190-193).
- Tripanpitak K, Tarvainen TV, Sönmezışık I, Wu J, Yu W. Design a soft assistive device for elbow movement training in peripheral nerve injuries. In 2017 IEEE international conference on robotics and biomimetics (ROBIO) 2017 Dec 5 (pp. 544-548).

- He S, Tripanpitak K, Yu W. Selective Stimulation of C-fibers for Chronic Pain Relief. In 2020 IEEE International Conference on Computational Electromagnetics (ICCEM) 2020 Aug 24 (pp. 133-135).
- Morant T, Tripanpitak K, Yu W. Analysis of EEG and Eye-Tracker for Object's Shape Recognition. In 2019 International Symposium on Info Comm and Mechatronics Technology in Bio-Medical and Healthcare Application (IS 3T-in-3A) 2019 Nov 12 (Poster session).

Contents

List of Figures

List of Tables

List of Abbreviations

ACF	Autocorrelation function
AUC	Area under the receiver operating characteristic (ROC) curve
DTW	Dynamic time warping
EEG	Electroencephalography
eEEG	Evoked electroencephalography
ERP	Event-related potential
FD	Fractal dimension
GC	Granger causality
GP	Grassberger-Procaccia correlation dimension
HFD	Higuchi's fractal dimension
MCC	Matthews correlation coefficient
MLP	Multilayer perceptron
NN	Neural network
VAR	Moving variance

Chapter 1

Introduction

In this chapter, we provide background, motivation, and goals for this Doctoral project. Firstly, we introduce pain mechanisms and the existing pain assessments. Next, we discuss an evaluation of pain through electroencephalography (EEG). Then, we give a literature review on objective pain assessment. After that, we state our challenges to deal with in this project. Finally, we discuss the project's goals followed by the structure of this thesis.

1.1 Background

1.1.1 Pain activation

The phenomenon of pain is a composition of physiological (sensory) and psychological (emotion) mechanisms reflected by individual experience [1]. Pain is one of the major healthcare problems that has a detrimental effect on the quality of life, especially chronic pain, which has persistent uncontrolled pain even without any external stimulation. The mechanisms responsible for pain are from the excitation of the major nociceptive afferent nerves, Aδ- and C-fibers. Due to their characteristics, these two nociceptive nerve fibers play different roles in pain. Aδ-fibers is a myelinated nerve with a diameter of 1-5 μm, the conduction velocity of around 5-30 m/s, while C-fibers is an unmyelinated nerve that has a thinner diameter of 0.2-1.5 μm and slow conduction velocity of less than 2 m/s (approximately 0.4-1.4 m/s) [2]. When pain stimulus induces nociceptors, the signals that transmit noxious information will be transmitted through the nociceptive Aδ- and C-fibers and interpret pain information as first pain and long-lasting second pain, respectively. Then, these nociceptive afferents of the peripheral nervous system transmit the impulses to the dorsal horn of the spinal cord, which the pain signals are conveyed to the brain via the ascending pathways, i.e., spinothalamic tract and spinoreticular tract, to perceive pain sensation. Accordingly, pain sensation occurs with activation of afferent either Aδ- or C-fibers, both of which respond to thermal, mechanical, and chemical noxious stimulation, carrying signals to the spinal cord.

There have been reported that the activation of myelinated Aδ-fibers, which is represented as first pain due to its short-lasting effect, predominantly involves a withdrawal reflex due to its fast-conducting properties [3] and can be inhibited by stimulating large-diameter non-nociceptive nerve, Aβ-fibers [4]. This implies that Aδ-fibers is associated with acute pain because of their short-lasting effect. In contrast, unmyelinated C is related to hyperalgesia after inflammation that resulted from a slow progression and poor localization of second pain [5], which was found in one of the chronic musculoskeletal disorders, fibromyalgia [6]. Thus, C-fibers principally refer to the chronic state of pain. Since different nociceptive fibers convey different pain information that leads to different types of pain, discrimination between Aδ- and C-fibers activations is important for clinical pain rehabilitation. There are two theories that explicate the inhibition of pain impulses from nociceptive fibers: gate control theory and endogenous opioid theory.

Gate control theory [4] has focused on the modulation of inputs in the dorsal horn of the spinal cord that relating to several techniques for pain rehabilitation, such as transcutaneous electrical nerve stimulation (TENS), electroacupuncture, and massage. A gate is responsible for facilitating or inhibiting the impulses from nociceptive fibers to the dorsal horn. The control of the gate depends on the activation of large-diameter fibers (non-nociceptive Aβ-fibers) and small-diameter (nociceptive Aδ- and C-fibers), which the former nerve fibers convey non-painful information that related to touch, while the latter nerve fibers carry pain information. As shown in Figure 1.1, the nerve fibers synapse onto the substantia gelatinosa (SG) and the transmission (T) cell in the dorsal horn of the spinal cord, which sends projections to the brain. The inhibitory SG interneuron plays a role in inhibiting inputs to the T cell by determining which afferent inputs should reach the T cell and then projects the signals further to the brain. When the gate is closed, it means that the SG is excited by large-diameter nerve fibers and preventing the transmission of the pain impulses through the T cells. Thus, the non-pain signals override the pain signals resulting in that pain is not perceived by the brain. In contrast, activity in small-diameter fibers opens the gate, which means that inhibitory neurons are inactivated. Activity of small-fibers facilitates the transmission of pain signals and produces pain. Therefore, this theory describes that the excited non-nociceptive nerve fibers block the signaling of nociceptive nerves, thereby reducing pain. However, this technique cannot produce a long-lasting analgesic effect.

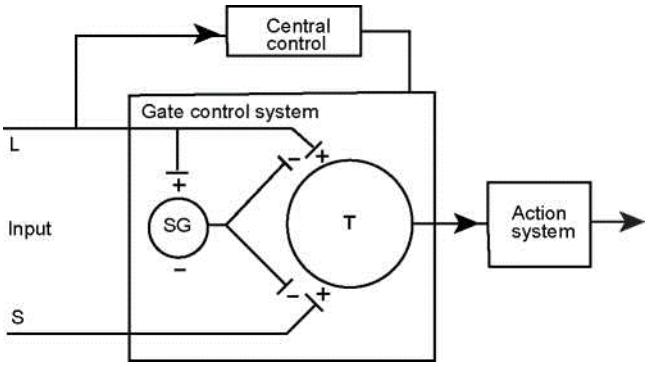

Figure 1.1 Schematic diagram of the gate control theory. The substantia gelatinosa (SG) and transmission (T) cells have received the signal through the large (L) and small (S) diameter afferent fibers. The inhibitory effect (-) of SG on the afferent terminals is activated by activity in L fibers, while inactivated by activity in S fibers [4].

Sometimes we need to prolong medication used like opioid analgesic for serious chronic pain cases, which may cause adverse effects and a high risk for addiction. Due to its large role of opioids in the pain modulatory system [7], an endogenous opioid theory is a significant mechanism for chronic pain relief. This theory is related to the binding of the secreted opioid substances to opioid receptors, which are found on Aδ and C nociceptors as well as SG and T cells. The endogenous opioid in the human body has the same analgesic effect as the synthetic opioid drug, so it has the potential to attenuate pain without addiction [8]. Different types of pain cause different endogenous opioid substances secretion to bind with their corresponding receptors. There have been reported that μ-receptor is the main target for pain moderate to severe pain management in the pharmacological field because it has the strongest analgesic effect corresponds to low frequency electrical stimulation, which involved stimulation to

nociceptive C-fibers [9]. Since then, there have been developed treatments using endogenous opioid theory to sustain analgesia for chronic pain relief, i.e., using electrical stimulation [10], laser [11], and heat [12].

According to the techniques mentioned above, pain inhibition has been involved in small-diameter nociceptive afferent Aδ- and C-fibers. The concomitant stimulation of Aδ-fibers reveals that the myelinated Aδ-fibers has a lower activation threshold than the unmyelinated C-fibers [13]. On the other hand, nociceptor of C-fibers has a significantly lower heat threshold than that of Aδ-fibers type [14]. Nowadays, several methods are based on gate control theory have been used for managing acute pain from Aδ-fibers activation, for example, TENS and massage. However, pain relief from these gate control theory based methods only lasts for a short term and still persists afterwards. Regardless of drug therapy, there are methods to selectively stimulate C-fibers for achieving long-lasting analgesic effect for chronic pain, such as electrical stimulation with pin electrodes [15] [16], laser [11] [17], and electroacupuncture [18], which the latter ones required expert users. Still, all these methods are only for laboratory or medical use. So, it is difficult to use pain relief technology with a high cost or requiring technical skills for public or daily living use. In the stimulation induced painful sensation for pain study, the evoked potentials elicited by electrical stimulation have been used as a neurophysiological tool for exploring pain-related brain responses. Application of electrical stimulation is more practical used because there is no cumulative heat effect in skin during stimulation that could cause skin damage, which is the critical disadvantage of laser application. That leads to no limitation of the number of stimuli (trials) for electrical stimulation. However, electric-evoked potentials contain more noise of non-nociceptive Aβ-fibers evoked potential due to the presence of Aβ coactivation [31]. For laser stimulation, it induced heat-pain through non-contact stimuli with the lack of stimulus artifacts compared with electrical stimulation. Even though electrical and laser stimulations have controllable parameters, i.e., intensity and duration, using laser is more difficult than electrical stimulation due to the complexity in setup. Generally, the laser intensity is measured in the units of Watt or Joule, which is not relatively indicate the characteristic of nociceptive fibers activation, i.e., degrees Celsius (°C) for heat threshold. For other methods such as contact heat and cold stimulations, the stimuli are natural and flexible to use but they cannot allow time locking of stimulus (in milliseconds) for EEG responses due to their slow rising and falling times.Thus, electrical stimulation could be used for evaluating pain levels from nociceptive nerves activation due to its cost-effective and friendly-user as paramedical or public use. Aδ-fibers serve the pain information relating to acute pain, which is relatively short-lasting, while C-fibers are described as long-lasting sensations. Therefore, it is important to have a way to evaluate pain perception levels from each nociceptive Aδ- and C-fibers activations.

1.1.2 Evaluation of pain

There are two types of methods to evaluate pain: subjective and objective assessments. A questionnaire is a subjective assessment method that has been used for decades. There are two compositions for the pain questionnaire: self-rating scale and disability index. The intensity of pain and treatment effect is mostly be assessed with a self-rating scale questionnaire, i.e., visual analogue scale (VAS) and numeric rating scale (NRS). The scales are oriented unidimensional from left to right, where 0 at the left end is “no pain” and the right end is the worst pain imaginable, which is 10 or 100 according to its version. The disability index

questionnaire is widely used to measure functional disability through questions about activities that a patient can do or cannot do and reveal that pain quality descriptors vary across different pain conditions. For example, Oswestry low back pain disability questionnaire [19] and McGill pain questionnaire [20] are considered as the gold standard of low back functional outcome tools. However, all questionnaires are inherently subjective in nature and can be influenced by multidimensional factors.

For objective assessment, devices such as an algometer (measuring mechanical pressure pain) and a monofilament (for measuring sensitivity) are used together with questionnaires in the clinical field. Besides mechanical pain, electrical stimulation has the potential to be used for investigating pain among the various types of noxious stimulation, as mentioned in Chapter 1.1.1. There is a commercial stimulator, Neurometer (Neurotron, Baltimore, MD, USA), to measure the current perception threshold (CPT) for Aβ-, Aδ-, and C-fibers activations [21] for investigating peripheral neuropathy in diabetes mellitus [22]. There have been studies using Neurometer to clarify neural correlates associated with pain processing in brain imaging studies such as functional magnetic resonance imaging (fMRI) [23] and functional near-infrared spectroscopy (fNIRS) [24] in a research field. Nevertheless, several studies have also been explored with other stimuli to investigate pain-related activation of the brain, mostly in cortical activation data from brain imaging studies.

Among the signal sources for brain-computer interface (BCI) technologies, electroencephalography (EEG) signals offer a high temporal resolution as non-invasive brain imaging. EEG measures brain activity directly, which provides precise and reliable information. Even though the other cortical imaging such as magnetic resonance imaging (MRI) and fMRI provide high spatial resolution than EEG, they have low temporal resolution. Besides, only structural information and blood-oxygen-level-dependent brain activity indirect measurement are provided by MRI and fMRI, respectively [25] [26]. The study using EEG recording during selective stimulation of nociceptive Aδ- and C-fibers showed a statistically significant correlation between the amplitude of evoked potential in the time domain and pain rating score, while avoiding co-stimulation of Aβ-fibers [15]. Besides analysis in the time domain of EEG, analysis in the time-frequency domain also revealed a distinct pattern of EEG response to noxious stimuli; for example, pain intensity from painful heat stimuli was associated with gamma oscillations in the medial prefrontal cortex [27] and the late components of the evoked potential of EEG, N2 and P2 waves, significantly mediated the effect of stimulus intensity on pain perception ratings under laser stimuli [28]. Additionally, within the frequency domain, it was founded that the peak frequency of alpha oscillations associated with the perception of tonic pain [29]. The fMRI studies demonstrated that the activations of the anterior cingulate cortex (ACC) and the posterior cingulate cortex (PCC) were involved in pain from noxious thermal stimuli [30], while the secondary somatosensory cortex (S2) encodes pain intensity responses to noxious electrical stimuli [23]. Even though these studies could reveal the association between brain regions and pain perception intensity, the dissociable regions that encode pain-related information were not decisive.

To monitor and measure pain stimuli related brain activity, BCI are well used because they can capture information on brain structures and functions. Even though the EEG analysis including event-related potentials (components of EEG in time domain), spectral density (components of EEG in frequency domain), and time-frequency representations can well reflect oscillatory nature of brain activity during pain, there are pitfalls for EEG interpretation, especially in the case of the presence of various types of artifacts, and limited training and experience of the user. Therefore, it is a challenge to interpret the outcomes of brain activity

without prior knowledge of the brain and nervous systems. Besides statistical analysis of neuronal responses from cortical measures, machine learning is one of the effective approaches that have been used for developing objective pain assessment system. The strength of machine learning is that, given a set of samples of different pain stimuli related brain activity (EEG signals), it can acquire a classifier that reflects the relationship embedded in the samples. Additionally, it also generalizes across a much wider solution space, which leads to the potential of clinical use of the objective pain assessment.

In the next section, we discuss more in-depth how the machine learning, and the features of the pain related EEG work for the classification of pain through machine learning.

1.2 Related work and problems

Recent developments in objective pain assessment have mainly explored on recognition of pain from the BCI such as EEG and fMRI. Another modality is physiological signals; for example, using blood volume pulse, electrocardiogram, and skin conductance level, achieved an average accuracy of 75% to predict 4-level pain intensity [32]. In the fMRI studies, pain was decoded by investigation of activity in the specific brain regions during painful stimulation and pain anticipation using multivariate pattern analysis [33]; besides, pain states were classified using combined support vector machine (SVM) [34].

The main difficulties in pain classification are in the effective features to predict multiple pain perception levels. Since a major problem lies in individual pain sensitivity, the improvement of features to predict a high pain range (multiple classes in classification) is needed. For predicting pain perception, features extracted from the time-frequency domain of EEG signals achieved an accuracy of 89.45% for a maximum of ten pain classes using a random forest model [35]. Time-frequency wavelet representations were also used to classify two-class of low and high pain perception with the accuracy of 89% [36] and 83% [37]. Besides, power spectrum density of theta (4-8 Hz), alpha (8-12 Hz), beta (13-30 Hz), and wide band (2-30 Hz) ranges were used to identify a risk of developing pain through classification between multiple groups of spinal cord injured patients at different pain states [38]. Furthermore, there has been a study using a combination approach for feature extraction in a single trial of EEG evoked by laser stimulation to predict low and high pain with an accuracy of 86.3% [39]. The existing state of the art approaches for predicting pain states from EEG are shown in Table 1.1

However, none of the existing studies have explored classifying between nociceptive fibers activations. Even though the work in [40] was considered about nociceptive-specific stimulation which can be induced by laser, their work did not show the differentiation of brain activity under pain between Aδ- and C-fibers activations. That lies in the fact that the threshold of unmyelinated C-fibers is higher than the myelinated Aδ-fibers, which result in higher stimulus intensity that is perceived as painful sensation to excite C-fibers, while Aδ-fibers get excited near the perception threshold [41]. Although C-fibers have a higher density distribution than Aδ-fibers [42], selective stimulation of C-fibers without activating Aδ-fibers is still challenging.

In addition, a challenging problem of pain prediction concerning nociceptive fibers activations has not been solved yet. It remains unclear whether to selectively activate Aδ- or C-fibers by electrical stimulation through surface electrodes or a high number of stimuli for generating a steady signal-to-noise ratio (SNR) that reliable to detect the C-fibers activation

[13]. Because there has been an issue about the concomitant activation of Aδ that suppresses the occurrence of C activation [43].

Table 1.1 Existing pain classification approaches.

Literature	Pain stimulation	Classifier	Feature	Number of features	Maximum number of classes	Accuracy
[35]	Heat	Random forest	Time-frequency representation	60	10	89.45%
[36]	Heat	SVM	ERSP [1]	3	2	89.58%
[37]	Laser	Healthy, Eyes opened	Time-frequency representation	15	2	83.00%
[38]	Mechanical	LDA [2]	Power spectrum density	9	2	> 85.00%
[40]	Laser	SVM	Time-frequency representation	Based on PLSR [3]	2	83.50%

[1] ERSP: event-related spectral perturbation; [2] LDA: linear discriminant analysis; [3] Number of features based on feature selection with partial least-squares regression (PLSR).

The clinical use of the objective pain assessment requires classification of pain from pain-related EEG within a period of time as short as possible. Nevertheless, there have been few studies on real-time processing and classification of EEG signals. It has been reported that it is possible to decode pain from EEG recordings using classification for a real-time reflex system in prosthesis [44], and to predict pain perception from single trial EEG in healthy subjects [39]. Regarding the application in the real-time analysis (online classification), the difficulties lie in the fact that within the limited acquisition data (low number of data points), EEG signal tends to decrease in SNR and increase in non-stationary. However, a varying trend due to the artifacts, such as ocular movement and environment, and the fluctuation of the EEG signals that somewhat affect not only the activity patterns of each brain region, but also the dynamic patterns of functional connectivity among brain regions.

1.3 Challenges

The challenges of the research area to be addressed were:

1) Significant variability in individual pain thresholds is a challenge to pain classification with EEG-based features due to the nonlinear characteristics in EEG signals. Thus, the classification system for multiple pain perception levels is not trivial. Therefore, a system to predict a wide range of pain perception levels is necessary. Only few studies were classifying multiple classes with time-frequency EEG [35], while the others were classifying binary classes with spectral EEG and time-frequency EEG [36] [37] [38]. Furthermore, none of the studies have attempted to classify multiple pain perception levels induced by electrical stimulation.
2) The concomitant stimulation of Aδ affects the occurrence of C-evoked responses. According to the characteristics difference between these nerves, the activation of unmyelinated small C-fibers has required a higher threshold than myelinated Aδ-fibers. Thus, the saliency of C-evoked potential is reduced by the preceding activation of Aδ-evoked potential, which means that C-evoked is overshadowed by Aδ-evoked [13]. Moreover, the amplitude of C-fibers activation is much smaller than Aδ. Thus, to

get sufficient stimulus repetitions for obtaining clear evoked potential of each nociceptive fiber and differentiating the activations between them is perplexing.

3) The non-stationary nature of EEG signals causes difficulty in analysis with a low number of data points in an online scenario. The number of data points, including channels and trials, that could provide a high SNR is still unclear.
4) The information from each single region or channel and their combination may reflect the 1-dimensional brain activity, though, they cannot capture the functional connectivity between different regions or channels. Thus, using functional connectivity of brain activities as features for pain classification has not been solved yet. In the brain network, one of the functional connectivity measures, Granger causality (GC), is used to demonstrate causal relationships between neuronal activations or brain regions by identifying the sources and sinks that play roles in respond to specific tasks or stimuli. Although GC has been used to estimate the connectivity between brain regions during low pain and high pain [45], none of the studies realize classification of pain from different nociceptive fibers activations.
5) The robustness of the proposed feature for real-time analysis has not been made clear. The restriction in the data points due to a real-time scenario (online classification) may affect the classification performances. Thus, within a limited number of data points in a real-time scenario, an effective straightforward pipeline including pre-processing, feature extraction, feature selection, and classification is needed to be developed.

1.4 Approaches

Variations of pain threshold and response time cause the individual pain perception levels and pain types (from Aδ- or C-fibers), respectively. This indicates that EEG signal has nonlinear nature. Then, we computed fractal dimension (FD), which is the dominant tools in nonlinear analysis, to deal with the nonlinear dynamical characteristic of EEG.

Moreover, we applied GC to investigate the functional connectivity between EEG signals to solve the difficulty in distinguishing C-evoked from Aδ-evoked. The concept of brain connectivity is used to characterize the interaction between neurons during the execution of a task or stimulus by calculating based on the statistical dependencies between variables (such as channels and brain regions, etc.) in which dependencies are directed [46].

In addition, we applied further feature extraction to GC features to be used for online classification. Due to a non-stationary behaviour of EEG and the overshadowing effect of Aδ-evoked on C-evoked, implementing only GC features for classifying activations of nociceptive fibers might be affected by the limited number of data. Thus, to detect functional connectivity patterns among brain regions related to pain, dynamic time warping (DTW) was applied to measure similarity between EEG signals [47]. The superiority of the DTW technique is that it is invariance against signal warping (shifting, compressing/expanding, and scaling in the time axis) which has become one of the preferable estimates in matching the pattern. Thus, removing the trends from the EEG signals and applying the DTW to the functional connectivity would allow the system to be more effective for the instantaneous classification of pain.

To solve the challenges in this Doctoral project, the development of the system for pre-processing EEG data, feature processing (feature extraction and feature selection), and the classifier structure was performed, especially the EEG-based features for classifying pain

perception levels and nociceptive fibers activations. By looking back at the feature, it may reflect the brain activity and pain-related information of the brain network responses to pain stimuli.

1.5 Goals and structure of the thesis

1.5.1 Goals

The main goal of this Doctoral project was to develop a pain classification system using features extracted from EEG signals responding to painful stimuli elicited by electrical stimulation that would allow being used as an objective pain assessment in the clinical practice than the existing pain assessment approaches. In addition, we aimed to provide an improvement of the classification performances of different features for three purposes:

1) Classification of pain perception levels including binary and multiple classes.
2) Classification of nociceptive fibers activations, Aδ and C.
3) EEG-based features that are capable of classification in an online scenario.

We expected that by investigating the features in terms of 1- and 2-dimensional systems, the effectiveness of the features for classifying pain levels and nociceptive fibers activations could be achieved. To achieve these goals, features related to the activities of single and multiple channels/components, domains, and regions were analyzed. We approached the feature extraction method based on a 1-dimensional system of a single domain of EEG and compared the results derived from the current approach with the other approach in related studies. Then, we approached the features extracted from the 2-dimensional system, i.e., the temporal-spectral domain and the brain's spatial pattern. Through this proposed pipeline, features for pain classification were developed. Additionally, we investigated the robustness of the proposed features by analyzing several channels and trials to achieve online classification.

1.5.2 Structure of the thesis

The contents of the thesis are divided into seven chapters (including the current chapter). It can be summarized as follows.

1) In Chapter 2, we provide all methods that we used throughout the project.
2) In Chapter 3, we describe the section of EEG data acquisition, electrical pain stimulation, and the experimental designs for pain experiments that were implemented throughout the project.
3) In Chapter 4, features based on nonlinear analysis for the classification of pain perception levels is presented. Several FD-based features derived from the nonlinear analysis were used for classification to investigate the improvement of overall accuracy. Then, the results were compared with the statistical-based features and combined with the feature vectors for improving multiple classification performance. Additionally, the features were analyzed based on an n-averaging trial for investigating the possibility of real-time assessment.
4) In Chapter 5, features based on GC analysis for the classification of nociceptive fibers activations is presented. The 2-dimensional system of the feature was explored. Besides the classification of Aδ- and C-fibers activations, the classification of pain perception levels was analyzed too. Additionally, the difference of GC groups about

pain levels and stimulation waveforms (targeting Aδ- and C-fibers) were performed as the clues for neuroscience perspective.

5) In Chapter 6, we provide a proof of concept for simulating online pain classification with GC features. GC features were extracted from the frequency domain of pain-related EEG signals with limited number of channels and trials for classifying Aδ- and C-fibers activations. To improve the classification accuracy, detrending and DTW techniques were applied to the GC features. Then, the results of the proposed features were compared with those of nonlinear features.
6) In Chapter 7, we summarize the contributions of the Doctoral project, limitations, future directions, and conclusions.

Chapter 2

Research Methodology

2.1 Introduction

This chapter provides all methods that we used throughout this Doctoral project, including pre-processing steps, feature extraction methods, the selection methods for EEG channels and features, and classification models. We describe sequentially the methods of the study of classifying pain perception levels, activations of nociceptive fibers, and classifying nociceptive fibers in an online simulation.

2.2 For classification of pain perception levels

2.2.1 EEG pre-processing

EEG pre-processing outline is shown in Figure 2.1. Data were analyzed offline in Matlab 2017b (Mathworks, Natick, MA, USA) with the EEGLAB toolbox [48]. We first used the pre-processing pipeline (PREP pipeline) [49] to remove artifacts from power line noise, eye blinks, and muscle movement. High-pass filtering at 1 Hz [50] was used in the PREP process to remove baseline drift. Next, data were downsampled to 256 Hz. Then, we rejected bad channels and removed high-variance artifacts by Artifact Subspace Reconstruction (ASR) [51]. Remain channels were interpolated and re-referenced to the average values of all ordinary channels. Then, applying Adaptive Mixture Independent Component Analysis (AMICA) [52], which performs independent component analysis, to reject other noisy components and artifacts. Trials with the artifacts exceeding five times of standard deviation were removed. The first trial of every data was rejected to avoid the bias caused by initial startle responses. Finally, 435 data points from 500 ms before to 1200 ms after stimulus onset were obtained for each trial.

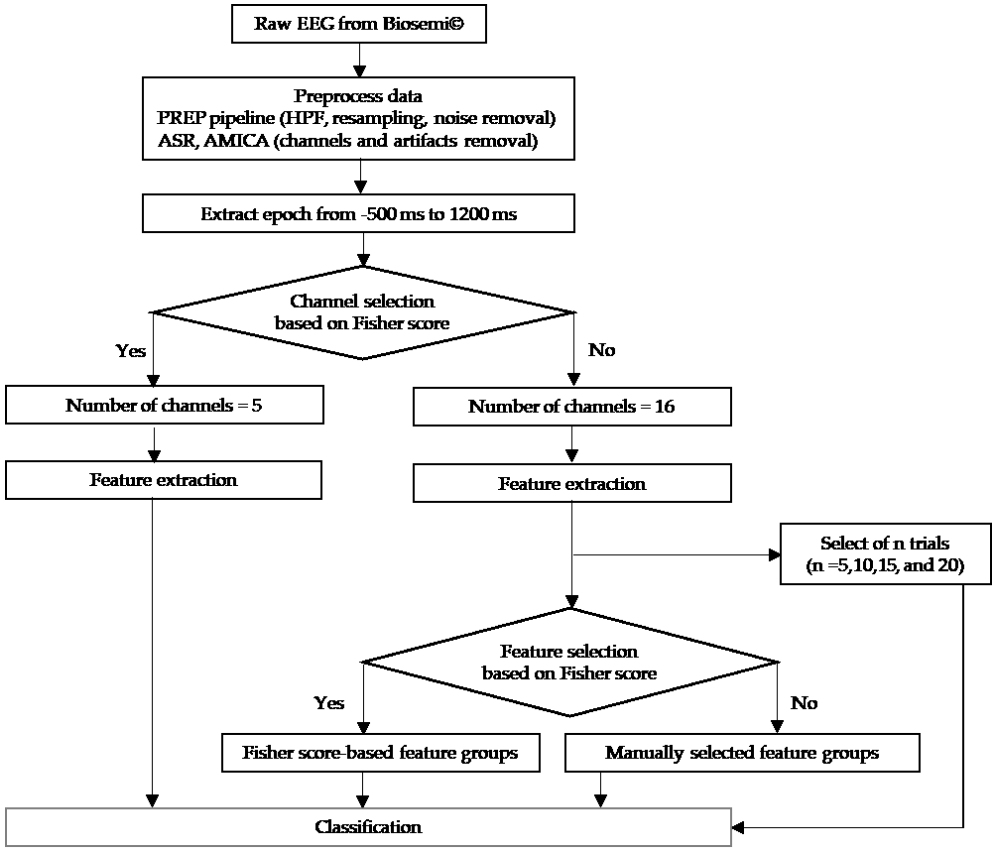

Figure 2.1 The flow of pain-ERP processing for analysis in Chapter 4.

2.2.2 Selection of EEG channels and features

The purpose of using the Fisher score [53] in this study was to select the EEG channels that had the high signal-to-noise (SNR) ratio and reduce redundancy feature problems for classification. Hence, we used Fisher score-based channel selection for selecting channels with high pain perception-related information. This Fisher score is used to determine the most discriminative channels or features and eliminate those noisy by remaining those data points with a maximum between-class and minimum within-class distance. The scatter matrices of within-class $\bar{\bar{S}}_w$ and between-class $\bar{\bar{S}}_b$ are calculated by Equations (1) and (2):

$$\bar{\bar{S}}_w = \sum_{i=1}^{c} P_i \left(\frac{1}{n_i} \sum_{j=1}^{n_i} (\bar{x}_{ij} - \bar{\mu}_i)(\bar{x}_{ij} - \bar{\mu}_i)^t \right) \quad (1)$$

$$\bar{\bar{S}}_b = \sum_{i=1}^{c} P_i \left(\frac{1}{n_i} \sum_{j=1}^{n_i} (\bar{\mu}_i - \bar{\mu})(\bar{\mu}_i - \bar{\mu})^t \right) \quad (2)$$

c denotes class which is equal to 4 for multiple-level scenarios in both channel selection and feature selection (for the study in Chapter 4), n_i is the training data samples in vector ($\bar{x}_{ij}$) for each class i (i = 1, …, c). For the simplicity of description $\bar{x}_{ij}$ is defined as a vector with n_i-dimensional, but in this study $\bar{x}_{ij}$ is a matrix of n_i-by-$n_{\text{channel\_num}}$, where $n_{\text{channel\_num}}$ is the number of EEG channels for a certain class i. The prior probability of class i is calculated by $P_i = \frac{n_i}{\sum_{i=1}^{c} n_i}$. $\bar{\mu}_i$ is the average training data of the ith class, $\bar{\mu}$ is the average of samples vector, and t denotes a transpose matrix. Fisher score of class separability for the kth feature is computed as:

$$Fisher(k) = \frac{S_b\,(k)}{S_w\,(k)} \tag{3}$$

where $S_b(k)$ and $S_w(k)$ are the kth diagonal elements of $\bar{\bar{S}}_b$ and $\bar{\bar{S}}_w$. Features with lower Fisher score indicate either irrelevant or noisy, which needs to be discarded; thus, a higher Fisher score is preferred.

In Chapter 4, six features with Fisher score-based channel selection and other six features without Fisher score-based channel selection were obtained. The feature was calculated from the data of each channel; thus, we had a feature vector of 5-dimensional and 16-dimensional for the case with and without channel selection, respectively.

2.2.3 Feature extraction with nonlinear analysis

There were four approaches of nonlinear analysis that were used for extracting features: Higuchi's fractal dimension (HFD), Grassberger-Procaccia (GP) correlation dimension, autocorrelation function, and moving variance function. The first two approaches were the methods that measure the complexity of the signal by using fractal dimension (FD) for calculating nonlinear deterministic of the signal, while the latter two were the further functions for feature extraction. Since both approaches of HFD and GP mainly analyzed the FD, the features extracted based on the nonlinear analysis were named FD-based features.

2.2.3.1 Higuchi's fractal dimension (HFD)

HFD measures the complexity of the time series based on the self-similar behavior without reconstruction of any strange attractors [54] [55]. Given N samples of time series $x(1)$, $x(2)$, …, $x(N)$, and k new time series are reconstructed for $m = 1, 2, \ldots, k$ as follows:

$$x_k^m = x(m), x(m+k), x(m+2k), \ldots, x\left(m + (\frac{N-m}{k})k\right) \tag{4}$$

where m is the initial time point, and k is the interval time. Then, the length $L_m(k)$ with normalizing factor $\frac{N-1}{\left(\frac{N-m}{k}\right)k}$ for each curve x_k^m could be defined as:

$$L_m(k) = \frac{1}{k}\left[\frac{N-1}{\left(\frac{N-m}{k}\right)k}\left(\sum_{i=1}^{\frac{N-m}{k}} |x(m+ik) - x(m+(i-1)k)|\right)\right] \tag{5}$$

The average curve length $L(k)$ of m curves with k interval times is estimated by:

$$L(k) = \frac{1}{k}\sum_{m-1}^{k}\left(L_m(k)\right) \qquad \text{if } L(k) \propto k^{-FD} \tag{6}$$

HFD is the slope of a plot $log(L(k))$ against $log(1/k)$, which can be calculated using the least-squares linear fitting. According to [56], the value of k was set to half of the N data samples. k = 217, which was half of the N = 435 data points for the study in Chapter 4.

2.2.3.2 Grassberger-Procaccia (GP) correlation dimension

GP [57] [58] is one of the FD approaches that evaluate the correlation dimension of a chaotic attractor in the phase space dimension. It is widely used to distinguish nonlinear deterministic or noise from the time series. For time series of data x_i, with M embedding dimension with and τ time delay, and reconstructed phase space vector of x_j. The correlation sum $C(r)$, which

is the fraction of pairs of point x_i in the phase space whose distance is smaller than r, is calculated as:

$$C(r) = \lim_{N\to\infty} \frac{1}{N^2} \sum_{i,j=1}^{N-(M-1)\tau} H\left(r - \left|x_i - x_j\right|\right) \quad (7)$$

where $\left|x_i - x_j\right|$ denotes the Euclidean distance between all pairs of points that are measured in the vector of data x_i and x_j. H is the Heaviside function, which is defined as $H(x) = 0$ for $x \leq 0$, otherwise $H(x) = 1$ for $x > 0$. r denotes a small value of the separation distance of the vectors and multiplier $\frac{1}{N^2}$ is added for normalizing the pairs of points on the attractor. The correlation dimension, D_2, is computed as:

$$D_2 = \lim_{r\to 0} \frac{\log(C(r))}{\log(r)} \quad (8)$$

GP is a slope of plot $\log(C(r))$ against $\log(r)$ at a given value M that led GP to saturation. $M = 12$ in the study in Chapter 4.

2.2.3.3 Autocorrelation function (ACF)

ACF measures the correlation between values of itself at different time steps to find the patterns or randomness in the data [59]. Given a time series $x(1)$, $x(2)$, …, $x(N)$, at lag k ($k = 0$, 1, …), its auto-covariance coefficient could be calculated as:

$$C_k = \frac{1}{N} \sum_{i=1}^{N-k} \left((x_i - \bar{x})(x_{i+k} - \bar{x})\right) \quad (9)$$

where C_0 is the variance of the time series. The ACF is calculated by:

$$ACF = \frac{C_k}{C_0} \quad (10)$$

In the study in Chapter 4, $k = 4$ and 15 for data with channel selection and without channel selection, respectively. Additionally, due to the calculation of ACF over EEG channels, we defined $N = 5$ for channel selection case and 16 for without channel selection case.

2.2.3.4 Moving variance (VAR)

VAR is a method that is mostly used to measure the statistics of streaming signals [60]. Each variance, V, is computed over sliding window lengths of five across each EEG channel in this study. For each sample $x(1)$, $x(2)$, …, $x(N)$, we calculated as:

$$V = \frac{1}{N-1} \sum_{i=1}^{N} (|x_i - \bar{x}|^2) \qquad \text{where} \quad \bar{x} = \frac{1}{N} \sum_{i=1}^{N} (x_i) \quad (11)$$

A sliding window with 5 and 16 data points for the case with and without channel selection, respectively, for the study in Chapter 4.

2.2.4 Single features and feature groups of FD features

The results of using this feature input are shown in Chapter 4. We extracted HFD and GP features from a series of 435 time points of pain-ERP for a single feature prior to forming feature groups, as presented in Figure 2.2. Then, both HFD and GP were extracted further by ACF and VAR. According to their extraction methods and functions, we named all features as "HFD" for features with Higuchi's method, "HFD_ACF" for Higuchi's with

autocorrelation, and "HFD_VAR" for Higuchi's with moving variance. Also, giving the same idea to the correlation dimension method by identifying the name "GP".

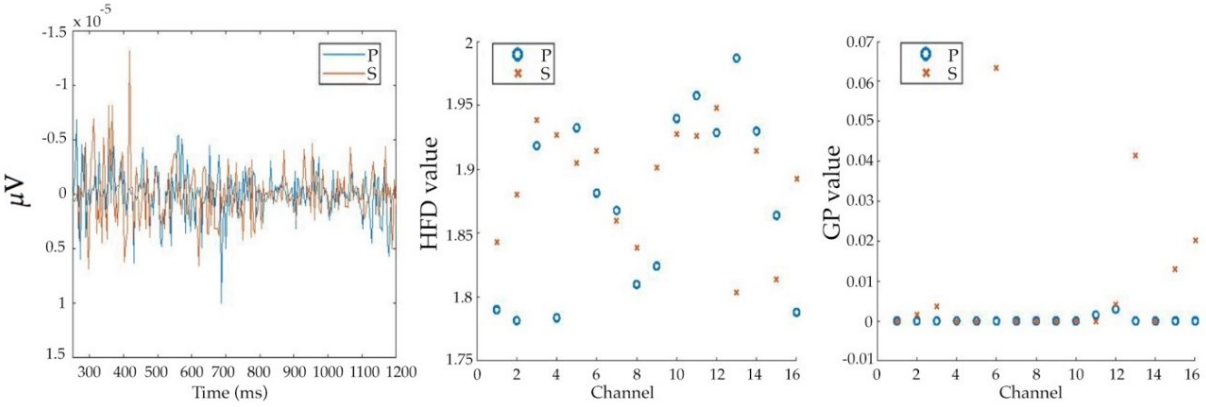

(**a**) (**b**) (**c**)

Figure 2.2 Feature extracted from pain-ERP (435 data points) of one subject for condition P and S. (a) a plot of pain-ERP data at Fz before feature extraction in range of 250 ms to 1.2 s to avoid the influence of the previous negative pulse, which might present from 0 to 250 ms; (b) a plot of HFD for each channel; (c) a plot of GP for each channel.

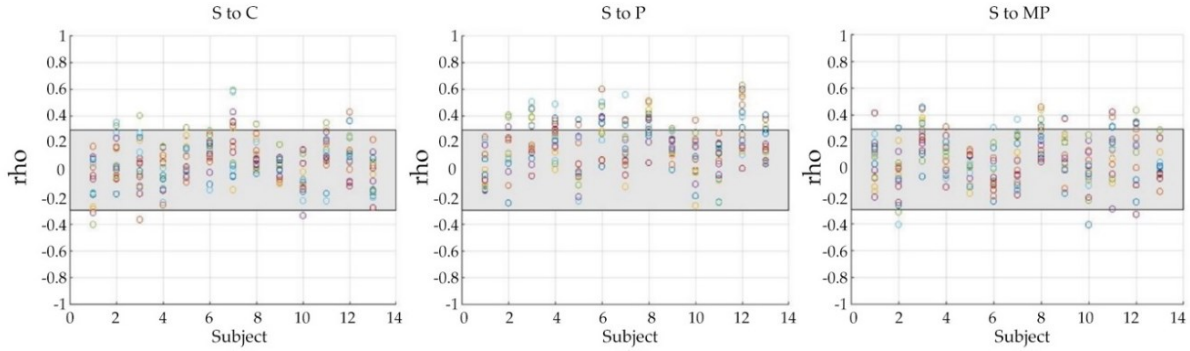

(**a**) (**b**) (**c**)

Figure 2.3 Plots of correlation between the signals for different pain perception levels and corresponding ratio of the number of points located outside the grey zone (the weak relationship boundary) to that of points located inside the grey zone. Horizontal axis represents subjects and vertical axis represents the spearman's correlation coefficients (rho). Each colour circle indicates the correlation between the data of a specific channel, and the grey area shows the weak correlation zone bounded by 0.3 and −0.3: (a) S to C is 0.10; (b) S to P is 0.27; (c) S to MP is 0.15.

After features were obtained, we observed the correlation between data features of different perception levels, as shown in Figure 2.2, demonstrating that some perception levels showed none or less discriminative to all the features. Thus, Spearman's correlation coefficient was used to calculate the correlation between data of different pain levels, displayed in Figure 2.3. To get a correlation ratio, we divided the number of points located outside of the grey zone by those points located inside the grey zone; thus, the higher the ratio, the strongly correlated to each other. Among the comparison of ratios between C and other pain levels, a

correlation ratio of 0.27 was found in 'S to P', which was higher values than those ratios 0.10 of 'S to C' and 0.15 of 'S to MP'. Still, the correlation ratio value of 'S to P' (0.27) was much higher when compared to the other pairs (0.07 of both 'C to P' and 'C to MP' and 0.21 of 'P to MP'). Due to the high correlation of data in S, the classifying pain levels were determined to perform for three types of classification: four-level classification (all perception levels including C, S, P, and MP), three-level classification (all perception levels excluding S), and two-level classification. Eventually, the sample numbers were 52, 39, and 26 for four-level classification, three-level classification, and two-level classification for a single feature.

To improve the multiple-level classification performances, the Fisher score was used to determine which feature extraction methods between the statistical method from the previous work on working memory [61] and the FD-based method (implemented in this study) is the better approach to predict pain levels. Also, we performed feature grouping according to the ranks of Fisher score to find the best features for multiple-level classifications.

For further investigation of the role of FD-based features, several feature groups were designated based on the following aspects of the features:

- Correlation-based (HFD, HFD_ACF, GP_ACF)
- Variance-based (GP, HFD_VAR, GP_VAR)
- HFD-based (HFD, HFD_ACF, HFD_VAR)
- GP-based (GP, GP_ACF, GP_VAR)

2.2.5 Classification model

Since we wanted to explore the feature, none of the development for the classifier model was performed. For investigating the effectiveness of FD-based features for multiple pain perception levels (Chapter 4), a traditional feed-forward neural network (NN) model was implemented in Matlab 2017b. The model structure is illustrated in Figure 2.4, which is composed of one input layer, one hidden layer with ten hidden units, and one output layer. Input data was divided into 75% training, 10% validation, and 15% testing sets. A NN model was trained by adjusting the weights based on a comparison between the output of the model and the ground truth (the real target of our data).

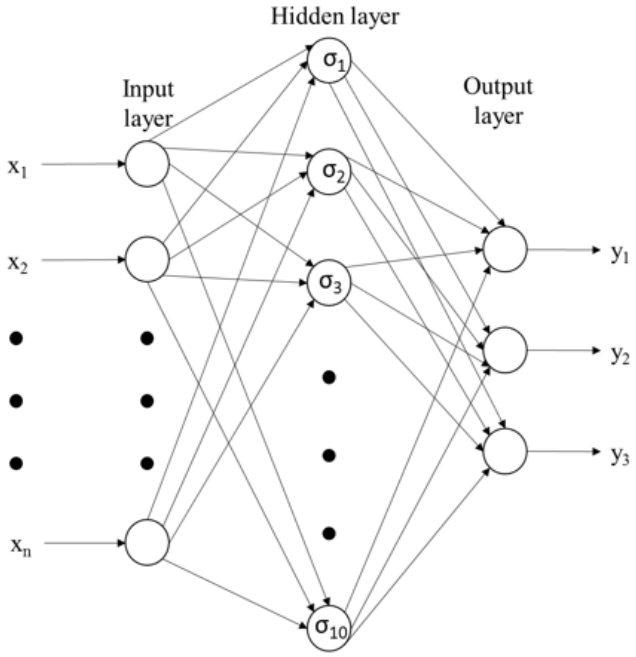

Figure 2.4 A scheme of NN model for pattern recognition. A hidden layer consists of ten hidden units (σ) *x* represents input features, and *y* represents the predicted output from the model.

2.3 For classification of Aδ- and C-fibers activations

2.3.1 EEG pre-processing

The evoked encephalography (eEEG) dataset, which was the evoked response to pain stimuli (see Chapter 3.2 for the details of experiment setting for acquiring the dataset), was pre-processed in Matlab 2017b (Mathworks, Natick, MA, USA) with EEGLAB toolbox [48]. EEG pre-processing was divided into two steps (Figure 2.5) to minimize artifact while maintaining the maximum quality of the extracted independent components (ICs) [62]. The first step was more aggressive in artifact removal. The selected independent component analysis (ICA) weights from the first step process were applied to the ICs of the second step to retain maximum information for further connectivity analyses.

In the first pre-processing step, the EEG data were downsampled to 512 Hz. Since the effect of artifacts from a power line and movement causes spurious causalities, high-pass filtered at 1 Hz and notch filtered at 50 Hz were reliable to use for artifact removal without misdetections of Granger causality (GC) components [63]. Next, bad channels and high-variance artifacts were removed by Artifact Subspace Reconstruction (ASR) [51]. Additionally, ASR was used to calibrate the pre-selected resting state and applied to the rest of the data. The remaining channels were re-referenced to channel-average, then the remaining data were divided into windows of 4 s (1 s before to 3 s after stimulus onset) for each trial. Epoched data were decomposed by Adaptive Mixture Independent Component Analysis (AMICA) [52]. ICA computed an unmixing matrix W with a given multivariate full ranked data series $X(N_{channels}, T)$ that generated source locations $S(N_{components}, T)$ were maximally independent, where $N_{channels}$ was a number of recording EEG channels (electrodes), $N_{components}$ was a number of ICs to be separated, and T was a number of time points in the trial. This was done by $WX = S$.

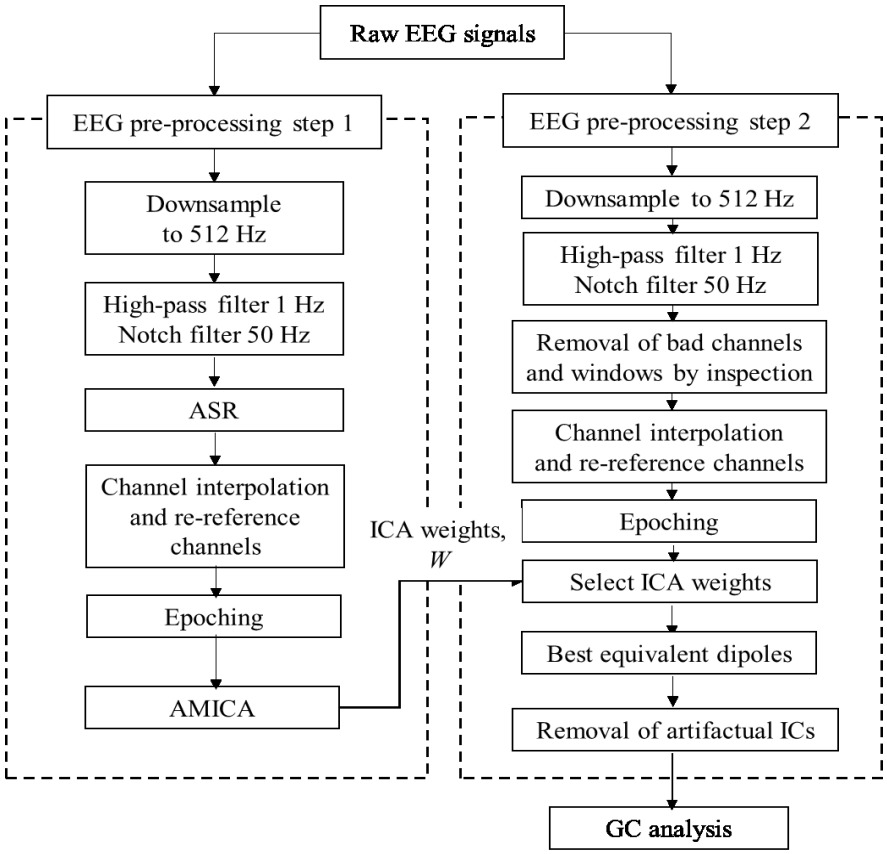

Figure 2.5 A schematic view of the EEG pre-processing for analysis in Chapter 5 and 6. First, the EEG was pre-processed and ICs were extracted. Then, the same ICs were applied to the second step. This two-step pre-processing procedure was helped the final data minimize the risk of artifact effects. Finally, epoched data with good ICs were obtained for further connectivity analysis.

ICA contributes to (1) The decomposition of EEG data into independent ICs and (2) Removing artifactual and highly interdependent ICs from eEEG signals. An example to indicate the effect of ICA on the eEEG signals is shown in Figure 2.6. In Figure 2.6a, which shows the signals from the FC5 channel before and after removing artifactual ICs identified by ICA and SASICA, it is clear that with ICA, the SNR of the signals was greatly improved. Nevertheless, the same effect could be confirmed for the other datasets of the other channels, stimulation level and waveforms. In Figure 2.6b, an example of average GC values over the frequency range of the gamma band (30-80 Hz) from the Cz to FC5 channels shows the higher value of $GC_{Cz \rightarrow FC5}$, which means that the past values of the Cz channel improve the prediction of the present values of the FC5 channel. However, the activities of the sites recorded by the two electrode channels shall have causal connections, as discussed in Chapter 5.3.3. Thus, applying ICA is necessary for EEG pre-processing in removing noise and computing causal connectivity.

In the second pre-processing step, raw EEG data were downsampled, filtered of 1 Hz and 50 Hz, and epoched to 4 s-window. No further artifact removal was done in this step except by inspection. Then, given ICA weights from the first step were applied to current data for acquiring maximized ICs quality while avoiding removal of brain activity that may come along with artifacts. DIPFIT toolbox with the Montreal Neurological Institute (MNI) brain

template was used to source localization of each IC. ICs based on these properties; noisy components with weak autocorrelation which derived from muscle artifact, and focal components which correspond to muscle activity and bad channels, were rejected by a semi-automated selection of independent components of the electroencephalogram for artifact correction (SASICA) [64] with Fully Automated Statistical Thresholding (FASTER) [65]. Finally, epoched data with good ICs for GC analysis were received.

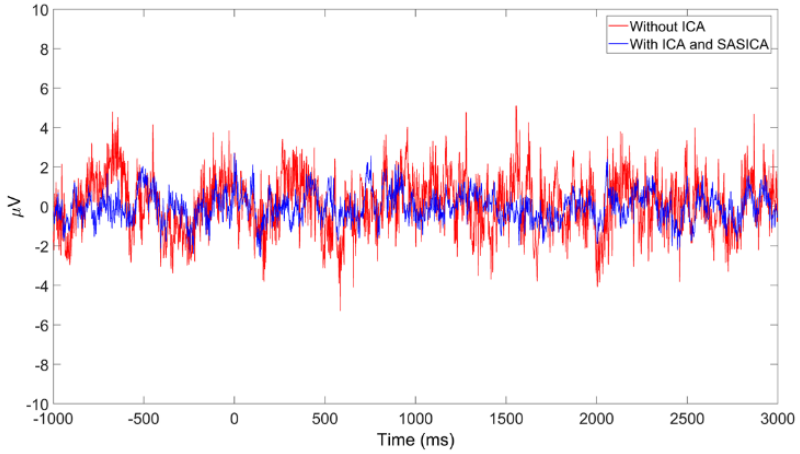

(**a**)

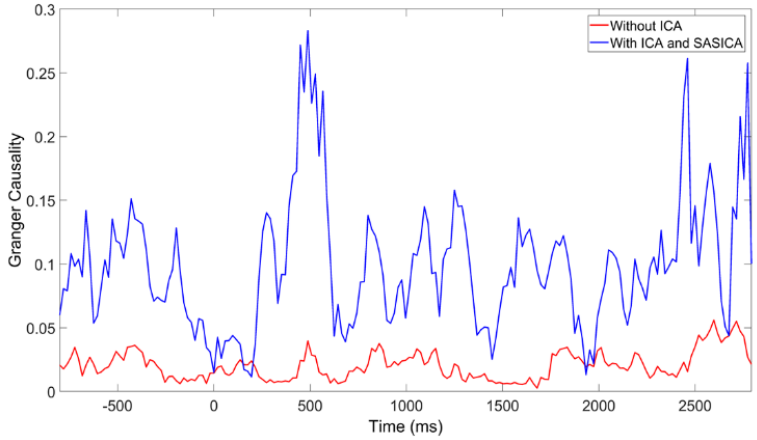

(**b**)

Figure 2.6 Effects of Removal of artifactual and highly interdependent ICs identified by ICA. These sample data were derived from eEEG signals recorded from the FC5 channel during a maximum pain level of 250 Hz stimulation to subject 2. (a) A plot of the eEEG signal in the time domain. The red line corresponds to eEEG before artifact removal (without ICA), and the blue line corresponds to eEEG after artifact removal with ICA, which contains both AMICA and SASICA; (b) A plot of average GC over the gamma band from the Cz to FC5 channels. Red and blue lines correspond to GC from eEEG without ICA and with ICA, respectively.

The eEEG signals elicited at both mild pain and maximum pain levels were collected for stimulation waveforms of 250 Hz and 5 Hz, but for stimulation of 1 Hz, the eEEG signals were collected only at the mild pain level due to the difficulty in distinguishing the elicited pain at different threshold values by the subjects. In summary, for each subject, five eEEG signal datasets were collected for analysis: 1 Hz (targeting C) at the mild pain level, 5 Hz (targeting C) at both the mild and maximum pain levels, and 250 Hz (targeting Aδ) at both the mild and

maximum pain levels, each of which consisted of 1 s of resting-state signals for calibration and the remaining signals during pain stimulation (stimulation part).

2.3.2 Feature extraction with Granger causality (GC) analysis

To investigate the event-related relationships between channels/components, Granger causality analysis was used for extracting GC features (Chapter 5). It measures based on the variances of the prediction error of univariate or multivariate autoregressive (AR) models. If the past values of time series x_2 can help predict the time series x_1, it means that x_2 "Granger causes" x_1 [46]. In this study, GC was computed in time-frequency based on SIFT toolbox [66] and Cohen's method [67].

The prediction of vector time series *x(t)* in univariate AR model (Equation 12) or multivariate AR model (Equation 13) are shown as follows:

$$x(t) = \sum_{i=1}^{p} a_i(t)\, x_1(t-i) + e_{x_1}(t) \tag{12}$$

$$x(t) = \sum_{i=1}^{p} a_i(t) x_1(t-i) + \sum_{i=1}^{p} b_i(t) x_2(t-i) + e_{x_1 x_2}(t) \tag{13}$$

where *i* is the number of lags in the process. a_i and b_i are estimated autoregressive coefficients for AR model of order *p*. e_{x_1} and $e_{x_1 x_2}$ are the prediction errors. Then, GC calculates in time series can be computed as:

$$GC_{x_2 \to x_1}(t) = ln \frac{var(e_{x_1})}{var(e_{x_1 x_2})} \tag{14}$$

where $GC_{x_2 \to x_1}(t)$ is the time series x_2 causal to the time series x_1. Then, the spectral GC at a given frequency, *f*, is estimated by:

$$GC_{x_2 \to x_1}(t, f) = ln\left(\frac{S(f)}{H(f) A H^*(f)}\right) \tag{15}$$

where *S(f)* is a spectral matrix, $H(f)$ is the transfer matrix. The covariance matrix of the whole system *A* is calculated by $\begin{bmatrix} e_{x_1}(t) \\ e_{x_2}(t) \end{bmatrix}$. The asterisk is defined as complex conjugation. GC in *t* time and frequency *f* (in range of [f_1, f_2]) is calculated as:

$$GC_{x_2 \to x_1}(t, [f_1, f_2]) = \frac{1}{f_2 - f_1} \int_{f_1}^{f_2} GC_{x_2 \to x_1}(f) df \tag{16}$$

Since covariance stationary was required for GC analysis, the time series data were windowed into short time segments of 400 ms with window sliding 20 ms. Due to the variance of the signals in GC analysis, demeaning and scaling were suggested to improve stationary. Any trial segments which were non-stationary and had a correlation structure in the residuals were excluded. AR model order was estimated based on the Bayesian Information Criterion (BIC) [66]. In this study, the model order of 18 was selected for all subjects without degraded performance. Then, the AR model was fitted with Vieira–Morf method and validated before calculating the connectivity.

Three categories of GC features were extracted: (1) GC between channel areas (GC_ChA), (2) GC between ICs of each frequency band (GC_CoF), and (3) GC between ICs of one stimulation waveform to another stimulation waveform (GC_CoW). The followings are the details.

2.3.2.1 GC between channel areas (GC_ChA)

A group of selected channels (or electrodes) was distributed according to the 10-20 system and previous study on Alzheimer's [68] [69]. In Figure 2.7, all 32 active electrodes were grouped into five brain areas: central (Fz, Cz, C3, C4, Pz, FC1, FC2, CP1, CP2), frontal (Fp1, Fp2, F3, F4, AF3, AF4), occipital (Oz, O1, O2, P3, P4, PO3, PO4), left temporal (Lt: F7, FC5, T7, CP5, P7), and right temporal (Rt: F8, FC6, T8, CP6, P8).

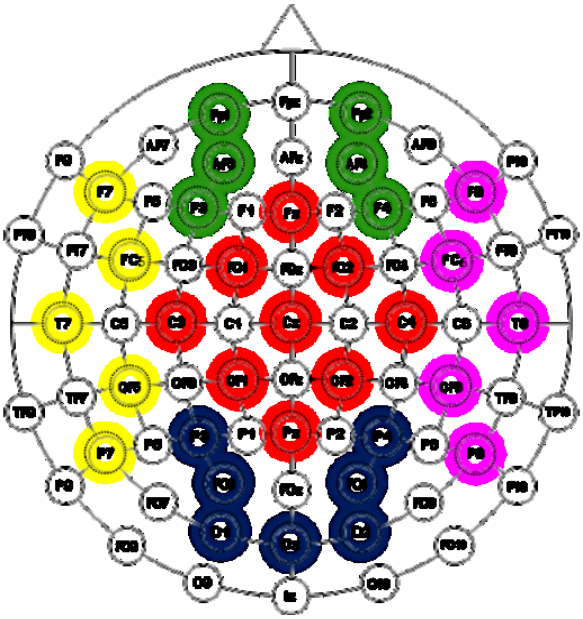

Figure 2.7 EEG electrode locations. All 32 active electrodes were clustered into five areas: red for the central area, green for the frontal area, blue for the occipital area, yellow for the left temporal area, and pink for the right temporal area.

It is noted that only this GC category was calculated according to [67] with the same pre-processing step for GC as in SIFT. Firstly, epoched EEG from the same waveform was merged into one dataset for each subject. Any trials with non-stationary and correlated residuals were removed after checking by Kwiatkowski–Phillips–Schmidt–Shin (KPSS) test and Durbin Watson test, respectively. Then, a Morlet wavelet transform was used to extract time-frequency representations. Wavelet coefficients of 50 frequency points on a logarithm scale were computed from a frequency range of 1-80 Hz. Therefore, each unidirectional pair of GC_ChA was defined as:

$$GC_{ChA_j \to ChA_i}(t,f) = \sum_{n=1}^{N} GC_{ChA_{jn} \to ChA_{in}}(t,f) \quad (17)$$

where *ChA* is the average channel of the selected channels from predefined areas indexed by i (i = 1,2,…,5) and j (j = 1,2,…,5). n is the index of the subjects (n = 1,2,…,N), and N denotes the total number of subjects (N = 14). There were three target classes in this GC category. The classes were labeled 1 Hz, 5 Hz (both targeting C), and 250 Hz (targeting Aδ). Each GC group consisted of the number of samples (*Nsample*) and relationships (*Nrelationship*) as follows:

Nsample = 3 waveforms × 14 subjects

Nrelationship = 126 time points × 50 frequency points

Each GC group had 42 samples and 6,300 relationships. Thus, 20 pairs of unidirectional GC estimations were received as follows:

$GC_{central \rightarrow frontal}$, $GC_{central \rightarrow occipital}$, $GC_{central \rightarrow Lt}$, $GC_{central \rightarrow Rt}$, $GC_{frontal \rightarrow occipital}$, $GC_{frontal \rightarrow Lt}$, $GC_{frontal \rightarrow Rt}$, $GC_{occipital \rightarrow Lt}$, $GC_{occipital \rightarrow Rt}$, $GC_{Lt \rightarrow Rt}$, $GC_{frontal \rightarrow central}$, $GC_{occipital \rightarrow central}$, $GC_{Lt \rightarrow central}$, $GC_{Rt \rightarrow central}$, $GC_{occipital \rightarrow frontal}$, $GC_{Lt \rightarrow frontal}$, $GC_{Rt \rightarrow frontal}$, $GC_{Lt \rightarrow occipital}$, $GC_{Rt \rightarrow occipital}$, $GC_{Rt \rightarrow Lt}$

2.3.2.2 GC between ICs of each frequency band (GC_CoF)

In this category, the GC relationship was estimated from one IC to another IC within the subject and waveform. Wavelet coefficients were computed for 80 frequency points on a linear scale, ranging from 1 to 80 Hz in this step. Five frequency bands were defined for each GC: delta (1-4 Hz), theta (4-8 Hz), alpha (8-13 Hz), beta (13-30 Hz), and gamma (30-80 Hz). Each pair of GC_CoF is defined as follows:

$$GC_{\mathrm{CoF}}(t, f_m) = \sum_{n=1}^{N} GC_{Co_{jn} \rightarrow Co_{in}}(t, f_m) \quad (18)$$

where f_m (m = 1,2, …,5) is a frequency band that is mentioned above from delta to gamma band. *Co* denotes the *i*th and *j*th IC, *n* and *N* indicate the subjects (n = 1,2,…,N) and the total number of subjects (N=14). The number of samples of this feature was varied based on the number of ICs (*Co*) in each frequency band. Furthermore, feature numbers were not equal in every sample due to different frequency points of each band, for example, four points in the delta band and eighteen points in the beta band. The target classes were labeled 1 Hz, 5 Hz, and 250 Hz (same as those of GC_ChA). Each GC group was composed as follows:

Nsample = 3 waveforms × 14 subjects × N_c

Nrelationship = 185 time points × f_m frequency points

where N_c corresponds to the number of ICs of each dataset after artifact removal, and frequency points denote each frequency band.

Each GC group had 24,744 samples and a range of 740-9,435 relationships. Thus, 5 pairs of unidirectional GC estimations were obtained as follows: GC_{delta}, GC_{theta}, GC_{alpha}, GC_{beta}, and GC_{gamma}.

2.3.2.3 GC between ICs of one stimulation waveform to another stimulation waveform (GC_CoW)

To investigate which directional flow of stimulation waveform has contributed to different pain levels, GC relationship was calculated IC of eEEG by one waveform and one IC of eEEG by another waveform. Even though the EEG signals evoked by different waveforms were not collected simultaneously in this study, they were used as virtual empirically related variables in the calculation of this GC category because they had the same processed that taking the onset time of stimulation as the point of reference with the same time span (4 s-window). Data of stimulation waveform of 1 Hz was excluded in this step because it was composed of only one mild pain level (low pain). Thus, 2 pairs of unidirectional GC estimations were shown as follows: $GC_{5Hz \rightarrow 250Hz}$ and $GC_{250Hz \rightarrow 5Hz}$. Each pair of GC_CoW is described as:

$$GC_{CoW_j \to CoW_i}(t,f) = \sum_{n=1}^{N} GC_{CoW_{jn} \to CoW_{in}}(t,f) \quad (19)$$

where *CoW* is an IC of the *i*th (*i* = 1,2) and *j*th (*j* = 1,2) stimulation waveform, and *f* denotes wavelet coefficient of 80 frequency points on a linear scale, which frequency ranging from 1 to 80 Hz. *n* and *N* are the index of the subjects (*n* = 1,2,…,*N*) and the total number of subjects (*N*=14), respectively. In this category, two target classes were labeled mild pain and maximum pain.

To classify pain levels (mild and maximum pain), information about GC flows between waveforms was used in this category. Each GC group consisted of sample and relationship numbers as follows:

Nsample = 2 pain levels × 14 subjects × N_c

Nrelationship = 185 time points × 80 frequency points

where N_c corresponds to the number of ICs of each dataset after artifact removal.

Consequently, each GC group had 914 samples and 14,800 relationships. Therefore, the 2 pairs of unidirectional GC estimations were $GC_{5Hz \to 250Hz}$ and $GC_{250Hz \to 5Hz.}$

In feature extraction of this study, there are three levels of GC from the highest level to the lowest level: GC categories, groups and relationships. GC categories corresponding to the purpose of the investigation, i.e., causal connectivity concerning channel areas, frequency bands and waveforms. GC groups are on the second level, reflecting the GC for the groups in each category, e.g., GC_{alpha} group for the alpha band. In this case, the Granger causality of the category is GC_CoF. GC relationships are on the lowest level and were analyzed for each IC pair in the group, e.g., the data within two different time windows in the alpha band, summed up to GC groups, e.g., GC_{alpha} group. Moreover, relationship maps and feature map examples of GC groups from GC_ChA, GC_CoF and GC_CoW are shown in Figure 2.8a, Figure 2.8b, and Figure 2.8c, respectively.

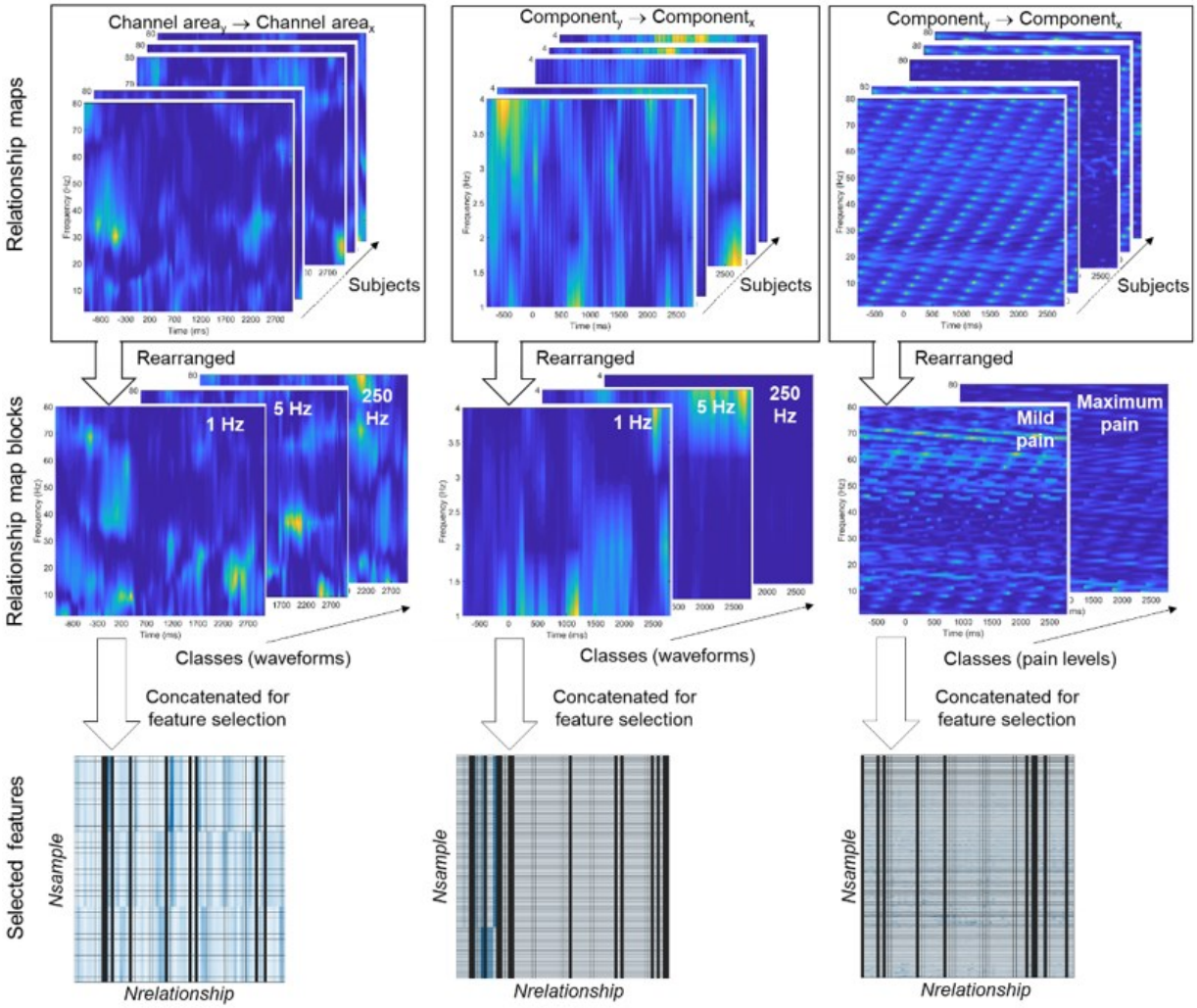

(**a**) (**b**) (**c**)

Figure 2.8 Relationship maps and feature maps of three GC groups from the three GC categories. (a) $GC_{frontal \rightarrow Rt.}$ from GC_ChA; (b) GC_{delta} from GC_CoF; (c) $GC_{5Hz \rightarrow 250Hz}$ from GC_CoW. The upper row shows relationship maps of a GC group (GC between 2 channel areas) of the GC_ChA category and a GC group (GC between two components, i.e., ICs) for the GC_CoF and GC_CoW categories with regard to a class (waveform or pain level). The middle row shows the relationship map blocks for classes (three waveforms or two pain levels), each of which corresponds to (subject number) pieces of relationship maps for GC_ChA and (subject number × N_c) pieces of relationship maps for GC_CoF and GC_CoW. The bottom row shows 30 selected features (bold black lines) with a background of a concatenation relationship map, which is a combination of relationship map blocks of all classes, i.e., (subject number × class number) pieces of relationship maps for GC_ChA and (subject number × class number × N_c) pieces of relationship maps for GC_CoF and GC_CoW.

2.3.3 Feature selection and sample optimization

For feature selection, the paired t-test and mutual information were applied. The paired t-test was performed between the frequency vectors, *f*, and the corresponding time point, *t*. GC relationships with p-value < 10^{-5} were chosen as selected features. Then, the mutual information was performed to get the top 30 features for each GC pair.

For sample optimization, the interpolation and clustering methods were used to increase spatial sampling density and separate samples in groups of equal variances, respectively, in which the former was used for the GC_ChA and the latter was used for the GC_CoF. In the GC_ChA, the original sample number of 42 for each feature was derived from a combination of subject numbers (14 subjects) and stimulation waveform numbers (3 waveforms of 1 Hz, 5 Hz, and 250 Hz). After applying univariate interpolation in the GC_ChA, 195 samples were obtained. The number of optimized samples was determined by trial and error. Due to a large number of combinations of ICs, subjects, and waveforms in the GC_CoF, there was a simple number of 24,744. Thus, a clustering method was used with the number of clusters, k = 3, determined by the sum of squared error (SSE). The best cluster was used as samples, which resulted in discarding less than 5% of the samples considered outliers. Accordingly, the samples number were varied according to the clusters. Only the samples after optimization were classified in this study.

Finally, 27 GC relationship features were obtained for classifying pain induced by different fibers activations and different pain perception levels: 20 from the GC_ChA, 5 from the GC_CoW, and 2 from the GC_CoF.

2.3.4 Classification model

The pipeline for the classification is displayed in Figure 2.9. One type of neural network, multilayer perceptron (MLP) with one input layer, one hidden layer of 100 hidden units and one output layer, was used for classifying GC features. The following hyperparameters were optimized to achieve better classification: a maximum number of iterations of 200, 500, and 1000 and limited-memory Broyden–Fletcher–Goldfarb–Shanno (LBFGS) and stochastic gradient descent (SGD) solvers. In this case, the solver was set to LBFGS for all GC features, but the maximum number of iterations was varying for each GC feature. A model structure with 200 bootstrap iterations with a replacement for training and testing sets (Figure 2.10) was implemented to ensure that obtained classification accuracy was from the input features' distribution. In this study, input features were resampling based on the dataset after sample optimization, as shown in Figure 2.9. However, we also look back to the original dataset (without sample optimization) and used it as input feature in a model structure. Moreover, we found that there was subtle difference between the classification rate of the optimized dataset and the original dataset, which means that features extracted from the optimized dataset contain the same information of pain as the original dataset. A sample size of a training set was set as 70% of data and the other samples which were not included in the training set were retrieved as a test set. The plot of difference between $GC_{central \rightarrow frontal}$ related dataset with and without bootstrap resampling was illustrated in Figure 2.11 as an example. Then, the model was run to optimized classification parameters and k-fold cross-validation.

The classification performance indices included Matthews correlation coefficient (MCC), accuracy, and F1-score were evaluated on the test set. MCC measures the correlation between actual and predicted classes, while accuracy and F1-score indices indicate how many correctly predicted results of the classification. The former focuses on true positives and true negatives and the latter focuses on false negatives and false positives. MCC ranges from -1 to 1 where 1 indicates the best classification and -1 indicates no correlation between the predicted values and actual observations. For F1-score, 1 means the classification model can give the best accurate results (high precision and fewer false positives).

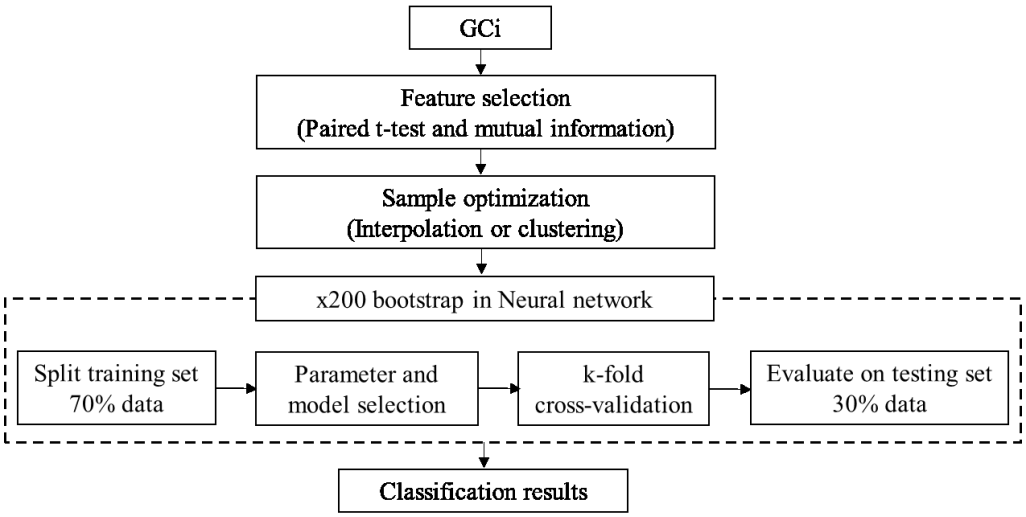

Figure 2.9 Schematic representation of classification steps for the neural network model. GCi was indicated as GC groups in different categories, where i = 1 for GC groups in GC_ChA, i = 2 for GC_CoF, and i = 3 for GC_CoW.

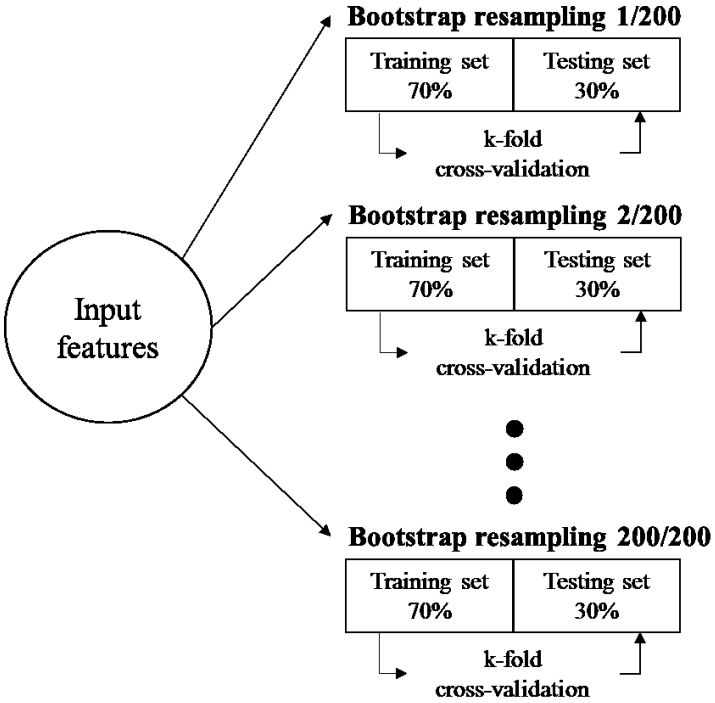

Figure 2.10 A scheme of classification model with a bootstrap method.

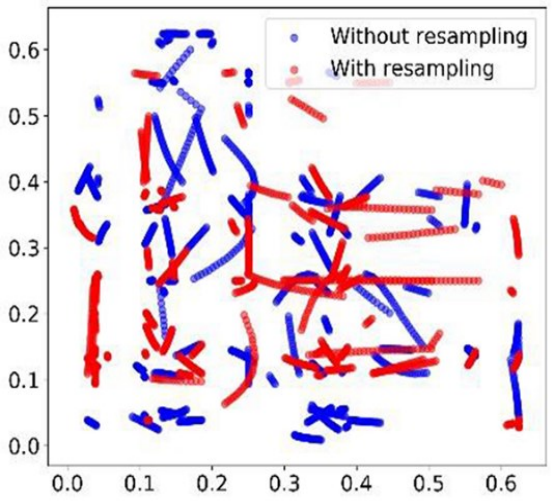

Figure 2.11 Data variation resulting from bootstrap resampling of $GC_{central \rightarrow frontal}$. Blue points represent the data points without resampling and red points represent the data points with resampling.

2.3.5 Statistical analysis

To compare classification accuracy of these GC categories, Wilcoxon rank sum test was used. Three different tests were performed: GC_ChA vs. GC_CoF, GC_ChA vs. GC_CoW, and GC_CoF vs. GC_CoW. Additionally, six different conditions of GC groups were analyzed; the three different waveforms (1 Hz and 5 Hz for targeting C and 250 Hz for targeting Aδ) for two pain levels (mild pain and maximum pain). All GC differences were estimated by subtracting GC estimates of one group from another group for all subjects. For GC differences calculation, a two-sample t-test was predominantly used to initiate t-score maps masked with an uncorrected $p < 0.01$. Then, multiple comparison correction, family-wise error rate (FWER) control, was used via 10,000 times permutation test with $p < 0.05$ as a critical value. Therefore, the pixel-by-pixel t-scores of GC in time-frequency representation that identify a significant difference between conditions were obtained.

2.4 For simulating an online classification

The experimental design is described in Chapter 3.2.3.2. We implemented the stimulation waveforms to elicit pain for Aδ- and C-fibers activations as we conducted in Chapter 5. Two stimulation waveforms of 1 Hz square waves [70] and 5 Hz sine waves were used for highly selective C-fibers, while another waveform of 250 Hz sine waves for Aδ-fibers. The latter two waveforms were corresponding to the parameter from Neurometer [21] [22] [71].

2.4.1 EEG pre-processing

We used the eEEG dataset (see Chapter 3.2 for the details of experiment setting for acquiring the dataset) and EEG pre-processing that were used in Chapter 5. We eventually obtained 2048 data points from 1 s before to 3 s after stimulus onset for each trial after EEG pre-processing. For this final implementation, we used the frequency domain of EEG to extract

features for all data to determine which frequency band was the most correlated to pain. The pipeline of this study is displayed in Figure 2.12

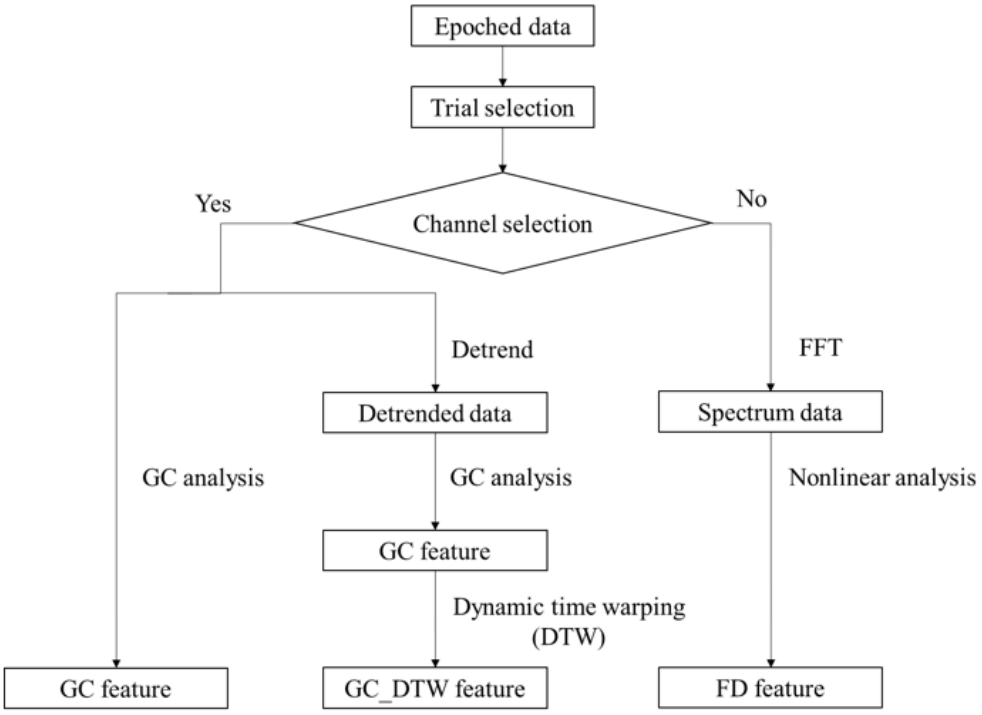

Figure 2.12 Overview of the proposed pipeline. GC feature and GC_DTW feature were processed with EEG channel selection due to the computation time cost in GC calculation. GC feature was only performed with GC analysis, while GC_DTW feature was pre-processed with detrend (remove trend from the signal), then performed with GC analysis and further extracted with dynamic time warping (DTW). Data was analyzed with fast-Fourier transform (FFT) and extracted by nonlinear analysis approaches for the FD feature.

After pre-processing data, epoched data was used to select the target trial(s) for simulating an online scenario, which has fewer number trials. Since the latency of the evoked Aδ-response is earlier than that of C-response, the time-locked of the pain stimulus (target trial) might affect the pain information corresponds to the trial. Thus, three ways of selecting target trial(s) were:

- N-trial averaging: n-trial were selected and then performed average.
- Single trial: only target trial was selected.
- First n-trial averaging: n-trial from the first appearance in the EEG signal was selected.

After that, EEG channel selection was performed with Fisher score. In this study, a range of 5-9 channels was investigated. The obtained data with few numbers of trials and channels were used for extracting features.

2.4.2 Feature extraction

2.4.2.1 Granger causality (GC) analysis

All methods of feature extraction were performed in the frequency domain of EEG within five frequency range of interest: delta (1-4 Hz), theta (4-8 Hz), alpha (8-13 Hz), beta (13-30 Hz), and gamma (30-80 Hz). After pre-processing, the data was analyzed with GC analysis and nonlinear analysis to get GC features and fractal dimension (FD) features, respectively.

To estimate GC between origin channel y and target channel x from spectral EEG, GC at frequency f can be computed as:

$$GC_{y\to x}(f) = ln\left(\frac{|S_{xx}(f)|}{\left|S_{xx}(f) - H_{xy}(f)A_{yy}H_{xy}{}^{*}(f)\right|}\right) \tag{20}$$

where S denotes the spectral matrix and H is the transfer matrix. A is the covariance matrix, and the asterisk denotes matrix transposition and complex conjugation.

According to the five frequency bands that we used in the analysis, the feature numbers were varied based on the frequency points of each band that used in the calculation, i.e., 12 for delta, 16 for theta, 20 for alpha, 68 for beta, and 200 for gamma, while the sample numbers composed of $N_{\text{subject}} \times N_{\text{waveform}} \times \sum_{x,y=1}^{N_{channel}} GC_{y\to x}$ where N_{subject} is the number of subjects (14 in this study), N_{waveform} corresponds to EEG data of 1 Hz stimulation at low pain, 5 Hz stimulation at low and high pain, and 250 Hz stimulation at low and high pain. $\sum_{x,y=1}^{N_{channel}} GC_{y\to x}$ is the number of channels (N_{channel}) pairs of a two-node network in GC calculation model.

Therefore, 5 GC features were: GCdelta, GCtheta, GCalpha, GCbeta, and GCgamma, which each GC feature composed of a number of samples (*Nsample*) and channel pairs of the two-node network (*Npair*) as follows:

Nsample = 14 subjects × 3 waveforms

Npair, which is the permutation of *Nchannel* = $\frac{Nchannel\,!}{(Nchannel-2)!}$. For example, *Npair* = 30 for 6 selected channels based on Fisher score, 20 *Npair* for 5 selected channels based on Fisher score, etc.

2.4.2.2 Dynamic time warping (DTW)

DTW technique [72] is used to find the optimal alignment between two time series even if a pair of these time series is asymmetric. By a nonlinear compression aims at aligning two time series and iteratively extension of the time axes (warping the time axis). Given two time series a ($a_1,a_2,\ldots,a_M$) and b ($b_1,b_2,\ldots,b_N$) of length M and N, respectively, and then compute time-normalized distance measure between two time series by:

$$D(a,b) = \frac{\sum_{k=1}^{K} d(p_s)\, w_k}{\sum_{k=1}^{K} w_k} \tag{21}$$

where the warping path, $p = (p_1,p_2,\ldots,p_k)$ with length K. A distance between mth sample of series a and nth sample of series b is $d(p_s) = \sum_{k=1}^{K}\left|a_{k,m} - b_{k,n}\right|$. w_s denotes the weighting coefficient, which is more than 0. An optimal warping path (optimal alignment) *DTW*, which has the minimal total cost among all warping paths, can be described as:

$$DTW = min \frac{\sum_{k=1}^{K} D(a,b)}{\sum_{k=1}^{K} k} \quad (22)$$

In this study, DTW was performed between two GC features, for example, between GCdelta and GCtheta. Within the GC feature at one frequency band of one subject, a matrix (*Nwaveform* × *Npair*) in which each vector of a pair of channels was analyzed with DTW against a vector from another GC feature. An example for DTW calculation between GC features of one eEEG dataset (data of one subject and one waveform) is illustrated in Figure 2.13. After that, all vectors of DTW values were merged into one GC_DTW feature, as displayed in Figure 2.14.

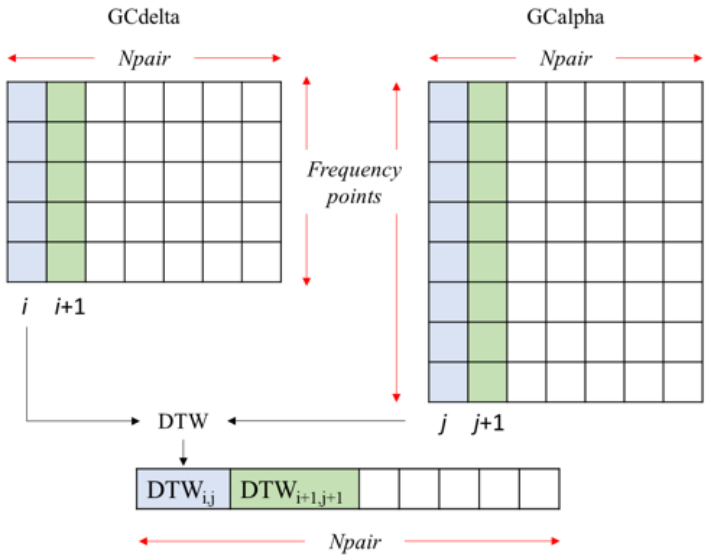

Figure 2.13 An example of the DTW calculation between GC features. Two GC features: GCdelta (12 frequency points × *Npair*) and GCalpha (20 frequency points × *Npair*) which each *Npair* vector of each GC feature was used to calculate DTW. Accordingly, a vector of DTW with a length of *Npair* was obtained for each eEEG dataset (one waveform and one pain level) of one subject.

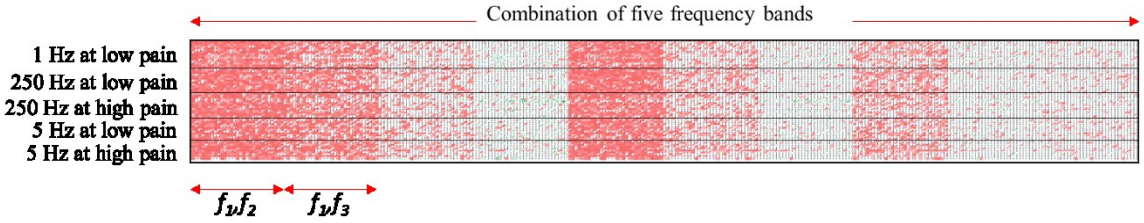

Figure 2.14 A matrix of GC_DTW feature. Each row of one class (one waveform at one pain level, for example, 1 Hz at low pain) corresponds to a subject and each column block corresponds to DTW between frequencies such as f_1f_2 denotes DTW between frequencies of delta and theta. With a combination of five frequency bands ($f = 1,2,\ldots,5$) of delta, theta, alpha, beta, and gamma, ten combinations were analyzed. Each column inside one column block corresponds to *Npair* according to Figure 2.13. Colour corresponds to the value of DTW.

2.4.2.3 Nonlinear analysis

Three approaches of nonlinear analysis, HFD, GP, and VAR, from Chapter 2.2 were used to extract FD features from EEG in the frequency domain. Firstly, epoched data was analyzed by fast Fourier transform with Hanning window. Then, the obtained data in terms of frequency components was calculated with the frequency range of interest (frequency band). The obtained spectral power estimates composed of 11 data points for delta, 17 data points for theta, 17 data points for alpha, 67 data points for beta, and 199 data points for gamma. Thus, the power spectral estimates for each frequency band was used to extract FD features by analysis with HFD and GP, and calculating further by VAR.

For calculating HFD (see Chapter 2.2.3.1) from the spectral power data, curve length *L(k)* with interval times k (k = 5, 8, 8, 33, and 99 for delta, theta, alpha, beta, and gamma, respectively) can be computed as:

$$L(k) = \frac{1}{k} \sum_{m-1}^{k} \left(L_m(k)\right) \tag{23}$$

where HFD is the slope of a plot $log(L(k))$ against $log(1/k)$.

For GP calculation (see Chapter 2.2.3.2), a correlation dimension (D_2) which is the relation between the correlation sum *C(r)* with a value of M = 1 for lower frequencies of delta, theta, and alpha, 2 for beta and gamma and hypersphere radii r, is calculated as:

$$D_2 = \lim_{r \to 0} \frac{\log(C(r))}{\log(r)} \text{ where } C(r) = \lim_{\mathrm{N} \to \infty} \frac{1}{N^2} \sum_{i,j=1}^{N-(M-1)\tau} H\left(r - \left|x_i - x_j\right|\right) \tag{24}$$

where GP is a slope of plot $\log(C(r))$ against $\log(r)$.

Then, both HFD and GP were extracted further by VAR, which performed a sliding window over 3 data points and named "HFD_VAR" and "GP_VAR", respectively.

Therefore, HFD, GP, HFD_VAR, and GP_VAR, were combined into one FD feature of each frequency band. Finally, 5 FD features were obtained: FDdelta, FDtheta, FDalpha, FDbeta, and FDgamma, which each FD feature consisted of the number of samples (*Nsample*) and features (*Nfeature*) as follows:

Nsample = 14 subjects × 3 waveforms

Nfeature = HFD, GP, HFD_VAR, GP_VAR = 4

2.4.3 Classification model

The model structure in this section was used for the third experiment (Chapter 6) to classify nociceptive fibers activations as the same as the second experiment, but performed in simulation for online analysis. This study implemented a more generalize classification model with nested cross-validation (CV). MLP with nested CV, which is a procedure to optimize the model parameters while also estimating the generalization error of the underlying model with the optimized parameters, was applied to this model structure, as displayed in Figure 2.15.

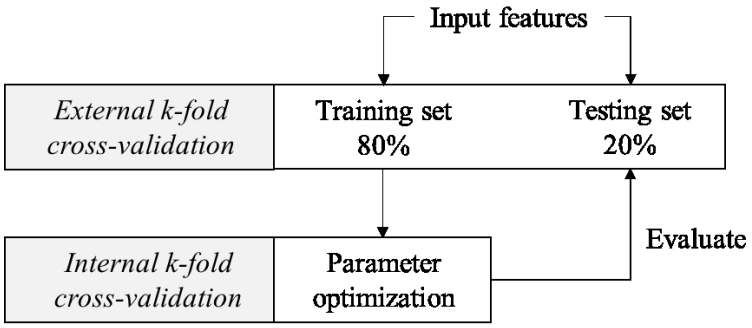

Figure 2.15 A scheme of classification structure using MLP with nested CV. k = 5 in this model structure

Nested CV consisted of a two-fold CV which was applied with k-fold (k=5) CV for both external and internal fold in the model structure. It consisted of two 5-fold CV scheme: an external and an internal, was performed. Firstly, the external 5-fold CV split the input features into 80% training and 20% testing. Secondly, the training set (80% of the input features) from the external CV was taken to perform with an internal 5-fold CV. The MLP model was trained and optimized within the internal CV with the training set (80%). Finally, evaluating the rest 20% testing set of the input features. This scheme of nested CV could give more robust and fair results compared with the traditional CV.

This scheme provided more robust and fair results compared with the model in the previous chapter. Furthermore, the imbalanced class of 1 Hz, which derived from only a low pain level, was oversampling to avoid bias in the training set.

2.5 Conclusions

All the processes of EEG pre-processing, selection of EEG channels and features, feature extraction with nonlinear analysis and GC analysis, post-processing and classification model used throughout the Doctoral project are described in this chapter.

In the next chapter, EEG data acquisition, electrical pain stimulation, and pain experiments are presented.

Chapter 3

Experiments

3.1 Introduction

This chapter provides the details of the designs of the experiment used in this Doctoral project. First, we describe EEG data acquisition. Then, we describe the stimulation waveforms and an overview of the pain experiments. All experiments in this project were approved by the Research Ethics Committee, Safety and Health Organization, Center for Frontier Medical Engineering, Chiba University (no. 01-09). This project was carried out following the rules of the Declaration of Helsinki of 1975 (https://www.wma.net/what-we-do/medical-ethics/declaration-of-helsinki/), revised in 2008.

3.2 Experimental design

In this section, we used stimulation waveforms and parameters according to the Neurometer [23] [71], simulation studies [70] [73] [74], and electrical stimulation-related study [75]. There were two experiments in this Doctoral project. The square waves with low frequency were used to activate mainly on C-fibers in the first experiment. The purpose of applying the waveforms that selectively stimulates C-fibers was to imitate chronic pain in this experiment. We applied three waveforms that selectively stimulate Aδ- and C-fibers to predict pain corresponding to these different nociceptive fibers for the second experiment.

3.2.1 EEG data acquisition

In the whole project, the EEG signals were measured using Biosemi ActiveTwo. In the first experiment (Chapter 4), 16 electrodes were used, while 32 electrodes were used in the rest of the experiments (Chapter 5 and 6). The locations of EEG electrodes are displayed in Figure 3.1. The electrode placements were described as follows.

- 16 electrodes: Fp1, F3, T7, C3, P3, Pz, O1, Oz, O2, P4, C4, T8, F4, Fp2, Fz, and Cz
- 32 electrodes: Fp1, Fp2, AF3, AF4, F7, F3, Fz, F4, F8, FC5, FC1, FC2, FC6, T7, C3, Cz, C4, T8, CP5, CP1, CP2, CP6, P7, P3, Pz, P4, P8, PO3, PO4, O1, Oz, and O2

It is necessary to pull data from this EEG device through proprietary software (ActiView), which is an open-source acquisition program for the Active Two system provided by the company. In this project, a sampling rate was set to 2048 Hz with a bandwidth of 400 Hz. In the ActiveTwo system, a USB2 receiver is used to convert the optical data from the AD-box and transmit the trigger from the other device, i.e., pain stimuli from the stimulator in this project, to the software. In the ActiView software, we can see the EEG data and the triggers from the stimulator separately in the graphical user interface, but both data are stored in one data file. All the triggers (pain stimuli) were used as a stimulus onset for windowing the data.

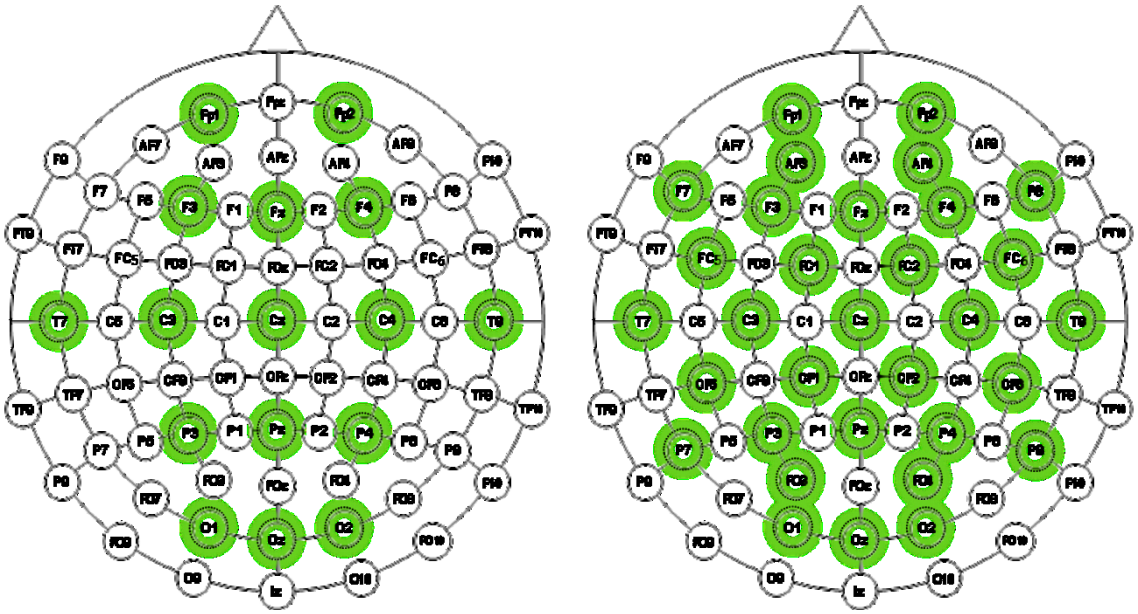

(a) (b)

Figure 3.1 EEG electrode locations. Channels to be used in this project were indicated in green colour. (a) 16 active electrodes for the first experiment (Chapter 4); (b) 32 active electrodes for the second (Chapter 5) and third experiments (Chapter 6).

3.2.2 Electrical stimulation waveforms

3.2.2.1 Waveforms for classification of pain perception levels

In the first experiment for classifying pain perception levels which will be performed in Chapter 4, one stimulation waveform was used to elicit pain. The pain stimuli were generated by Electro-stimulator NS-101 (Unique Medical Co., Ltd., Tokyo, Japan) through a diameter of 1 cm of disposable electrodes (Neurotron Co., Ltd., Baltimore, MD, USA). We delivered electrical pain stimuli to the side of the right middle phalanx of the middle finger. According to [75], which found that square waves induced pain more than sine waves, bipolar square waves with a frequency of 5 Hz were applied in this study to activate one of the major pain conduction nerves, C-fibers. The other parameters of the waveform were 50 double pulses, 5 ms of pulse duration [76], 95 ms of inter-pulse interval, and 1 s of inter-stimulus interval (ISI) [75] [77]. The stimulation waveform has displayed in Figure 3.2.

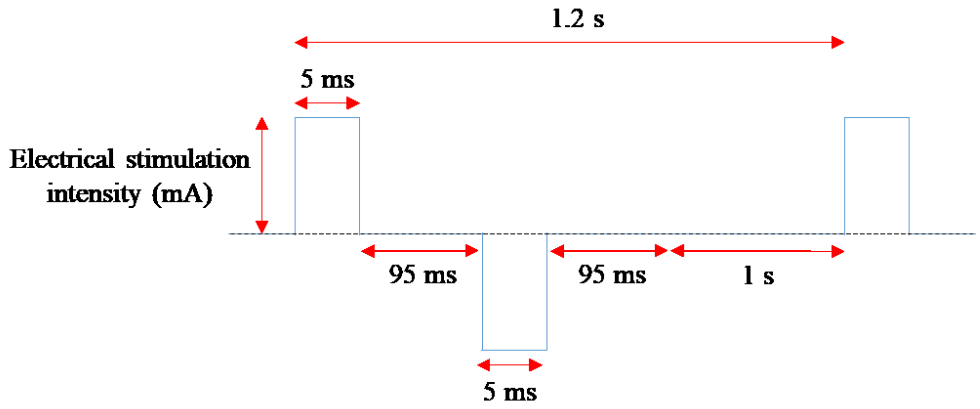

Figure 3.2 Stimulation waveform for the first experiment. 5 Hz Square waves with a pulse duration of 5 ms, inter-pulse interval of 95 ms, and inter-stimulus interval of 1 s. A stimulation period is 1.2 s.

3.2.2.2 Waveforms for classification of nociceptive fibers activations

To selectively stimulate nociceptive fibers, Aδ and C, three stimulation waveforms were implemented in the second and the third experiment (Chapter 5 and 6), as shown in Figure 3.3. Two waveforms of 1 Hz square waves and 5 Hz sine waves were targeting C-fibers, while another waveform of 250 Hz was targeting Aδ-fibers. 5 Hz and 250 Hz sine waves were referenced based on Neurometer [21] [22] to selectively activate C- and Aδ-fibers, respectively. However, due to the concomitant of Aδ-fibers activations that difficult to avoid, we gave waveform of 1 Hz square waves for high C-selectively over Aδ [70].

Painful stimuli were elicited by multifunction generator WF1974 (NF Techno Commerce, Yokohama, Japan). A custom adhesive pad (Omron Healthcare, Kyoto, Japan) of 4 cm^2 was used as an active electrode attached to the dorsal surface of the left hand, with a ground electrode of 25 cm^2 at 5 cm proximal to the active site. According to [70] (Figure 3.3a), three-pulse train bipolar square wave of 1 Hz with pulse duration 50 ms, inter-pulse interval 950 ms, polarity asymmetry ratio (the quotient of the amplitude of the cathodal stimulus and anodal stimulus) of 1:6, and a carrier frequency of 10 kHz were used for targeting higher C-selectivity over Aδ. Other waveforms according to [21] [22] to stimulate C-fibers (Figure 3.3b) and Aδ-fibers (Figure 3.3c) were sine waves with the frequency of 5 Hz and 250 Hz, respectively. The ISI of all three waveforms was 15 s. The first 1 s of EEG data was collected as a rest state and used as a baseline, followed by 40 stimuli.

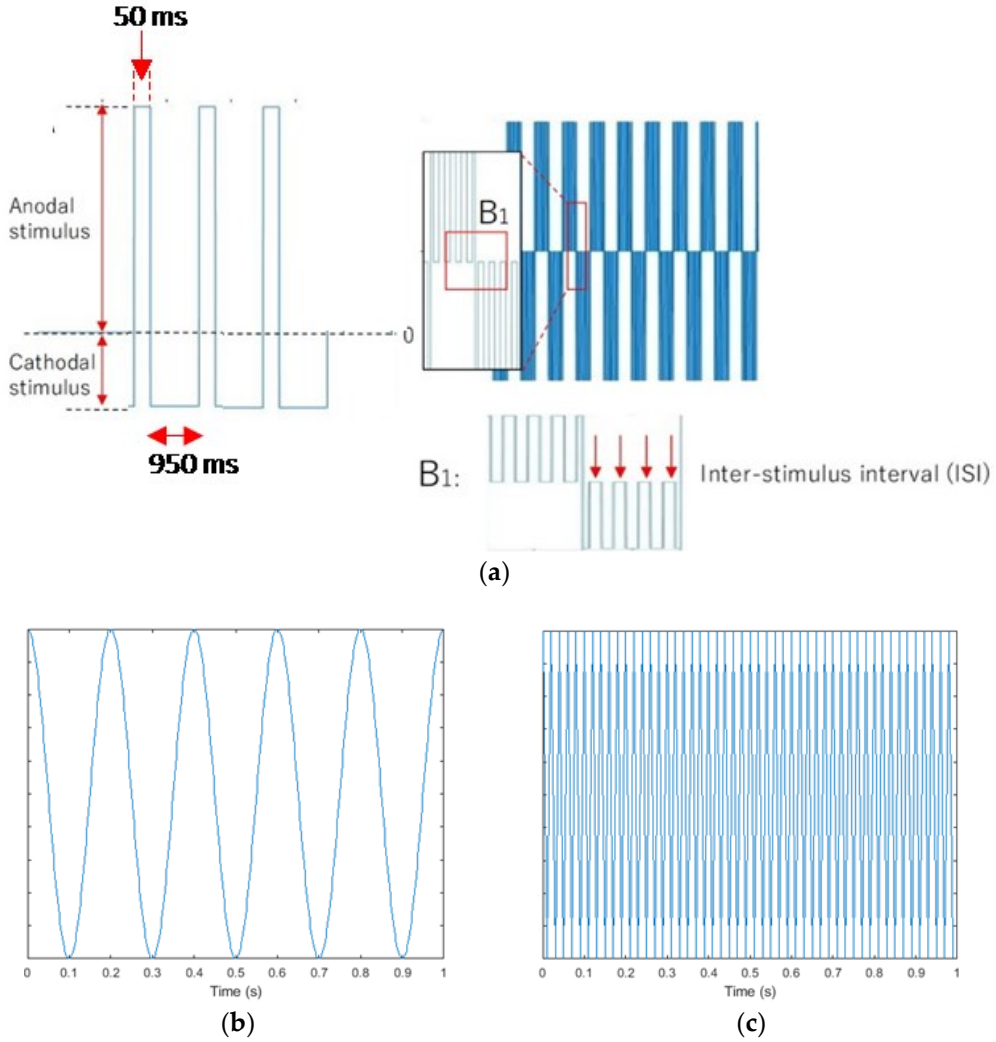

Figure 3.3 Stimulation waveforms for the second experiment. (a) Waveform for selectively stimulate C-fibers: 1 Hz bipolar square waves which each period contains a pulse duration of 50 ms, inter-pulse interval of 950 ms, a polarity asymmetry ratio (cathodal stimulus: anodal stimulus) of 1:6, the carrier frequency of 10 kHz, and ISI of 15 s (B1) [70]; (b) Waveform for selectively stimulate C-fibers: 5 Hz sine waves with a period of 200 ms and ISI 15 s; (c) Waveform for selectively stimulate Aδ-fibers: 250 Hz sine waves with a period of 4 ms and ISI 15 s.

3.2.3 Pain experiments

3.2.3.1 Electrical stimulus for classification of pain perception levels

Experiment subjects

Thirteen healthy subjects (8 males and 5 females, mean age 33.2 ± 7, range 20 – 52) participated in the experiment. No signs of neuropathy disease, impaired sensation, headache, and regular medication use were reported in all participants. All participants were informed that they could stop the experiment at any time.

Experiment setup

This experimental design was used in Chapter 4. Pain stimuli were generated by an electrical stimulator while recording EEG signals with 16 electrodes: Fp1, F3, T7, C3, P3, Pz, O1, Oz, O2, P4, C4, T8, F4, Fp2, Fz, and Cz that following the 10-20 system (see Chapter 3.2.1).

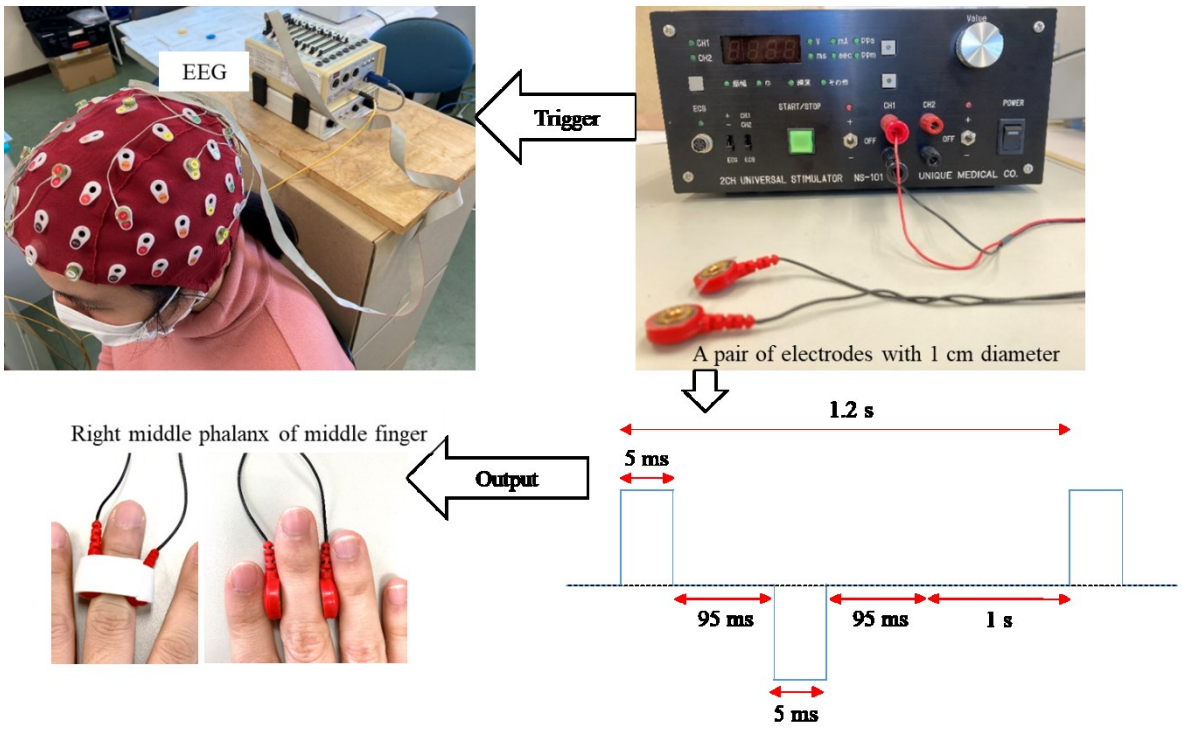

Figure 3.4 Experimental design of the first experiment. Pain stimuli were elicited by stimulator through electrode with 1 cm diameter at right middle phalanx of a middle finger while recording EEG through 16 electrodes.

We performed 50 stimuli per session and two sessions for each subject with a 5 s pause between the two sessions. Eventually, each subject received 100 trials, which lasted approximately 2 minutes in total, for each pain perception level. Here, four levels of pain perception were recorded as follows:

- Control (C): do not feel anything from the stimuli
- Sensation (S): feel something but not reach painful sensation
- Pain (P): feel pain
- Maximum pain (MP): feel maximum pain as tolerate

Before the experiment, all subjects received a test to determine their threshold for each pain perception level. The threshold for C was recorded with the minimum stimulation intensity that the subject could not perceive any sensation, which was set to 0.1 mA. For S, the minimum stimulation intensity induces non-painful sensation. The threshold of P was set to induce any minimal painful sensation, irritated feeling, or unpleasant feeling, and that of MP was set to the highest stimulation intensity, which let the subjects perceived the highest painful sensation as they could tolerate.

3.2.3.2 Electrical stimulus for classification of nociceptive fibers activations

Experiment subjects

An eEEG dataset of 14 healthy subjects (9 male, 5 female, mean age 28.07 ± 5.65) was used in the experiment. None of the subjects had any impaired sensations, neurological diseases, and cognitive impairments. All subjects participated voluntarily and gave informed consent without receiving any incentives. They were informed that they could stop the experiment at any time.

Experiment setup

This experimental design was used for the rest of the experiments in this project (Chapter 5 and 6). EEG (Biosemi ActiveTwo) with 32 active electrodes (see Chapter 3.2.1) was used to record eEEG at a sampling rate of 2048 Hz. The electrode placement sites of Fp1, AF3, F7, F3, FC1, FC5, T7, C3, CP1, CP5, P7, P3, Pz, PO3, O1, Oz, O2, PO4, P4, P8, CP6, CP2, C4, T8, FC6, FC2, F4, F8, AF4, Fp2, Fz, and Cz were chosen based on the 10-20 system. Subjects were asked to concentrate on the stimulation site and try to stay still. This study performed two levels of pain: mild (low) and maximum (high) pain. By rating the subjects' threshold with NRS, mild pain level referred to the scale ranges from 1-6, while maximum pain level was from scale ≥ 7.

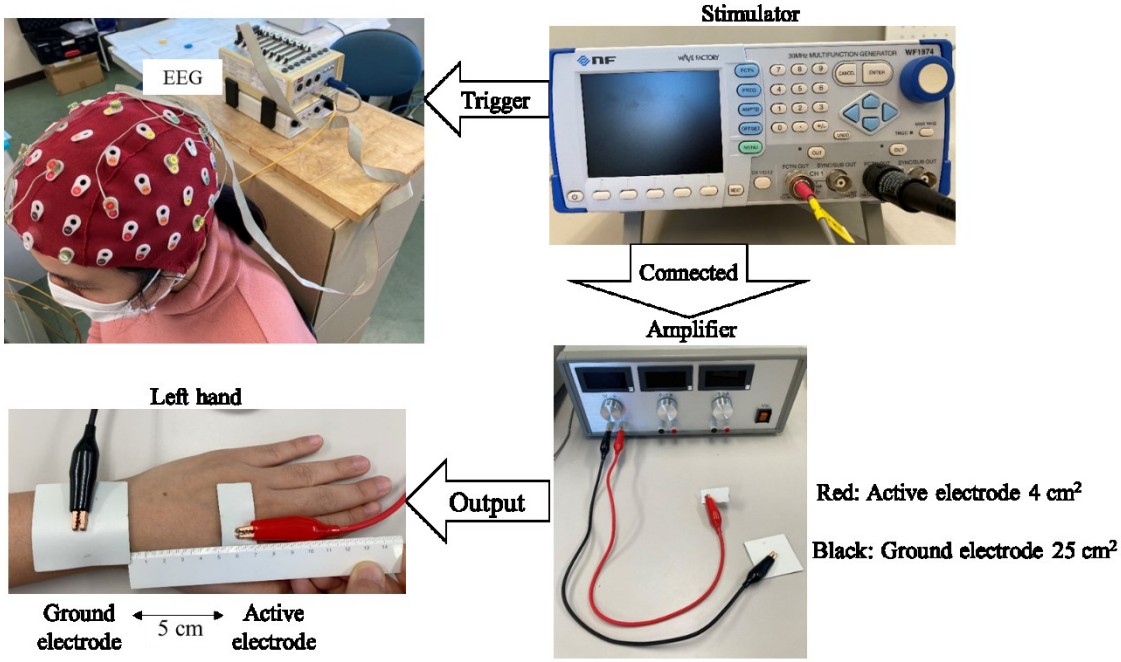

Figure 3.5 Experimental design of the second experiment. Three stimulation waveforms were elicited through an active electrode with 4 cm² with a ground electrode with 25 cm².

Pain stimuli were elicited through a 4 cm² active electrode, which was placed at the dorsal side of the left hand between second and third metacarpal bones, with a large ground electrode of 25 cm². Here, the NRS was used to rate the subjects' pain and identify each level of low (mild) and high (maximum) pain. The scale ranges from 1 to 6, which indicates mild to moderate pain, will be used as mild pain level, and a scale of ≥ 7 indicates severe pain will be

used as maximum pain level. All subjects were asked to receive a test to determine their individual painful and maximum painful threshold, which the latter was collected at the level that the subject could tolerate before the experiment.

Three stimulation waveforms of 1 Hz square waves, 5 Hz sine waves, and 250 Hz sine waves, were used to stimulate pain induced by nociceptive fibers activations. Since a new scheme of stimulation to selectively simulate C-fibers, which was 1 Hz square waves based on simulation in [70] is implemented the first time in vivo, the discrimination point to distinguish between each level of pain has not been deceived before. During the experiment, maximum stimulus intensity was set to 20 mA for safety. Nevertheless, within a range of 20 mA, it is difficult for the subject to interpret the threshold as a high pain level. Thus, the only low pain level was performed for the stimulation of 1 Hz square waves for targeting C-fibers, while mild pain and maximum pain levels were collected for stimulations of 250 and 5 Hz.

In summary, for each subject, five eEEG signal datasets were collected for analysis: 1 Hz (targeting C) at the mild pain level, 5 Hz (targeting C) at both the mild and maximum pain levels, and 250 Hz (targeting Aδ) at both the mild and maximum pain levels. Each dataset consisted of 1 s of resting-state signals for calibration and the remaining signals during pain stimulation (stimulation part contains 40 stimuli).

3.3 Conclusions

All pain experiments, including electrical pain stimulation and EEG recording, are provided in this chapter. In the following chapters, we present the investigations of features extracted by nonlinear analysis from pain-event related potential to classify multiple pain levels, while extracted by GC analysis from EEG to improve the classification of nociceptive fibers activations for both offline and future online.

Chapter 4

Fractal Dimension-Based Classification of Pain Perception Level

4.1 Introduction

For this first study, we focused on investigating EEG features for classifying multiple pain perception levels. The proposed features were compared with the other features in the literature to verify their effectiveness. This study was published in the open-access journal *Sensors,* under the Creative Commons Attribution license, on March 9th, 2020 [78].

4.1.1 Background and related research

Questionnaire-based methods have been known as a standard tool for pain measurement for decades. However, it is limited due to some factors, such as the bias from self-reporting and the inability of the people to feel or express the pain. Thus, objective pain assessment is necessary to implement in the clinical field even though it is challenging to deal with the individual difference in pain perception. The event-related potential is a technique that measures brain activity during task performance or response to the stimulus. Several studies on healthy subjects were used components of pain-event-related potential (pain-ERP) to estimate pain perception [29], i.e., time-frequency representation [37]. Besides pain-ERP analysis, there have been works reported on using EEG-based for classifying two pain levels (low pain and high pain) that elicited by different types of stimulation (see Table 1.1 for the details of existing pain classification studies)

Even though those studies could achieve a fair amount of accuracy for classifying two pain levels, none of them so far have achieved high classification accuracy from pain-ERP for multiple pain levels. A major obstacle for multiple pain levels classification might be the lack of feature extraction and feature selection investigation. The existing feature extraction methods that used EEG analysis are not enough to succeed in predicting multiple pain levels. Additionally, there is another challenge to deal with for evaluating pain-ERP: the nonlinear and complex nature of EEG. It is seen that nonlinear analysis is widely used to determine disorder symptoms like Alzheimer [79] and depression [80] by several nonlinear techniques such as Higuchi's fractal dimension (HFD), Hausdorff dimension, Grassberger-Procaccia correlation dimension (GP), Entropy, etc. Especially, HFD and GP examine the dimensional complexity of time series data [55], which would be helpful to estimate pain-ERP. Therefore, it is essential to find the feature that contains most pain information from nonlinear signals of ERP, while challenging on keeping the noise robustness.

4.1.2 Goals

In this study, we concentrated on exploring the effect of nonlinear feature extraction based on pain-ERP for predicting multiple pain perception levels. Our hypothesis was a feature based on the nonlinear analysis (fractal dimension, FD) that could take more information from pain-ERP responding to electrical stimulation. Firstly, the performances of features based on nonlinear analysis for binary and multiple pain perception levels classifications were demonstrated, together with the effect of using Fisher score as a channel selection. Then, using Fisher score again for selecting features and combined into groups to improve the classification performances. Finally, the possibility of online pain measurement by analyzing a few trials that could receive an accurate classification was investigated.

4.2 Results

4.2.1 Effect of feature selection on classification

We investigated the effects of channel selection by the comparison of classification between pain-ERP processed data with and without the selection, while the effects of feature selection were investigated following the results of the channel selection.

Table 4.1 The top five channels based on Fisher score.

Subject	1st channel	2nd channel	3rd channel	4th channel	5th channel
1	Fp1 (0.642)	Fp2 (0.354)	C3 (0.349)	P3 (0.238)	F3 (0.195)
2	Fz (0.237)	O1 (0.217)	Oz (0.157)	F4 (0.157)	Fp1 (0.142)
3	Fp1 (0.445)	C4 (0.097)	T7 (0.082)	P4 (0.075)	C3 (0.056)
4	Fp1 (0.063)	Fz (0.036)	Fp2 (0.032)	P4 (0.022)	P3 (0.018)
5	Oz (0.546)	P3 (0.311)	Fz (0.288)	Fp2 (0.132)	C3 (0.115)
6	F4 (0.272)	O2 (0.179)	Fz (0.132)	O2 (0.122)	F3 (0.072)
7	O1 (0.429)	O2 (0.301)	Oz (0.249)	C3 (0.180)	F3 (0.142)
8	F4 (0.348)	Pz (0.319)	Oz (0.262)	O2 (0.251)	Fp2 (0.246)
9	Oz (0.517)	Fz (0.424)	O2 (0.366)	F3 (0.244)	O1 (0.242)
10	Oz (0.281)	Pz (0.217)	F3 (0.208)	O1 (0.176)	O2 (0.174)
11	F3 (0.435)	O2 (0.303)	Oz (0.303)	Fz (0.252)	Fp1 (0.219)
12	Fz (0.215)	F4 (0.213)	F3 (0.174)	C4 (0.142)	O1 (0.140)
13	F3 (1.349)	O2 (0.868)	Oz (0.755)	FO1(0.499)	Fz (0.472)

Fisher was used to select the top five channels, as shown in Table 4.1, and then used these chosen channels for further feature extraction. Since each feature was derived from calculating each channel (as mentioned in Chapter 2.2.3), we received five feature values for Fisher score-based channel selection, while the case without Fisher score-based channel selection had sixteen feature values.

All the classification accuracies of data with and without Fisher score-based channel selection were compared in Table 4.2. The accuracy results of binary and multiple-level classification with the features extracted from the selected channels are listed in the upper part of Table 4.2, while those of the features extracted from all channels are listed in the lower section of Table 4.2. It is seen that most of the results from features without channel selection showed better accuracy than those features with channel selection.

Table 4.2 Classification accuracy (%) of features from the whole trial. The highest accuracy is shown in bold.

Feature	4 Level	3 Level	C vs. MP	C vs. P	P vs. MP	S vs. C	S vs. P	S vs. MP	Average of 2-level
With Fisher score-based channel selection									
HFD	37.5	50.0	75.0	50.0	50.0	50.0	25.0	50.0	50.0
HFD_ACF	12.5	33.3	50.0	25.0	50.0	25.0	50.0	25.0	37.5
HFD_VAR	50.0	75.0	**100**	50.0	75.0	75.0	50.0	50.0	66.7
GP	25.0	33.3	50.0	50.0	50.0	50.0	75.0	50.0	54.2
GP_ACF	25.0	33.3	50.0	75.0	50.0	50.0	50.0	50.0	54.2
GP_VAR	50.0	83.3	75.0	**100**	75.0	75.0	75.0	75.0	79.2
Without Fisher score-based channel selection									
HFD	37.5	50.0	75.0	75.0	50.0	75.0	50.0	50.0	62.5
HFD_ACF	37.5	66.7	50.0	50.0	75.0	50.0	25.0	50.0	50.0
HFD_VAR	62.5	83.3	**100**	75.0	**100**	75.0	25.0	50.0	70.8
GP	25.0	33.3	50.0	50.0	50.0	25.0	25.0	50.0	41.7
GP_ACF	25.0	33.3	50.0	50.0	75.0	50.0	50.0	25.0	50.0
GP_VAR	75.0	**100**	**100**	**100**	**100**	75.0	75.0	75.0	87.5

Among all the performances, the further feature extraction by the VAR approach, GP_VAR, and HFD_VAR, produced good outcomes in this study. GP_VAR achieved the best performances for two-level classification with mean accuracies of 87.5% (without channel selection), 79.2% (with channel selection), and reached an excellent performance of 100% for the three-level classification without channel selection. Meanwhile, HFD_VAR achieved accuracies of 70.8% and 66.7% for two-level classification, 83.3% and 75% for three-level classification without channel selection and with channel selection, respectively. However, none of the features were achieved good accuracy for four-level classification, as shown in the two-level and three-level classifications. For four-level classification, the best accuracy was just a fair amount of 75.0% and the lowest accuracy was 12.5%.

Furthermore, the Wilcoxon rank sum test was used to investigate the significant difference between the accuracies of data processed with and without Fisher score-based channel selection in each type of classification. For four-level, three-level, and two-level classification, the Wilcoxon rank sum test values were 0.49, 0.25, and 0.91, respectively, which demonstrated that there were all insignificant differences between features with and without Fisher score-based channel selection.

4.2.2 Comparison of classification results between with and without using feature selection

Fisher score-based feature selection was applied to the feature extraction methods: statistical [61] and FD-based, to investigate the practicability of combined features. Three features from both feature extraction approaches corresponding to the highest and lowest Fisher scores are shown in Table 4.3. Notably, FD-based features had a higher Fisher score than those statistical-based features for both best and worst ranks. The results showed that GP, HFD_VAR, and GP_VAR were the best three features.

Table 4.3 The highest three and the lowest three features based on Fisher score.

Best three feature		**Worst three feature**	
Statistical feature	**FD-based feature**	**Statistical feature**	**FD-based feature**
Min (1.535)	GP (2.438)	SD (0.093)	HFD (0.139)
Max (1.033)	HFD_VAR (1.278)	Skewness (0.095)	HFD_ACF (0.168)
Variance (0.418)	GP_VAR (1.044)	Mean (0.097)	GP_ACF (0.167)

Mixing FD-based features with statistical features randomly was done to observe how statistical features affect accuracy, as shown in Table 4.4. For accuracy derived from features based on high Fisher score in four-level classification, the mixing features group (GP, HFD_VAR, Min) had a better performance of 50.0% than 37.5% of statistical features but still lower than 87.5% of FD-based features. Meanwhile, three-level classification accuracy based on low Fisher score showed that the mixing features group (HFD, HFD_ACF, SD) had the worst accuracy of 25.0% than both statistical and FD-based features. A group of random mixing features obtained the same accuracy as the statistical features group for high and low Fisher scores for three-level classification.

Table 4.4 Comparison of classification accuracy (%) between combined statistical features and FD-based combined features selected by the Fisher score. The highest accuracy is shown in bold.

Feature		**4-Level**	**3-Level**
Statistical feature	Low Fisher score (Skewness,Mean,SD) [1]	37.5	50.0
	High Fisher score (Min,Max,Variance) [2]	37.5	66.7
FD-based feature	Low Fisher score (HFD,HFD_ACF,GP_ACF)	37.5	66.7
	High Fisher score (GP,HFD_VAR,GP_VAR)	**87.5**	**100**
Mixing feature	Low Fisher score (HFD,HFD_ACF,SD)	25.0	50.0
	High Fisher score (GP,HFD_VAR,Min)	50.0	66.7

[1] Fisher scores of Skewness, Mean, and SD are 0.120, 0.121, and 0.123, respectively; [2] Fisher scores of Min, Max, and Variance are 1.008, 0.751, and 0.192, respectively.

Then, features from each feature extraction method were combined to form a group based on Fisher score for multiple-level classification improvement, as shown in Table 4.5. A group of variance-based features showed the best accuracies of 87.5% and 100% for four-level and three-level classifications, respectively. All the FD-based features groups could achieve better results than the statistical features group, except for the correlation-based features. Here, we

used the Wilcoxon rank sum test to calculate the statistical difference between the statistical features and FD-based features at a p-value < 0.05. To compare with the statistical features group, a significant difference with p-value < 0.0001 was found only for the variance-based group, while the p-value of the others were 0.36, 0.31, and 1.92 for correlation-based, HFD-based, and GP-based, respectively. The results from both Table 4.4 and Table 4.5 revealed that FD-based features achieved better accuracy than statistical-based features.

Table 4.5 Comparison of classification accuracy (%) between combined statistical features and FD-based combined features manually grouped. The highest accuracy is shown in bold.

	Feature	4-Level	3-Level
Statistical feature	Min, Max, Mean, SD, Variance, Skewness	37.5	66.7
FD-based feature	Correlation-based (HFD, HFD_ACF, GP_ACF)	37.5	50.0
	Variance-based (GP, HFD_VAR, GP_VAR)	**87.5**	**100**
	HFD-based (HFD, HFD_ACF, HFD_VAR)	75.0	83.3
	GP-based (GP, GP_ACF, GP_VAR)	50.0	66.7

Furthermore, the results of the classification model with k-fold cross-validation (k = 5) are shown in Figure 4.1. The best accuracies of 94.4% and 100% were obtained for four-level and three-level classifications, respectively, from the variance-based group. In contrast, the worst accuracy was from the correlation-based group, which showed 29.3% and 41.1% for four-level and three-level classifications.

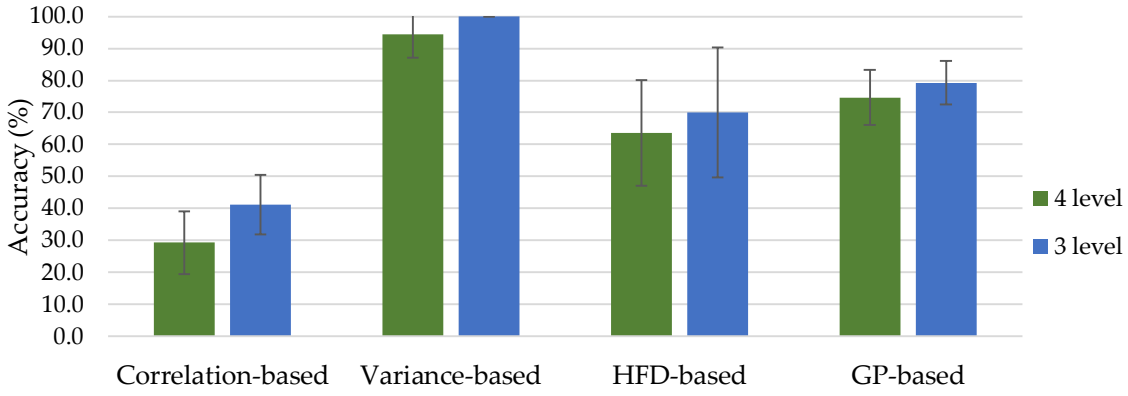

Figure 4.1 5-fold cross-validation accuracy (%) based on different combined features. The error bars are the standard error with regard to the mean.

4.2.3 Combined features based on n-trial averaging

We split data into several numbers of trials: whole trial, 50 trials, 20 trials, 15 trials, 10 trials, and 5 trials to test the possibility of a fast pain perception level evaluation (Figure 4.2 and Figure 4.3). Besides taking the whole trial into account, 50-trial data averaging showed classification rates comparable to those of whole-trial data averaging, as shown in Figure 4.2. Notably, the variance-based group achieved similar classification rates for both four-level and three-level classifications. Nevertheless, this study revealed that using data with a small number of trials causes a decrease in classification accuracy. In addition, all of the four-level classification accuracies had worse performances than three-level classification. Among the three-level accuracies of using fewer trials averaging (5-trial, 10-trial, and 15-trial), none of them reached an acceptable accuracy of 80%. Meanwhile, the only variance-based group from averaging of 50-trial and whole-trial could get the same fair performance rate for four-level classification. Consequently, classifying pain perception levels with the data averaging from the number of trials less than 20 is impossible even with the best combined features group of GP, HFD_VAR, GP_VAR.

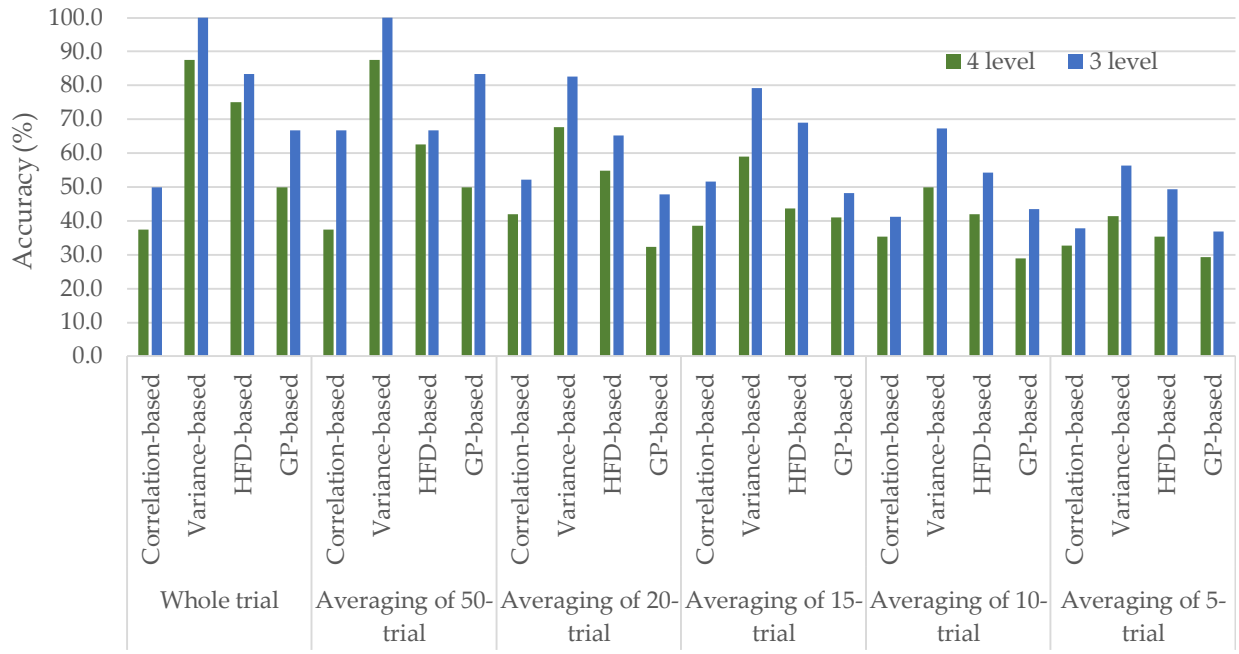

Figure 4.2 Classification accuracy (%) of n-trial averaging with different feature groups.

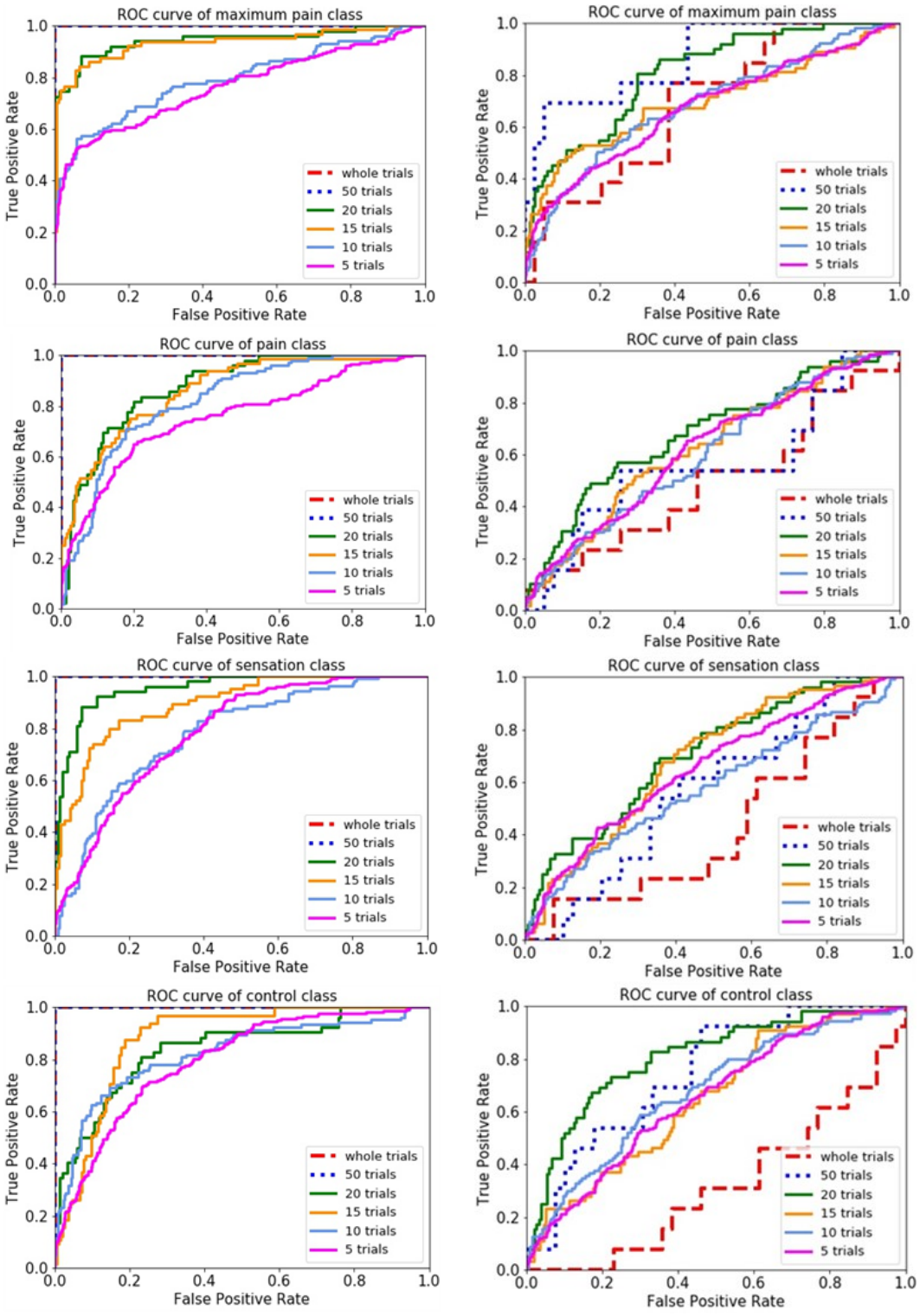

Figure 4.3 ROC curves of different n-trial averaging for each class in four-level classification with the best and worst combined features. (a) Variance-based group (the best combined features); (b) Correlation-based group (the worst combined features).

4.3 Discussion

Our main goal was to evaluate the capability of features extracted by the nonlinear approach from pain-ERP in predicting pain perception levels. The best feature that achieved a good classification accuracy is to indicate how much the pain information is contained. Thus, GP and HFD were used to estimate the complexity of EEG, which relevant to the different brain's state [55], while applying ACF and VAR for improving the SNR with the sliding window technique.

4.3.1 Distribution of the pain information over EEG channels

In this study, Fisher score was used to select the most discriminative channels for investigating the distribution of the pain information over the EEG channels. In Table 4.2, the results showed that the classification without channel selection performs better performance than classifying with channel selection. Even though two features from using five selected channels based on the Fisher score, HFD_VAR and GP_VAR, could achieve the highest accuracy of 100% for two-level classification cases of C vs. MP and C vs. P, respectively, the rest of the results still showed lower performances than those without channel selection. One possible reason is might because pain-related information has a broader distribution than expected, even Fisher score has chosen a subset of channels that contains a higher density of pain-related information, but the other channels also have their contribution too.

4.3.2 Role of fractal dimension-based feature for binary classification

4.3.2.1 Higuchi's fractal dimension vs. Grassberger-Procaccia correlation dimension

All average accuracies of GP-based features (GP, GP_ACF, GP_VAR) and HFD-based features (HFD, HFD_ACF, HFD_VAR) are shown in Table 4.6 to demonstrate the comparisons between nonlinear methods of GP and HFD.

Table 4.6 Comparison of averaging classification accuracy (%) between GP-related and HFD-related features. SD is shown in parenthesis.

Feature	With channel selection			Without channel selection		
	4-Level	3-Level	2-Level	4-Level	3-Level	2-Level
GP-based	33.3 (11.8)	50.0 (23.6)	62.5 (15.0)	41.7 (23.6)	55.5 (31.4)	59.7 (23.8)
HFD-based	33.3 (15.6)	52.8 (17.1)	51.4 (19.5)	45.8 (11.8)	66.7 (13.6)	61.1 (20.8)

These two nonlinear approaches calculate the changes at boundaries of fragmentation of time-series by different algorithms. GP estimates the fractal dimension of its reconstructed phase space [57] [58], while HFD calculates the self-similarity of a time series without phase space reconstruction [54]. Therefore, the outcomes of these two methods are different in this study. Using HFD, we can compute the value in a short time due to the small number of points required for its calculation. However, more noise-sensitive than GP, which generally requires a large number of points to calculate in high-dimension chaos [81].

4.3.2.2 Auto correlation function vs. moving average

Here, we compared the average accuracies of extension of feature extraction methods, VAR-related features (HFD_VAR and GP_VAR) and ACF-related features (HFD_ACF and GP_ACF) for different types of classification in Table 4.7.

The results showed that the average accuracies of features that applying VAR were improved for all binary and multiple-level classifications, while the performances of using ACF did not lead to any improvement. Both VAR and ACF were applied to the FD features for spatial filtering purposes, which were calculated along the channels in this study. To compare these methods, VAR succeeded in improving FD features by evaluating over the trend-cycle, which is similar to detrend function that removes a distortion or a cumulative error from all EEG channels, while ACF failed to do that due to its sensitivity to the variability of EEG over channels [59].

Table 4.7 Comparison of average classification accuracy (%) between VAR-related and ACF-related features. SD is shown in parenthesis.

Features	With Channel Selection			Without Channel Selection		
	4-Level	3-Level	2-Level	4-Level	3-Level	2-Level
VAR-related	50.0 (0)	79.2 (4.2)	72.9 (16.0)	68.8 (6.3)	91.7 (8.4)	79.2 (22.4)
ACF-related	18.8 (6.25)	33.3 (0)	45.8 (13.8)	31.3 (6.3)	50.0 (16.7)	50.0 (14.4)

Nevertheless, nonlinear features resulted in characterizing the different brain states of EEG. Due to the long-range correlation properties of biological signals, i.e., EEG [82], GP and the auxiliary post-processing by VAR (calculates based on the scaling properties) could increase prognostic utility more than the statistical features that lie in the data distribution.

4.3.3 Feature grouping for multiple-level classification

4.3.3.1 Fractal dimension-based features vs. statistical features

In Table 4.3, we can see that GP achieves the highest separability from Fisher score for pain-ERP (2.438), while HFD gets the lowest score (0.139), which even worse than the statistical features (1.535, 1.033, and 0.418 of Min, Variance, and Max, respectively). Due to the feature extracted by statistical methods that depend on the randomness of the data frequently used for qualitative and quantitative analysis for stationary and linear datasets, the statistical features could take a fundamental property of bio-signal [61]. As shown in the Fisher score result of Min that had a higher score than most of the FD-based features (except for GP with a score of 2.438) but could not get a good performance when grouped with other statistical features. For four-level classification, combined Min with the best two FD-based features based on Fisher score resulted in an accuracy reduction of 87.5% (FD-based group) to 50% (mixing group). This indicates the disadvantage of statistical features that take a few characteristics of signals' details into account. Consequently, the FD-based feature group can catch the information and perform classifying pain perception levels from pain-ERP than the statistical ones.

4.3.3.2 Feature grouping based on feature selection

In Table 4.4, the FD-based features (GP, HFD_VAR, GP_VAR) achieved higher accuracy than the statistical features and the mixing features (GP, HFD_VAR, Min), which consisted of the three features based on the highest Fisher score from both FD-based and statistical features. Notably, the Fisher score of Min (1.535) was higher than that of GP_VAR (1.044). This might be from the sensitivity to outliers of the statistical methods. Although combined Min with the other two statistical features or FD-based features based on the highest Fisher score, it could not obtain higher accuracy than the FD-based group.

In Figure 4.4, we can see that GP has a better diagnostic ability than HFD_VAR and Min but has a similar tendency to GP_VAR (75% accuracy), even with the low accuracy of 25% itself. This means GP can correctly predict most of the pain class out of all classes, as shown in Figure 4.4a. Meanwhile, as shown in Figure 4.4b, GP has the proportion of true negative predictions much more than true positive predictions; this is because accuracy is the ratio of correctly classified to all predictions that include true positives and true negatives. Besides, GP_VAR shows high values of both probability and accuracy; on the contrary, Min shows the lowest values. The results of Figure 4.4, which shows how FD-based feature and statistical feature with high Fisher score is complementary to each other, explain why GP_VAR is more compatible with the GP and HFD_VAR than Min.

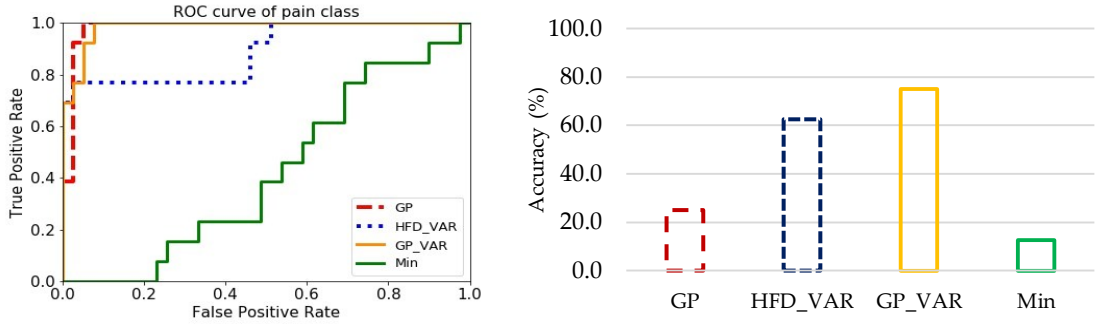

(**a**) (**b**)

Figure 4.4 Comparison between the features of two feature groups: Variance-based (GP, HFD_VAR, GP_VAR), and Fisher score-based (GP, HFD_VAR, Min) for four-level classification: (a) ROC curves of each FD-based feature and Min for pain perception levels; (b) Classification accuracy of each FD-based (corresponding to results without Fisher score-based channel selection from Table 4.2) and Min.

Moreover, we found that VAR helps classify pain information because both HFD_VAR and GP_VAR could obtain a high Fisher score (Table 4.4). Although GP_VAR had the lowest Fisher score among the best three features group (Table 4.3), it performed the highest accuracies of 100% for most of the two-level and three-level classifications (Table 4.2). Due to the ratio of the variability of between-group to that of within-group, a higher Fisher score implies that a feature is more discriminative; however, it does not reveal mutual information, which measures the dependency between multiple features. Even though the Fisher score of GP_VAR is lower than that of GP, when these two features are combined for classification, they can contribute to differentiate perception levels that are difficult for mixing feature groups.

Compared with the results of no cross-validation (Table 4.5), the variance-based group analyzed with 5-fold cross-validation (Figure 4.1) could improve accuracy by 6.9% for four-

level classification. On the other hand, the correlation-based group obtained worse performances by 8.2% and 8.9% for four-level and three-level classifications. Therefore, forming a combination of features that are based on GP and VAR from the variance-based group can characterize the complexity of the pain-ERP by calculating more pairs of points, which shows more robustness than other combination groups. Eventually, our findings suggest that FD features based on higher Fisher scores are related to pain information more than those with a lower Fisher score.

4.3.4 Possibility of online analysis

A short duration of collecting data is necessary for online analysis in future work. There have been reported using about 150-500 data points, which is a reliable data length for calculation in real-time [55]. Since we had 435 data points in this study, our data were enough to test the feasibility of online pain classification with nonlinear features. Figure 4.2 and Figure 4.3 show that the averaging of the whole trial (maximum number of trials was 98) and 50-trial can maintain the classification performances. Even though classifying with FD-based features group can differentiate between pain perception levels, when the number of collected trials for averaging further decreases, the classification performances continue to decline. This would mean that despite the data length, the trial numbers should also be considered. Our findings showed that at least 20-trial, which corresponds to 24 s (1.2 s per trial) is necessary for the current features and classifications to obtain the accuracies of 67.7% and 82.6% for four-level and three-level classifications from EEG.

However, the possibility of online classification was analyzed from the data collection viewpoint, i.e., the number of EEG trials required for getting certain accuracy, while the pre-processing steps were done in an offline manner due to their long computation time. Therefore, objective pain assessment in real-time is preferable, in which online pain classification might take a role in clinical practice.

4.3.5 Contributions and limitations of the study

The features based on nonlinear analysis extracted from pain-ERP for classifying pain perception levels were proposed in this study. Throughout the analysis, the use of FD-based features demonstrated improved classification performances compared with the other features (statistical features). Besides, the possibility of analysis pain-ERP in real-time was investigated through the features based on n-trial averaging.

However, collecting a sufficient number of samples and trials is necessary for validating and generalizing the pain classification method. Still, more trials lead to longer experiment times that might cause both uncomfortable and habituated pain perception. For further investigation, the neurologic pain disease people should be included in the subjects for validation.

4.4 Conclusions

This study aimed to demonstrate that classifying pain perception levels by the FD-based feature of pain-ERP. We were expecting that the effectiveness of nonlinear features would improve the classification performances. Firstly, we presented the accuracy derived from using a single FD-based feature for classification with and without channel selection. Second, we investigated the effect of the Fisher score on feature selection to form a group of combined features to improve the multi-class classification. Combined features were examined on both FD-based and statistical features. Finally, averaging n-trial to evaluate the possibility of online analysis.

The results showed that GP with VAR is the best feature for two-level classification and achieves the highest accuracy for three-level classification. Additionally, we infer that applying channel selection does not show a significant difference in accuracy from without channel selection. Based on our results without channel selection, a variance-based group achieves the best accuracies of 87.5% and 100% for four-level and three-level classifications, respectively, which is also better than combined statistical features. Furthermore, averaging the n-trial showed that more EEG trials have better classification performance due to more data points to calculate.

Although pain level is a significant problem for pain treatment, pain induced by different pain-conducting nerve fibers is another problem we should consider due to each nerve activation that causes different pain states. Thus, we provide the effectiveness of other feature extraction methods for classifying pain corresponding to nociceptive Aδ- and C-fibers activation in the next chapter.

Chapter 5

Granger Causality-Based Pain Classification Using EEG Evoked by Electrical Stimulation Targeting Nociceptive Aδ- and C-fibers

5.1 Introduction

For this second study, we aimed to use connectivity of EEG as features for classification of nociceptive fibers activations. We analyzed connectivity among channel areas and independent components of each frequency band to classify pain induced by three different stimulation waveforms, of which two waveforms were selectively stimulate C-fibers and one waveform was stimulate Aδ-fibers. We also computed connectivity between stimulation waveforms to classify two pain perception levels. Moreover, we performed the significance test to compare between connectivity at different pain levels (mild pain vs. maximum pain) and stimulation waveforms (5 Hz targeting C vs. 250 Hz targeting Aδ). This study was published in the open-access journal *IEEE Access*, under the Creative Commons Attribution-NonCommercial-NoDerivatives license, on January 8th, 2021 [83].

5.1.1 Background and related research

Pain is associated with the activation of nociceptive fibers, myelinated Aδ and non-myelinated C induced by noxious stimuli. These nociceptive fibers activations are important to the first pain and the second pain carried by Aδ- and C-fibers, respectively, which is a particularly challenging issue in pain relief. Due to the outlasting effect difference of nociceptive fibers activations, Aδ-fibers likely explain acute pain, while C-fibers refer to chronic pain. In the Neurometer (Neurotron, Baltimore, MD, USA) [22], sine waves with the frequencies of 250 Hz and 5 Hz are used to stimulate Aδ- and C-fibers, respectively, for measuring their current perception threshold (CPT). Additionally, new stimulation schemes have been explored in simulation studies [70] [73] [74]. However, there is still a lack of evaluation of the effect of selective electrical stimulation, especially for C-fibers stimulation. Therefore, developing an effective objective system for pain assessment is necessary to achieve better pain management.

The classification of stimulation-responding physiological and bio-signals is used to explore the multiple combinatory features without prior knowledge of the information processing of the brain and nerve system. Then, the features of the pain could be identified by looking back at the features resulting in better classification. Many EEG studies used evoked electroencephalography (eEEG) for the classification of pain. For example, previous works explored the stochastic features of pain-related signals by using temporal-spatial patterns [35] [37] and nonlinear features [78] for classifying pain perception levels. Furthermore, differentiating between nociceptive fibers activations, Aδ- and C-fibers, has remained unsolved. Due to the fact that the small amplitude of C evoked-potential that is overwhelmed

by Aδ activation in most cases of various pain intensities [13], it causes difficulty in finding features that could capture the difference between the Aδ- and C-responses.

Even though the existing EEG-based feature extraction approaches have succeeded in determining brain markers of pain occurring, only the temporal-spectral were assessed, not the spatial pattern of pain responses. Due to the complexity of pain mechanisms, pain cannot be revealed through only analyzing a single region or single domain of pain-related bio-signals such as electric-evoked potentials in this study. It is important to investigate multiple regions containing different functional neural systems and interactions between them in a different domain to understand pain perception. Thus, the connectivity analysis is possible to play an important role in C-response identification. Here, Granger causality (GC) [46] was used to classify Aδ and C activities and identify important property features. GC is a method to investigate causality between variables in a time series by testing the variance of one signal to predict variance in another signal. If there is GC between variables (nodes or signals), it can be said that one node contains information about the future of another node. GC was used as a feature to classify human actions [84] and differentiate awake from anesthetized state [85]. Besides the classification, GC was also applied to reveal connectivity patterns such as distinction in motor and perceptual visuo-spatial working memory [86] and analysis of anesthesia [87]. In the pain-related study [88], the results of GC analysis showed the flow between these pain regions: primary somatosensory cortex (S1), secondary somatosensory cortex (S2), and anterior cingulate cortex (ACC). It was reported that pain-related information did not carry through S1 to S2 during pain but conveyed independently. Furthermore, [45] demonstrated the connectivity between cortical areas was marked by changes in the alpha band. Still, those studies were analyzed GC between the brain regions that already reported related to pain processing. However, none of the studies used GC to either classify pain response to Aδ and C or identify these nociceptor-related brain networks. Therefore, the GC-based classification would benefit the understanding of nociceptive fibers induced pain by looking back at the features containing the important causality connection.

5.1.2 Goals

Compared with our previous approach dealing with the nonlinear dynamical aspects of EEG [78], the current approach focused on the interaction patterns in the brain. In this study, the investigation of causal connectivity in the pain system was proposed using GC as features for the classification of pain eEEG responsive to nociceptive fibers (Aδ- and C-fibers) and corresponded to pain intensity. The proposed pipeline is displayed in Figure 5.1. The purpose of investigating the causal connectivity that enables two types of classification were defined as follows:

1) The classification of three painful stimulation waveforms that is resulting in acute (Aδ-response) and chronic pain (C-response): 1 Hz square waves and 5 Hz sine waves both targeting C-fibers, and 250 Hz sine wave targeting Aδ-fibers, which were analyzed based on: a) channel areas (central, frontal, occipital, left temporal, and right temporal) as GC_ChA features (see Chapter 2.3.2.1); b) EEG components (i.e., ICs) at different frequency bands as GC_CoF features (see Chapter 2.3.2.2).
2) The classification of mild pain (low pain) and maximum pain (high pain) by EEG components (i.e., ICs) from different waveforms as GC_CoW features (see Chapter 2.3.2.3).

Moreover, GC relationships resulted in significant differences among different waveforms, and different pain perception levels were analyzed to obtain findings of nociceptive fibers activations related to brain activity.

Our hypotheses were made based on the findings in the literature.

1) According to the location of the central area that is close to the S1, the causal flow involved with the central area would be a good predictor for differentiating pain from Aδ-fibers and C-fibers activations.
2) Due to a lack of findings that reported the association between lower frequencies and pain, GC relationships from lower frequencies would be worse than those higher frequencies.
3) Due to the concomitant stimulation of Aδ- and C-fibers, GC relationships from 250 Hz (targeting Aδ) to 5 Hz (targeting C) would be related to low pain intensities (mild pain level in this study) more than high pain intensities (maximum pain level in this study).

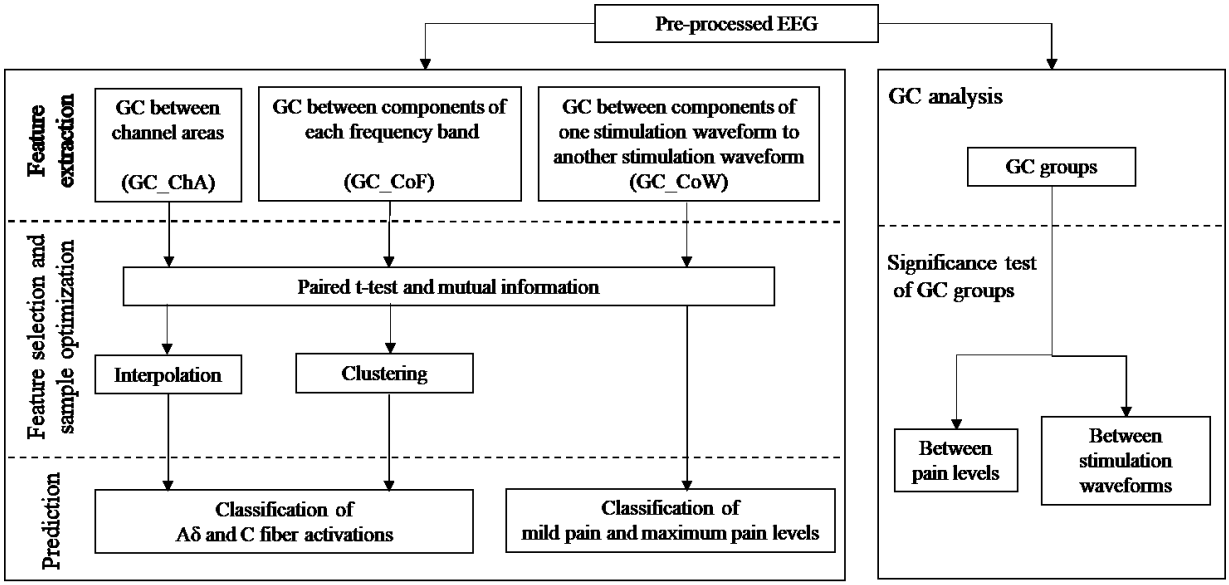

Figure 5.1 Overview of the proposed pipeline. (Left) The flow of pain classification; (Right) The flow of GC differences analyses among stimulation waveforms and pain levels.

5.2 Results

5.2.1 Comparison between GC groups as features

Classification results of 30 GC features are presented in Table 5.1. The number of samples was varied after interpolation and clustering, as mentioned in Chapter 2.3.3. As shown in Table 5.1, the classification results after clustering are presented in two different ways, discarded samples as data of a reject class and discarded samples as misclassification, as a worst-case scenario that might happen even with the clustering process. Here the worst-case scenario means that the outlier samples in the test trial or real-time implementation in the near future may be completely different from those that appeared in the training dataset. Although the MCC and average accuracy derived for the two ways were different, they still showed a similar tendency.

Table 5.1 Classification results: MCC and average accuracy (SD is shown in parenthesis) resulted from selected GC relationships from the GC group as features. For each GC group, the best accuracy is shown in bold.

GC category	GC group	Sample number [1]	MCC	Average accuracy (%)
GC_ChA	$GC_{central \rightarrow frontal}$	195	0.18	64.20 (8.63)
	$GC_{central \rightarrow occipital}$	195	0.21	72.25 (6.07)
	$GC_{central \rightarrow Lt}$	195	0.37	**82.99 (7.71)**
	$GC_{central \rightarrow Rt}$	195	0.14	67.35 (8.69)
	$GC_{frontal \rightarrow occipital}$	195	0.26	67.10 (11.90)
	$GC_{frontal \rightarrow Lt}$	195	0.30	69.74 (11.80)
	$GC_{frontal \rightarrow Rt}$	195	0.28	71.88 (9.72)
	$GC_{occipital \rightarrow Lt}$	195	0.33	71.47 (10.61)
	$GC_{occipital \rightarrow Rt}$	195	0.22	66.65 (8.96)
	$GC_{Lt \rightarrow Rt}$	195	0.31	69.08 (10.24)
	$GC_{frontal \rightarrow central}$	195	0.29	72.63 (12.52)
	$GC_{occipital \rightarrow central}$	195	0.49	80.79 (8.97)
	$GC_{Lt \rightarrow central}$	195	0.20	68.19 (7.54)
	$GC_{Rt \rightarrow central}$	195	0.24	60.57 (9.63)
	$GC_{occipital \rightarrow frontal}$	195	0.12	71.81 (9.12)
	$GC_{Lt \rightarrow frontal}$	195	0.24	69.09 (10.12)
	$GC_{Rt \rightarrow frontal}$	195	0.09	58.93 (11.76)
	$GC_{Lt \rightarrow occipital}$	195	0.27	75.55 (6.15)
	$GC_{Rt \rightarrow occipital}$	195	0.51	79.49 (7.51)
	$GC_{Rt \rightarrow Lt}$	195	0.41	65.46 (10.02)
GC_CoF	$GC_{delta,}$	23892	0.92 / 0.76*	94.99 (2.28) / 89.75 (4.75)*
	GC_{theta}	23731	0.80 / 0.77*	88.58 (2.84) / 88.13 (4.38)*
	GC_{alpha}	24439	1.00 / 0.83*	**99.71 (0.59) /** 98.98 (0.73)*
	GC_{beta}	23703	0.93 / 0.81*	97.20 (3.65) / 98.50 (0.25)*
	GC_{gamma}	24440	0.96 / 0.83*	98.66 (1.95) / 99.13 (0.13)*
GC_CoW	$GC_{5Hz \rightarrow 250Hz}$	914	0.03	**99.35 (1.21)**
	$GC_{250Hz \rightarrow 5Hz}$	914	0.32	69.93 (9.76)

[1] Sample number after optimization, * Classification results of the data after clustering which using the discarded samples as misclassification class.

In Table 5.1, the GC_CoF achieved the best classification for the three different stimulation waveforms (1 Hz and 5 Hz stimulations for C and 250 Hz stimulation for Aδ) among all GC categories, with MCC values of all GC groups ranging from 0.8 to 1. In contrast, most GC groups in the GC_ChA and the GC_CoW had MCC values lower than 0.4, except for $GC_{occipital \rightarrow central}$, $GC_{Rt \rightarrow occipital}$, and $GC_{Rt \rightarrow Lt}$ (0.492, 0.512, and 0.415, respectively). In the GC_CoW, $GC_{5Hz \rightarrow 250Hz}$ achieved the second-highest accuracy of 99.35% of all results but received the lowest MCC of 0.033. This might be due to the imbalanced samples of mild pain and maximum pain caused by the varying number of EEG independent components (ICs) in each dataset that had an effect on the accuracy but not on the MCC.

For average accuracy results, GC_{alpha} from the GC_CoF achieved the best accuracy of 99.71 %, followed by $GC_{5Hz \rightarrow 250Hz}$ with accuracy of 99.35%, while $GC_{Rt \rightarrow frontal}$ resulted in the lowest

accuracy of 58.93 %. Furthermore, the GC_ChA showed the lowest accuracy among all GC categories. The results of Wilcoxon rank sum test between GC categories were as follows:

- GC_ChA vs. GC_CoF: p-value < 0.001
- GC_ChA vs. GC_CoW: p-value = 0.230
- GC_CoF vs. GC_CoW: p-value = 0.857

5.2.2 Contribution of GC categories to nociceptive fibers activations and pain levels

The normalized F1-score results of the GC_ChA and the GC_CoF to classify the three waveforms (targeting Aδ- and C-fibers) are presented in Figure 5.2a and Figure 5.2b, respectively. Regarding to the stimulation waveforms of 1 Hz, 5 Hz, and 250 Hz, the medians of the normalized F1-score of GC_ChA were 0.393, 0.425, and 0.550, respectively, while those of GC_CoF were 0.989, 1, and 0.851 for 1 Hz, 5 Hz, and 250 Hz, respectively. For waveforms targeting C-fibers, the normalized F1-score results were similar for the GC_ChA and the GC_CoF. Nevertheless, the normalized F1-scores of GC_CoF were higher than those of GC_ChA, which means that GC_CoF could be a better feature for classification pain-eliciting waveforms than the GC_ChA, because a higher F1-score indicates more contribution of a GC to the classification. However, compared with the GC_CoF, the GC_ChA category resulted in much lower normalized F1-score for all three stimulation waveforms. That is, the GC_CoF is better than the GC_ChA as the features of classification.

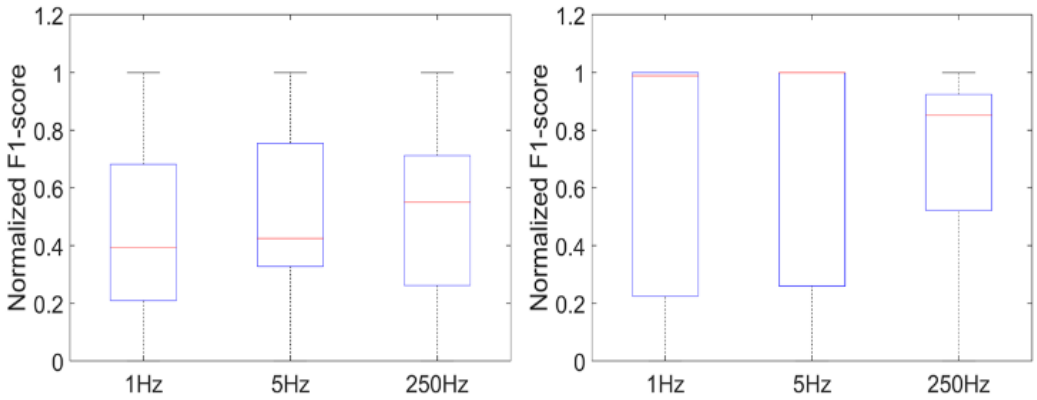

(**a**) (**b**)

Figure 5.2 Box plots of normalized F1-score of classification results of stimulation waveforms targeting different nociceptive fibers: (a) GC_ChA; (b) GC_CoF.

Table 5.2 False positive rates of classification results of waveforms: 1Hz vs. 250 Hz, 5 Hz vs. 250 Hz and 1 Hz vs. 5 Hz.

GC category	1 Hz predicted as 250 Hz	5 Hz predicted as 250 Hz	1 Hz predicted as 5 Hz
GC_ChA	0	0.551	0.255
GC_CoF	0.056	0.004	0

The false positive rates that waveform targeting C-fibers (1 Hz and 5 Hz) were incorrectly predicted as waveform targeting Aδ-fibers (250 Hz) and stimulation waveform of 1 Hz were incorrectly predicted as that of 5 Hz are presented in Table 5.2. By comparison of the

classification results of two waveform targeting C-fibers (1 Hz and 5 Hz) the false positive rates of 1 Hz vs. 250 Hz, 5 Hz vs. 250 Hz, and 1 Hz vs. 5 Hz by GC_ChA were 0, 0.551, and 0.255, respectively, whereas in the case of the GC_CoF, they were 0.056, 0.004, and 0, respectively.

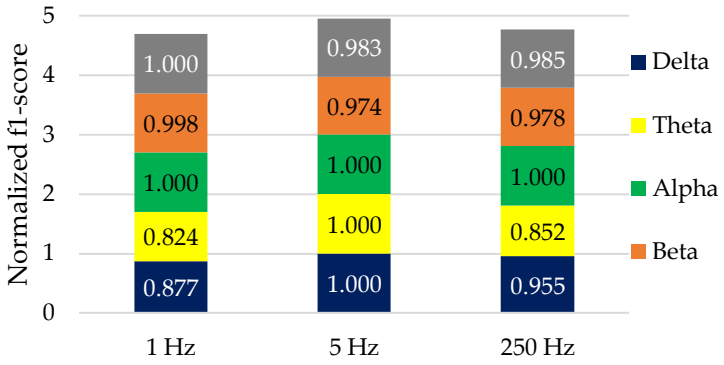

Figure 5.3 Normalized F1-score of each GC group (frequency band) of GC_CoF category for the classification of different waveforms targeting Aδ- and C-fibers.

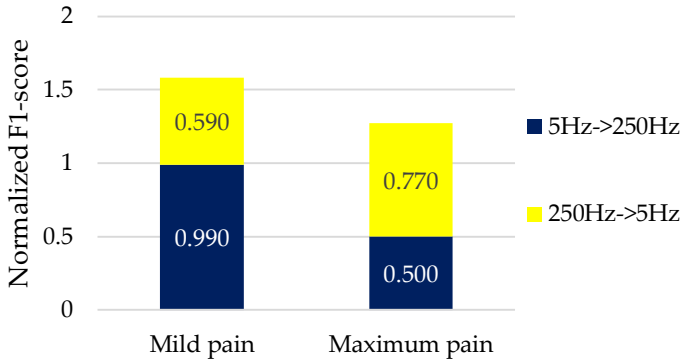

Figure 5.4 Normalized F1-score of each GC_CoW for different pain levels.

The contribution of each frequency band to the classification of nociceptive fibers activations was observed through normalized F1-score in Figure 5.3. Alpha band resulted in the maximum values of 1.000 for all three waveforms. Besides the alpha band, the stimulation waveform of 1 Hz and 5 Hz, which both targeting C-fibers, achieved the best score in gamma and lower frequency band, i.e., delta and theta, respectively. Since all frequency bands achieved a score higher than 0.8, none of the frequency bands effectively differentiated the two stimulation waveforms targeting C-fibers.

Normalized F1-score results for classification of pain levels (mild pain and maximum pain) of GC groups in the GC_CoW are presented in Figure 5.4. Compared with $GC_{250Hz \rightarrow 5Hz}$, $GC_{5Hz \rightarrow 250Hz}$ resulted in a higher score for mild pain level (0.990 vs. 0.590) but obtained a lower score for maximum pain level (0.500 vs. 0.770).

5.2.3 Significance test of different GC groups

To investigate both the difference between GC groups of different pain levels and the difference between GC groups of different waveforms, the following pairs were analyzed: 5Hz_Max – 5Hz_Pain, 250Hz_Max – 250_Pain, 250Hz_Max – 5Hz_Max, 250Hz_Pain – 5Hz_Pain, 5Hz_Pain – 1Hz_Pain, and 250Hz_Pain – 1Hz_Pain, where the name of stimulation

ended with '_Max' denotes the maximum pain level at a specific stimulation frequency, and the name ended with '_Pain' denotes mild pain level. According to the explanation in Chapter 3.2.3.2 that there was no data from the maximum pain level of 1 Hz stimulation, six pairs were obtained for analysis. The results of t-scores of GC connectivity for brain regions and frequency bands are summarized in Table 5.3.

Table 5.3 Results of the difference between GC groups of different pain levels and the difference between GC groups of different waveforms.

Comparison	GC direction	Frequency band	p-value	Related to previous studies
5Hz_Max – 5Hz_Pain	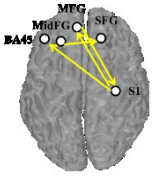	Rt. S1 → Lt. BA45	Beta and gamma	< 0.001	N/A
		Lt. MFG → Rt. SFG	Beta	0.007	N/A
		Lt. MedFG → Rt. S1	Beta	0.005	N/A
		Rt. S1 → Lt. MedFG	Gamma	0.004	N/A
250Hz_Max – 250Hz_Pain	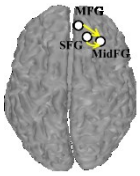	Rt. SFG → Rt. MFG	Gamma	0.015	N/A
		Rt. MedFG → Rt. MFG	Gamma	0.015	N/A
250Hz_Max – 5Hz_Max		Rt. MedFG → Rt. SFG	Gamma	0.034	N/A
		Rt. SFG → Rt. MedFG	Alpha and low beta	0.001	N/A
		Rt. MFG → Rt. SFG	Beta	0.001	N/A
250Hz_Pain – 5Hz_Pain	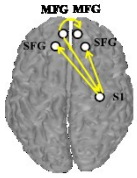	Rt. S1 → Lt. SFG	Beta	< 0.001	o
		Lt. MedFG → Rt. S1	Beta	< 0.001	N/A
		Rt. S1 → Rt. SFG	Beta	0.002	o
		Lt. MedFG → Rt. MedFG	Alpha and beta	0.001	N/A
5Hz_Pain – 1Hz_Pain	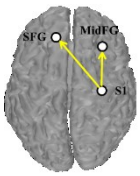	Rt. S1 → Lt. SFG	Delta and gamma	0.050	o
		Rt. S1 → Rt. MFG	Gamma	0.015	N/A
250Hz_Pain – 1Hz_Pain	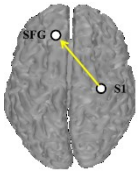	Rt. S1 → Lt. SFG	Alpha and gamma	0.034	o

Lt. = left, Rt. = right, S1 = postcentral gyrus, BA45 = inferior frontal gyrus (pars triangularis) of the frontal lobe, SFG = superior frontal gyrus of the frontal lobe, MFG = middle frontal gyrus of the frontal lobe, MedFG = medial frontal gyrus of the frontal lobe, o Agree with the existing studies

In terms of brain regions, five brain regions associated with the results of GC groups difference were postcentral gyrus (corresponding to S1), inferior frontal gyrus (pars triangularis) of the frontal lobe (corresponding to Brodmann area 45, BA45), superior frontal gyrus of the frontal lobe (SFG), middle frontal gyrus of the frontal lobe (MFG), and medial frontal gyrus of the frontal lobe (MedFG). For some of these regions, a significant difference was shown in both left (Lt.) and right (Rt.) hemispheres. The connectivity of GC from Rt. S1 to Lt. SFG was the most frequently found among all the results, with a p-value of < 0.001 for 250Hz_Pain – 5Hz_Pain, 0.050 for 5Hz_Pain – 1Hz_Pain, and 0.0034 for 250Hz_Pain – 1Hz_Pain, followed by the causal flow from Lt. MedFG to Rt. S1 with a p-value of 0.005 for 5Hz_Max – 5Hz_Pain and < 0.001 for 250Hz_Pain – 5Hz_Pain.

In terms of frequency bands, such significant differences were observed in higher frequencies of beta and gamma than those of lower frequencies, i.e., delta, theta, and alpha. Besides, the significant differences were found only at higher frequencies of beta or gamma for analysis between pain levels scenario, i.e., 5Hz_Max – 5Hz_Pain and 250Hz_Max – 250Hz_Pain. Furthermore, in the analysis compared with 1Hz_Pain, i.e., 5Hz_Pain – 1Hz_Pain and 250Hz_Pain – 1Hz_Pain, the results showed a significant difference in GC flow from Rt. S1 to Lt. SFG at low and high frequencies with a p-value of 0.050 and 0.034, respectively. However, no GC relationship that is consistent throughout the pairs containing pain levels (mild pain and maximum pain) or frequency of stimulation (1, Hz, 5 Hz, and 250 Hz) could be identified from Table 5.3.

5.3 Discussion

This section discusses the potential of GC features for the classification of different nociceptive fibers activations and pain levels. First, we consider using three categories of GC relationships (GC_ChA, GC_CoF, and GC_CoW) in the general classifier, multilayer perceptron (MLP), which is training with bootstrap method and k-fold cross-validation. Then we discuss how the GC feature could be effective in between-class and within-class differentiation. We also summarize the results of a significant difference between pairs regarding pain levels and pain-eliciting stimulation waveforms in terms of brain regions and frequency bands. Finally, we consider the contribution and limitation of this study and our plans for the next step.

5.3.1 GC features for classifying activations of nociceptive fibers

GC relationships were analyzed from pain eEEG as features in this study to develop a system for classifying the activation of different nociceptive fibers, C elicited by stimulation waveforms with the frequencies of 1 Hz and 5 Hz, and Aδ by 250 Hz. Due to the comparison of prediction error in GC analysis, GC is appropriate to analyze the signals with randomness like EEG. Thus, using GC analysis would help improve an understanding of 2-dimensional systems in the pain field study. Furthermore, by using MLP, which is an efficient classifier that filtering the important information from the input data by training with different initial weights on each iteration, it could make full use of the potential of GC features. To receive the consistent performances, the classification model was guaranteed by implementing 200 bootstrapping and inner k-fold cross-validation. Finally, the classification results can be used to assess the competence of GC relationships as features to differentiate the activation of different nociceptive fibers.

In the literature review between this study and other pain-related eEEG signal classification studies (Table 5.4), the classification of multiple pain perception levels has been investigated by a fair number of research groups, but none of them achieved the classification of pain induced by Aδ- and C-fibers activation. Additionally, classification of pain perception levels by using GC was also performed, although more class numbers need to be challenged. Therefore, this study contributed to pain assessment by introducing GC for the first time as a feature of pain-related eEEG classification.

Table 5.4 A comparison between this study and the other pain-related eEEG signal classification studies.

Reference	Type of pain stimulation	Classifier	Feature	Feature numbers	Class	Class numbers	Accuracy (%)
This study	Electrical	MLP	GC	30	Nociceptive fibers activation	3 [1]	99.71
					Pain perception level	2	99.35
[78]	Electrical	MLP	Fractal dimension (nonlinear analysis)	3	Pain perception level	4 [2]	87.50
[36]	Heat	Support vector machine (SVM)	Event-related spectral perturbation	3	Pain perception level	2	89.58
[35]	Heat	Random Forest	Time-frequency representation	60	Pain perception level	10	89.45
[37]	Laser	Combined SVM [3]	Time-frequency representation	15	Pain perception level	10	83.00

[1] Classes correspond to 3 waveforms: 1 Hz and 5 Hz stimulations, both targeting C-fibers; and 250 Hz stimulation for targeting Aδ-fibers; [2] Maximal class number; [3] Multivariate pattern analysis (MVPA) combining feature selection techniques with a support vector machine (SVM).

5.3.2 Evaluation of classification performances

Indices of MCC and average accuracy were used for between-class differentiation to differentiate the activation of Aδ-fibers from that of C-fibers and low pain (labeled as mild pain) from high pain (labeled as maximum pain). Although these two indices have different calculation methods, there is a strong correlation between them [89]. Unlike accuracy, MCC calculates the samples regarding the ratio of positive and negative cases that resulted in an advantage over imbalance classes or samples [90]. The classes of the GC_ChA were imbalanced due to the class of 1 Hz stimulation that derived from only mild pain level, while the classes of 5 Hz and 250 Hz stimulations were received from mild pain and maximum pain levels. The samples of the GC_CoF were imbalanced due to the varying number of EEG components.

In Table 5.1, the obtained values of MCC and average accuracy from two ways of counting discarded samples in the GC_CoF showed that the clustered samples could result in effective classifiers, even in the worst-case scenario. Therefore, rejecting the outliers by the clustering is helpful to improve classification performance. The average accuracy values had a similar tendency to those of MCC for all GC groups, except for $GC_{5Hz \rightarrow 250Hz}$. The causal influence of 5 Hz stimuli on 250 Hz stimuli showed the accuracy of 99.35% but obtained a low MCC of 0.033. Since accuracy does not consider the true negatives as MCC does, it would mean that the

positive and negative cases affected the prediction outcomes in $GC_{5Hz \rightarrow 250Hz}$ but not in $GC_{250Hz \rightarrow 5Hz}$.

Furthermore, F1-score was used to determine the potential of the GC relationship associated with one of the three stimulation waveforms targeting different nociceptive fibers and with one of two pain levels, describing the within-class contribution of the GC relationship (Chapter 5.2.2). Due to the imbalanced classes in this study, F1-score would be better for measuring the classification outcomes because of its calculation regarding the weight of false positives and false negatives that affect precision and recall, respectively. As presented in Figure 5.2, the GC_CoF contributes more to the differentiation of the C-fibers activated by 1 Hz and 5 Hz stimulations from Aδ-fibers activated by 250 Hz stimulation than the GC_ChA. Additionally, through the same index, it is possible to identify how much each GC group in the GC_CoF and the GC_CoW affects the classification of nociceptive fibers activations (Figure 5.3) and pain perception levels (Figure 5.4), respectively.

5.3.3 The importance of GC features to the identification of nociceptive fibers activations and pain levels

5.3.3.1 Association of GC features with between-class discrimination

Among all GC groups in Table 5.1, GC_CoF achieved the highest average accuracy and MCC. Our results of classification accuracy were significantly improved compared with previous works [35] [36] [78]. According to the results among all GC groups, GC measures between ICs at frequency bands (GC_CoF) were not only more accurate (higher average accuracy) but also more correlative (higher MCC) to Aδ-response (elicited by 250 Hz stimulation) and C-response (elicited by 1 Hz and 5 Hz stimulations). However, not all the GC categories achieved high accuracy, i.e., GC measures between channel areas (GC_ChA) did not reveal a contribution to GC measures between ICs (GC_CoF and GC_CoW). The reason might lie in the calculation with average channels of GC_ChA could not localize the source of brain activity as calculation with ICs.

According to the EEG montage [91], the central area in this study covered areas of S1 and the medial prefrontal cortex (mPFC), which are associated with the processing of pain-related information [92]. Due to the interaction between sensory and affective components in a pain phenomenon, the left temporal area in this study is related to BA47, which is located in the left hemisphere and corresponds to the emotion-related procedure [93]. In the GC_ChA, which obtained the lowest classification performances among all GC categories, the best GC group that achieved 82.99% accuracy was the GC relationship between the areas as mentioned earlier, i.e., $GC_{central \rightarrow Lt}$. Besides, the GC relationships related to the occipital area, which is mainly associated with vision, achieved accuracy of 80.79% and MCC of 0.492 from $GC_{occipital \rightarrow central}$ and accuracy of 79.49% and MCC of 0.512 from $GC_{Rt \rightarrow occipital}$. This means stimulation targeting Aδ- and C-fibers also produced the causal influences of the occipital area too. The occipital area and right temporal area involved in pain responses from nociceptive fibers might be from the focus of the subjects on the pain stimuli and its role in emotion processing, respectively. Moreover, the pain studies showed that S1 [94] and S2 [95] were most activated during pain. Therefore, P3/P4 (near the occipital area) and CP5/CP6 (left/right temporal area), which are the neighbour of some parts of S2 region, may yield the causal connectivity between these areas.

In the GC_CoF, it was found that the alpha band provided the best classification performances, followed by the gamma band, which agrees with other pain studies using thermal stimuli [37] [45]. However, those studies have described frequency components in the time-frequency power aspect but have not disclosed the role of each frequency band in causal connectivity of the brain. The contribution of GC relationships in the frequency band (GC_CoF) can be supported by the finding that different types of pain stimuli induced different response mechanisms in the brain [37].

The GC_CoW was used to classify binary classes of pain perception: mild pain and maximum pain. The results in Figure 5.4 showed that the past of eEEG induced by 5 Hz stimulation (targeting C) helped in the prediction of eEEG induced by 250 Hz stimulation (targeting Aδ) for mild pain, while the past of 250 Hz stimulation helped in prediction of 5 Hz stimulation for maximum pain. These outcomes related to the finding that the C-response has a higher possibility of not being overshadowed by the Aδ-response at the low pain level [13].

5.3.3.2 Association of GC features with within-class discrimination

The results between the GC_ChA and GC_CoF in Figure 5.2 showed that GC_CoF contributed more to pain elicited by different stimulation waveforms (different nociceptive fibers activations) than the GC_ChA. A variation in contribution to all waveforms of GC_ChA was more than the GC_CoF. Due to the two stimulation waveforms of 1 Hz and 5 Hz that targeting C-fibers, within-class differentiation (Table 5.2) were performed to identify the most contributive feature for C-fibers activations. The results of 1 Hz showed more distinctive from 250 Hz than 5 Hz. This agrees with [70] which revealed that 1 Hz square waves gave higher C selectively over Aδ than 5 Hz sine waves.

In the GC_CoF, the results in Figure 5.3 showed that the alpha band was the most contributive feature to both Aδ- and C-fibers. For waveforms targeting C-fibers, gamma and theta bands achieved high contributions to 1 Hz and 5 Hz stimulations, respectively. This agrees with the power changes of these two frequency bands in thermal pain stimuli [36]. However, due to a low variation in the normalized F1-score from all frequency bands (all bands achieved normalized F1-score > 0.8), the results were not decisive enough to identify that different frequency bands were affected by different nociceptive fibers activations.

In the classification of two pain perception levels using GC_CoW in Figure 5.4, 5 Hz and 250 Hz stimulations were associated with mild pain (low pain) and maximum pain (high pain), respectively. This agrees with the fading-out of C-response caused by the appearance of Aδ-fibers activation at higher pain intensity [43]. Furthermore, the activation threshold of C-fibers was lower than that of Aδ-fibers at stimulation frequencies lower than 100 Hz, which means that both Aδ- and C-fibers were activated at higher pain intensity [70].

5.3.4 Significance test of different GC groups

The significant difference between pairs regarding pain levels and pain-stimuli waveforms showed that the cortical area that responds to pain was contralateral S1, which corresponds to the stimulation site at the left hand. This agrees with [90] which found that pain-evoked activation in contralateral S1. Most of the significant differences were presented at higher frequency bands of beta and gamma in the significance test of GC group pairs regarding pain levels, i.e., 5Hz_Max – 5Hz_Pain and 250Hz_Max – 250Hz_Pain. In the significance test of GC

group pairs corresponding to mild pain, the significant differences with p-values of < 0.001 (250Hz_Pain – 5Hz_Pain), 0.050 (5Hz_Pain – 1Hz_Pain), and 0.034 (250Hz_Pain – 1Hz_Pain) were presented at the causal flow from contralateral S1 (Rt. S1 in this study) to Lt. SFG. Nevertheless, the causal flows between S1 and SFG, found in the GC group pairs at mild pain, were not presented in maximum pain. This might result due to the concomitant activation of Aδ- and C-fibers during low stimulus intensity [13]. However, no consistent causal connectivity between brain regions was presented.

According to the role of S1 (related to sensation) [94] and SFG (corresponds to the self-awareness related to the sensory input) [96], the causal flow from Rt. S1 to Lt. SFG in this study revealed that these two regions are involved in the pain network. In addition, the regions that had significant differences were Lt./Rt. MFG, Lt./Rt. MedFG, and Lt. BA45 are associated with contextual conditioning of pain perception [97], motion, and semantic processing [98], respectively. The involvement of these regions can be justified by perceiving pain system, movement, and semantic decision during the experiment of the subject. However, some regions were found in this study but not presented in other studies (Lt./Rt. MedFG and Lt. BA45) and regions shown in literature but were absent in this study (such as ACC and S2 etc.). This might be from this study's condition that explored only the differentiation of Aδ-response and C-response and that of mild pain and maximum pain.

One possible reason to explain about no consistent GC relationship was found across either pain levels (mild pain and maximum pain) or pain types (acute pain from Aδ-fibers and chronic pain from C-fibers), as presented in Table 5.3, might lie in the complexity of pain network. In pain-related information processing, mild pain, maximum pain, acute pain, and chronic pain might be processed in different brain regions or even by different mechanisms. Moreover, the areas identified with significant differences were small and might be lacking compared with the findings from neuroscience studies, but it still provides important clues related to neuroscience, such as dichotomizing concomitant phenomena.

5.3.5 Contributions and limitations of the study

A novel feature to classify pain elicited by Aδ- and C-fibers activations through different electrical stimulations and pain levels, which provided 2-dimensional results from GC connectivity was proposed in this study. The major contribution of the study can be summarized as follows.

1) The features based on causality that quantifies causal flows between regions, components, and frequency bands were used for the first time to classify pain eEEG rather than using the features related to the activities of a single region, single component, and single frequency band.
2) Using C-response and Aδ-response elicited by corresponding electrical stimulation was first classified by a machine learning method with the GC-based features. As a result, the highest accuracy was achieved.
3) Throughout the analysis of the GC features contributing to the differentiation of nociceptive fibers or pain levels, some of the significant causal relationships agree with those identified in a neuroscience research area, and others that have been addressed in the literature could serve as clues for further investigation.

However, the number of stimuli was one possible uncertain factor in this study. As clarified in [13], collecting 40 stimuli for each experimented trial may not reach a steady SNR to detect C-response because of the nature of concomitant activation of Aδ and C and

relatively small amplitude of C-response. Thus, it is difficult to detect C-response with less than 80 stimuli. Yet, this is not commonly known; there has been a study averaging the eEEG responding to 10 stimuli to investigate the changes in Aδ- and C-fibers activations [15].

After this study, we continued investigating features for the classification of pain induced by different nociceptive fibers activations from electrical stimulation and pain levels. In the near future, further experiments will be done to decide the number of stimulation sufficient for the classification of Aδ- and C-response. After discovering the appropriate GC-based features, online objective pain evaluation can be realized with a general classifier.

5.4 Conclusions

This study aimed to demonstrate the effectiveness of the features extracted from three GC categories: GC based on channel areas, frequency bands, and stimulation waveforms, analyzed from pain eEEG signals, in the classification of two different types of pain, acute pain and chronic pain. We expected that the classification systems with the GC features would improve the classification performances by evaluating MCC, average accuracy, and F1-score. For the classification of activation of different nociceptive fibers, GC features from alpha band achieve the highest MCC and average accuracy of 1.000 and 99.71%, respectively. The features that contribute most to the differentiation of Aδ- and C-fibers are found in the alpha band feature, too. Still, each nociceptive fibers activation contribution is not decisive due to the low variation of the results. The results of GC flow between 5 Hz and 250 Hz waveforms revealed that waveform targeting C-fibers (5 Hz) are associated with low pain, while waveform targeting Aδ-fibers is related to high pain. Through this investigation, it has been demonstrated that applying GC relationships as features could improve the classification performances for differentiating two different types of pain elicited by nociceptive fibers activations and the prediction of pain perception levels.

In the next chapter, we expand the investigation of the GC feature in this study in a simulation with an online manner. We extract features from the frequency domain of EEG with different channels and trials and then compare the classification results with FD features for differentiating nociceptive fibers activations.

Chapter 6

Final Implementation of Simulating for Online Classification with Granger Causality Features

6.1 Introduction

In the third experiment, we explored the features extracting with Granger causality (GC) analysis from spectral power (frequency domain) of EEG with limited channels and trials for classification of nociceptive fibers activations in an online manner (simulation for real-time analysis). We investigated the robustness of features for the classification of nociceptive fibers activations by comparing the results between current GC features and FD features. In addition, we applied detrending and dynamic time warping (DTW) to GC features for improving the classification accuracy. The chapter consists of material that has not been published yet.

6.1.1 Background and related research

The previous chapters showed that the EEG-based features extracted with our approaches (nonlinear analysis and GC analysis) could improve the classification accuracy for differentiating multiple pain perception levels and nociceptive fibers activations. Within analysis using various data in the time domain (the first experiment in Chapter 4 [78]) and time-frequency domain (the second experiment in Chapter 5 [83]), the results showed that data with frequency-related gave more information that could improve classification accuracy than without frequency-related. Our findings also agree with the pain-related study that alpha and gamma frequency provided a neuronal response to pain [37]. Even though GC has been used to identify rhythmic brain activity in response to pain stimuli, the frequency dominance correlates to pain stimuli were not determined. However, the effect of pain types between acute pain from Aδ-fibers activation and chronic pain from C-fibers activation on the frequency band of EEG were not decisive. Still, not only the frequency component affects the classification accuracy but also the feature extraction technique. Therefore, an association of frequency band and EEG-based feature with pain response from Aδ- and C-fibers is needed to be investigated.

In order to apply the GC features in real-time analysis, it needs to be investigated with a low number of data points, which weaken the stationary of the signal and causes difficulty in GC calculation. Furthermore, further feature extraction in different data is also needed to examine the robustness of our results.

6.1.2 Goals

In this final implementation, our goal was to show that the use of GC features extracted from spectral EEG would be applicable for pain classification even in an online manner. We aimed to investigate the effective GC features that would classify pain induced by nociceptive fibers activations (Aδ and C) in the scenarios of a low number of trials and channels. For this, we compared the classification results between different features, i.e., GC features vs. fractal dimension (FD) features. Besides, the salient effect of the detrending and DTW on the GC features to improve the classification accuracy was discussed.

6.2 Results

6.2.1 Effect of channel numbers on accuracy

With the different number of channels selected by Fisher score, the results are shown in Figure 6.1, and their corresponding Fisher scores are presented in Table 6.1. The results of GC features (Figure 6.1a) analyzed with whole trials and a range of 5-9 channels were compared with those of FD features (Figure 6.1b) to investigate the variation of accuracy due to the low number of channels. It showed that the average accuracies of GC features over frequency bands with channel numbers of 5, 6, 7, 8, and 9 were 40.87 ± 2.62%, 42.10 ± 1.63%, 41.63 ± 2.21%, 41.67 ± 1.97%, and 40.85 ± 2.23%, respectively. Besides, one-way ANOVA was performed to test the relationship between channel numbers and classification accuracy. As a result of the ANOVA, p-value = 0.980 was obtained, which indicates that the number of used channels in GC analysis had an insignificant effect on the classification accuracy. Thus, the further outcomes were analyzed based on six EEG channels which obtained the average accuracies of 39.74 ± 2.11%, 39.54 ± 1.18%, 37.93 ± 1.18%, 40.34 ± 3.68%, and 45.57 ± 3.02% for delta, theta, alpha, beta, and gamma, respectively.

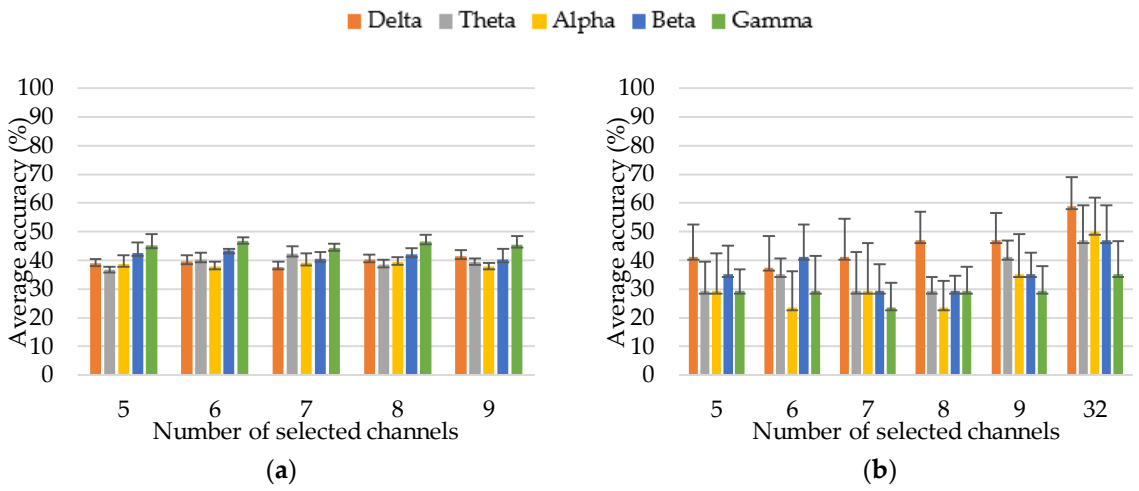

Figure 6.1 Average accuracy results for different selected EEG channel numbers. (a) GC features; (b) FD features.

In comparison between GC and FD features, FD features with different channel numbers in Figure 6.1b show the fluctuations in average accuracy values caused by a lower number of data points to be calculated in nonlinear analysis. However, analysis based on all 32 channels achieved the better accuracies of 58.82 ± 10.23%, 47.06 ± 12.13%, 50.00 ± 11.79%, 57.06 ± 12.06% and 35.29 ± 11.52% for delta, theta, alpha, beta, and gamma, respectively, than the accuracy results of using few channel numbers that selected by Fisher score.

Table 6.1 The top channels based on Fisher score.

Subject	Channel								
	1st	2nd	3rd	4th	5th	6th	7th	8th	9th
1	Oz: 0.048	AF3: 0.046	C3: 0.025	Fp2: 0.024	O2: 0.016	F7: 0.015	CP6: 0.012	FC6: 0.012	P3: 0.012
2	T8: 0.045	CP5: 0.030	F3: 0.013	F7: 0.012	Fz: 0.012	F8: 0.011	AF4: 0.010	Pz: 0.008	F4: 0.006
3	O1: 0.013	P7: 0.010	F3: 0.10	FC2: 0.007	CP2: 0.006	PO4: 0.006	T8: 0.005	FC5: 0.004	Pz: 0.003
4	Fp1: 0.090	O2: 0.063	CP2: 0.063	Oz: 0.056	FC5: 0.036	O1: 0.032	AF3: 0.024	Pz: 0.022	C4: 0.014
5	T8: 0.003	AF3: 0.003	Cz: 0.003	P7: 0.002	F3: 0.002	FC6: 0.002	P4: 0.002	P8: 0.002	O2: 0.001
6	Fp1: 0.045	Fp2: 0.021	FC5: 0.011	C3: 0.008	P3: 0.008	FC1: 0.007	CP2: 0.006	O1: 0.005	F8: 0.004
7	P8: 0.042	AF4: 0.016	F3: 0.013	Fz: 0.006	AF3: 0.006	O2: 0.006	T7: 0.004	Cz: 0.004	FC1: 0.003
8	FC1: 0.005	Fp2: 0.005	CP1: 0.004	F3: 0.003	Pz: 0.003	CP6: 0.003	C3: 0.002	CP5: 0.002	Fp1: 0.002
9	Fp1: 0.076	T7: 0.075	F8: 0.056	FC6: 0.047	F7: 0.035	F4: 0.032	T8: 0.032	C3: 0.030	CP5: 0.029
10	O2: 0.020	F8: 0.019	O1: 0.015	CP5: 0.014	T8: 0.010	FC2: 0.010	Oz: 0.010	F7: 0.007	CP5: 0.007
11	AF3: 0.030	T7: 0.029	Fp2: 0.028	P7: 0.023	FC2: 0.019	O1: 0.016	O2: 0.011	CP6: 0.010	P3: 0.010
12	F3: 0.326	C4: 0.148	P7: 0.116	Fp1: 0.081	F7: 0.073	T7: 0.072	CP2: 0.070	O1: 0.045	PO4: 0.040
13	T7: 0.010	P8: 0.010	F3: 0.008	FC2: 0.007	O2: 0.005	P4: 0.005	F7: 0.005	CP6: 0.004	C4: 0.004
14	CP6: 0.007	F7: 0.004	O1: 0.003	F7: 0.003	PO4: 0.003	PO3: 0.003	Fp1: 0.002	F8: 0.002	T8: 0.002

6.2.2 Effect of trial numbers on accuracy

The average accuracy of GC and FD features analyzed with different n-trial averaging are shown in Figure 6.2a and Figure 6.2b, respectively.

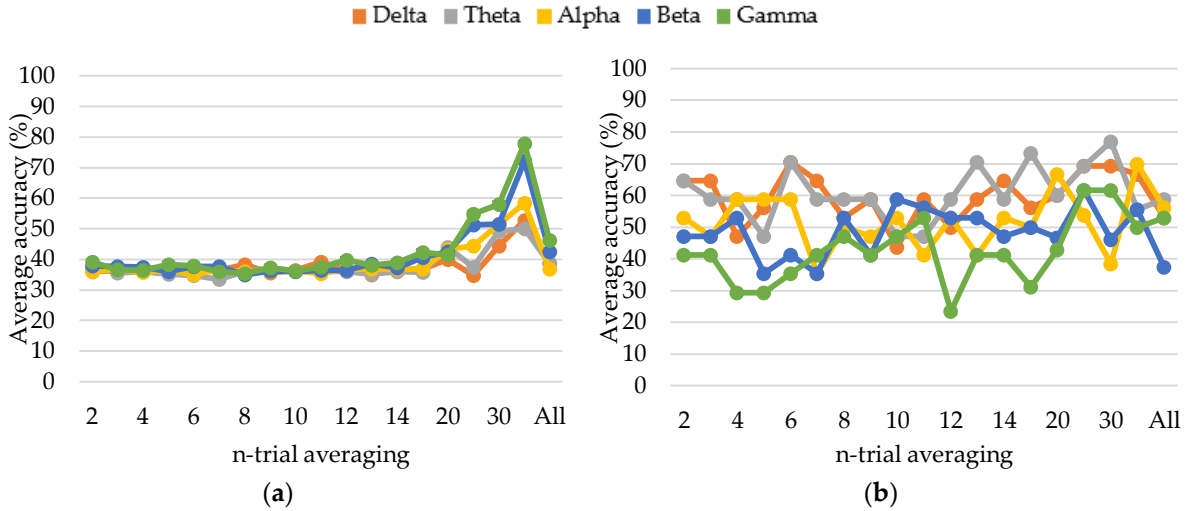

Figure 6.2 Average accuracy results of each frequency band from the feature with n-trial averaging. (a) GC features extracted from top six channels by Fisher score; (b) Nonlinear features based on all 32 channels.

In the case of GC features which analyzed with six channels based on Fisher score (Figure 6.2a), a low variation in accuracy (in a range of 36.11-42.42%) was presented at all frequency bands during analysis with the trials lower than 25-trial averaging, while increasing averaging

accuracy was observed when trial number increases as 25, 30, and 35. The highest accuracies were found in 35-trial averaging, which were 52.78%, 50.00%, 58.33%, 72.22%, and 77.78% for GCdelta, GCtheta, GCalpha, GCbeta, and GCgamma, respectively. In contrast, accuracies were depreciated to 52.94%, 58.82%, 56.25%, 37.50%, and 52.94% for GCdelta, GCtheta, GCalpha, GCbeta, and GCgamma, respectively, for analysis using all trials. In contrast, FD features analyzed with all 32 channels showed a high variation in accuracy when the number of averaging trials was increased. The highest accuracy was 76.92% from FDtheta at 30-trial averaging.

6.2.3 Effect of detrending and dynamic time warping (DTW) on online classification scenario

In a scenario for the recording of data within a short time, which has few data points, analyses with a single trial of 1, 2, 3, 4, and 5 and first n-trial (n = 1,2,…,5) averaging were performed and the results are displayed in Figure 6.3. All frequency bands' accuracy in both analyses of single trial and first n-trial averaging with GC features showed poor results, which were lower than 50%. On the other hand, most of the analysis with GC_DTW features provided improved accuracies. GC_DTW features obtained accuracies of 59.42 ± 14.96%, 56.58 ± 16.09%, 57.92 ± 9.47% for analysis with single trial of 1, 2, and 3, respectively, and accuracies of 58.08 ± 12.66%, 56.75 ± 14.85%, 64.42 ± 12.30%, and 57.83 ± 13.06% for analysis with averaging first 2, 3, 4, and 5 trial, respectively. However, GC_DTW with a single trial of 4 and 5 had accuracies of 43.75 ± 8.18%, and 49.00 ± 10.92%, respectively, could not get better accuracy than GC features.

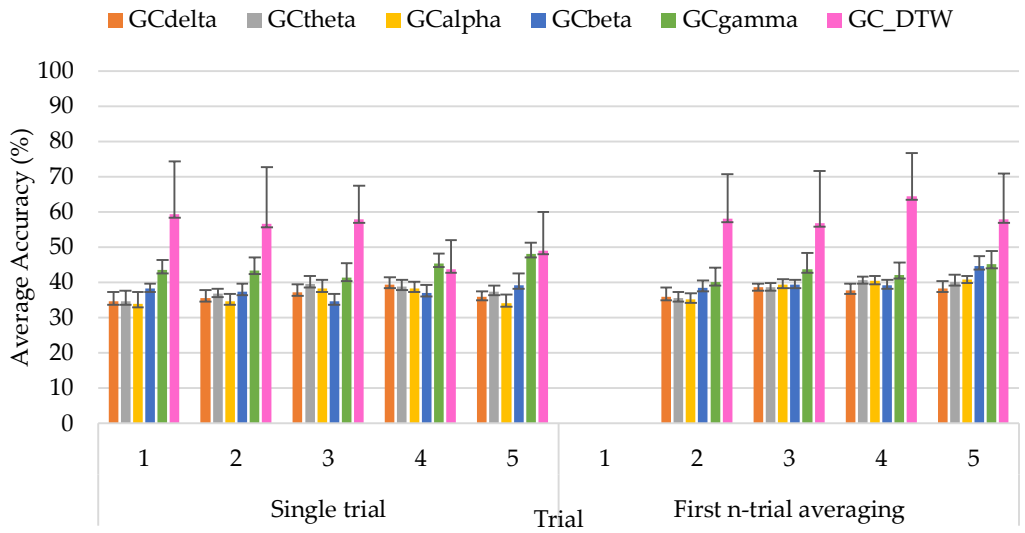

Figure 6.3 Average accuracy of GC features vs. GC_DTW features at different single trial and first n-trial averaging.

We also used GC_DTW with different channels to investigate the effect of DTW application on GC, as shown in Figure 6.4. Classifications with six channels selected based on Fisher score and different grouped channels are displayed in Figure 6.4a and Figure 6.4b, respectively. For all grouped channels that are shown in Figure 6.4b, they were selected based on the following: 1) C3 and C4 cover over sensorimotor cortex area; 2) the late and ultra-late components of EEG signals due to the activations of Aδ- and C-fibers, respectively, were found at the vertex, Cz [99];

3) CP1 and CP2 electrodes were adjacent to the vertex; 4) there have been reported that complexity of the brain activity may contribute to pain response [100] in the parietal (P3/P4) region which is associated with psychological pain [101]. It is noted that the accuracy results of classification with channels based on Fisher score in Figure 6.4a was the same as the plot of GC_DTW (shown in pink color) in Figure 6.3. Figure 6.4b shows the highest accuracy of 85.74 ± 7.94% from using the grouped three channels of C3, CP1, and P3 with single 1st trial, while the lowest accuracy of 44.56 ± 7.78% from five channels of C3, CP1, Cz, C4, and CP2 with single 5th trial. Besides, in classification with first n-trial averaging, we achieved the accuracy with a range of 48.68-66.84%. The values of the accuracy results are presented in Table A 1 (see Appendix).

Therefore, compared with the results of GC features (Figure 6.3), the results of GC_DTW analysis with several channels (Figure 6.4) were all improved.

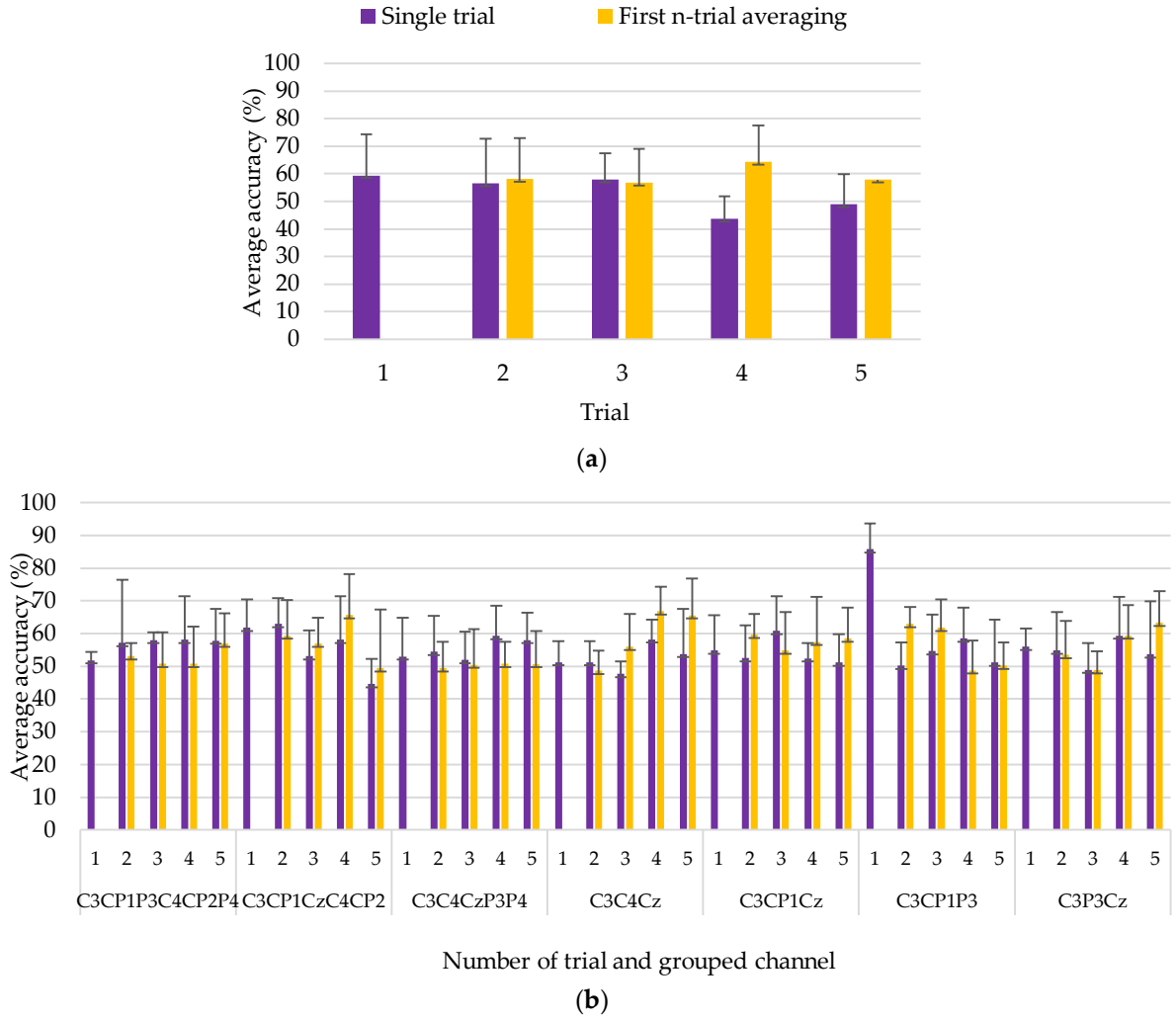

Figure 6.4 Average accuracy of GC_DTW features with different channel selection methods. (a) Selecting EEG channels based on the top six Fisher score (see Table 6.1 for details of each channel); (b) Selecting EEG channels based on [99]- [101].

6.2.4 Differentiation between nociceptive fibers activations

In this study, two waveforms of 1 Hz and 5 Hz were used to selectively stimulate C-fibers [13] [70]. Figure 6.5 shows a box plot depicting the performances for two-class classification. For

classification results between Aδ- and C-fibers activations in Figure 6.5a, it is seen that waveform of 1 Hz, which used for high selectively stimulate C-fibers, can differentiate from Aδ-fibers activation (waveform of 250 Hz) better than waveform of 5 Hz that targeting C. By using the waveform of 1 Hz to stimulate C-fibers, classifying the activations of C-fibers from Aδ-fibers (250 Hz) achieved a range of 64.00-84.00% with a median value of 76.00 for average accuracy, a median of 77.81 for F1-score of class C-fibers, and a median of 72.64 for F1-score of class Aδ-fibers. The classification between C-fibers activations from the waveform of 5 Hz and Aδ-fibers activations from the waveform of 250 Hz resulting in a range of 34.36-57.64% with 51.64 of median value, while the median values of 49.88 and 50.91 for F1-score of class C-fibers (5 Hz) and class Aδ-fibers (250 Hz), respectively. For the comparison between the classification of 1 Hz (C) vs. 250 Hz (Aδ) and 5 Hz (C) vs. 250 Hz (Aδ), the paired t-test was performed. The t-test results showed significant differences with p-value = 0.001, 0.023, and 0.004 for average accuracy values, F1-score of C-fibers activation, and F1-score of Aδ-fibers activation, respectively.

Figure 6.5b, which is the classification between waveforms that both target C, shows the average accuracy ranges from 71.27-81.09% with a median of 75.46, median F1-score of 76.89 for class 1 Hz stimulation waveform, and median F1-score of 74.06 for class 5 Hz stimulation waveform.

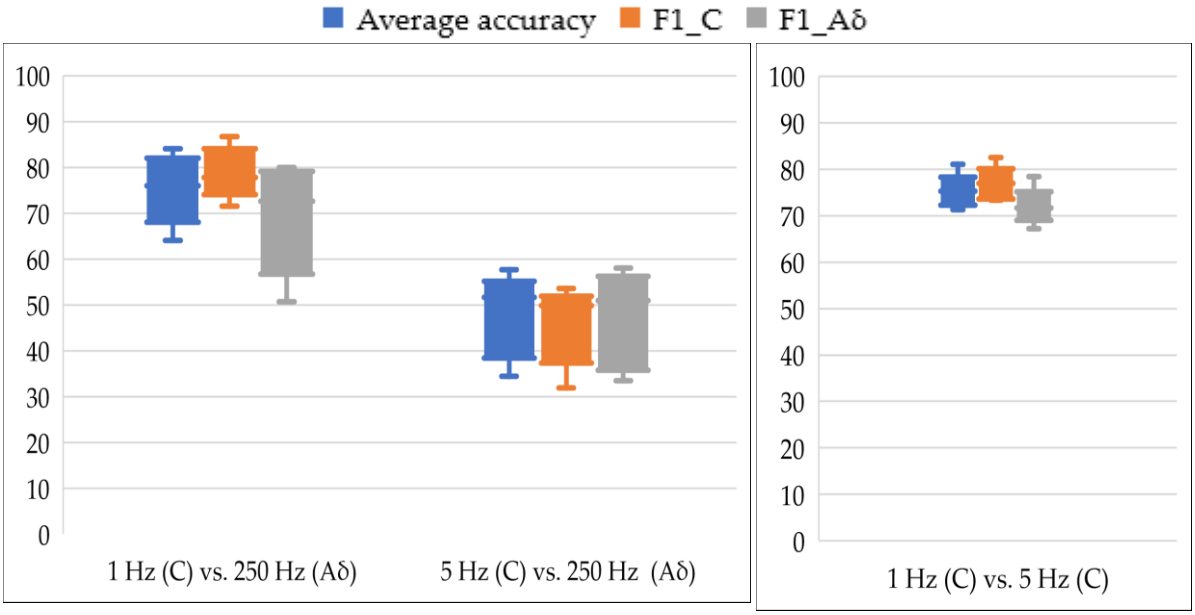

(a) **(b)**

Figure 6.5 Classification results for binary classes. (a) Classifying between the activations of Aδ- and C-fibers; (b) Classifying between different stimulation waveforms for targeting C-fibers.

6.3 Discussion

6.3.1 Number of channels used for GC features in online analysis

The results in Figure 6.1 show that the higher number of channels used in GC analysis does not give higher accuracy for all frequency bands. On the other hand, FD features with all 32

channels achieve higher accuracy than using few channels for extracting FD features. This means that even if we used the most discriminative channels (selected by Fisher score), some channels do not reveal the causal relationships for pain-related information. This is because the causal interaction in the GC feature is associated with spatial distribution less than the fractal dimension in the FD feature. Furthermore, a number of channels has not effect on the GC frequency band-related relationships.

6.3.2 Number of trials used for GC features in online analysis

For the GC analysis with n-trial averaging in Figure 6.2a, a lower number of n-trial averaging shows low variation in accuracy results. There is a tendency to increase accuracy when we analyzed with 25-trial and reached a peak at 35-trial, which achieved a range of 50.00-77.78% accuracy and depreciated when using all trials. That is because we included all subjects into analysis when we wanted to use all trials, but analysis with n-trial the subjects whose trials could not reach the target n-trial will be excluded. Accordingly, the accuracy of using all trials is worse than using 25-35 trials. This might agree with our previous findings [78] in Chapter 4, which found that with the trial numbers at least 20 was sufficient to get the acceptable accuracy of 67.7% and 82.6% for four-class and three-class in the classification of pain perception levels. Thus, even though there is no tendency of the results in FD features analyzed with a number of n-trial averaging ≥ 20 (Figure 6.2b), there is a fluctuation in the classification accuracy. Furthermore, averaging a higher number of trials ≥ 25 could give better accuracy because it contains more data points to be calculated. Additionally, only the subjects that reach the target trials were included in this study. Hence, using all trial averaging provides lower classification accuracy than n-trial averaging in this study because all subjects were used for analysis with all trials, while some subjects were selected and used for analysis with n-trial averaging. However, the difference between the results of FD features in our previous study and the current study might come from the information of pain-evoked potential that was analyzed in different domains of EEG signals.

Nevertheless, the current study extracted from the spectral power (frequency domain) may be affected by the frequency components rather than time components. This might be related to the relationship between neural oscillations in frequency band activity and pain states, as they found that the low frequencies of delta, theta, and alpha showed a global reduction in power response to thermal pain stimulation [45]. Even though the evoked potential (in time domain analysis) could reflect cortical responses to electrical pain stimulation, low SNR in the evoked potential is inevitable [15]. Therefore, brain responses to pain might correlate to the frequency component more than the temporal component.

However, among the trial selection of n-trial averaging (Figure 6.2), single trial (Figure 6.3), and first n-trial averaging (Figure 6.3), it requires at least 35-trial averaging for classification of nociceptive fibers activations using the current GC feature, while single trial and first n-trial averaging are not sufficient enough to get a fair accuracy from the classification with the current GC feature. By using single trial and first n-trial averaging as a simulation for online classification, the current GC features needed to be improved by applying detrending and DTW to GC feature processing which will be discussed in the next section.

6.3.3 The contribution of detrending and DTW to GC features

GC feature analyzed based on gamma band with 35-trial averaging (Figure 6.2a) achieved 77.78 ± 10.02% accuracy, but other GC features which analyzed based on other frequency bands and different n-trial averaging could not achieve the acceptable accuracy. Even though there has been reported using GC features extracted from the time-frequency domain of EEG data were effective for the classification of nociceptive fibers activations [83], the current GC features extracted from spectral EEG still needed to be improved. Thus, detrending and DTW were applied.

Detrending allows identifying the fluctuations of the data by removing a trend from the data. The components of the EEG time series after decomposition are presented in Figure 6.6. Thus, we can address it explicitly and indicate the tendency of the signal. Here, a trend component might contain some artifacts that remained from the pre-processing steps. Then, we removed the trend component (detrend) and used the remainder components (seasonal and residual) of the data. We used this detrended data to extract features with GC analysis, which calculates based on the covariance of the data and requires stationary data. Since non-stationary behavior can be dominant trends, performing detrending helps improve the stationary of the EEG data. Therefore, using detrending helps in the improvement of GC features without distorting the data.

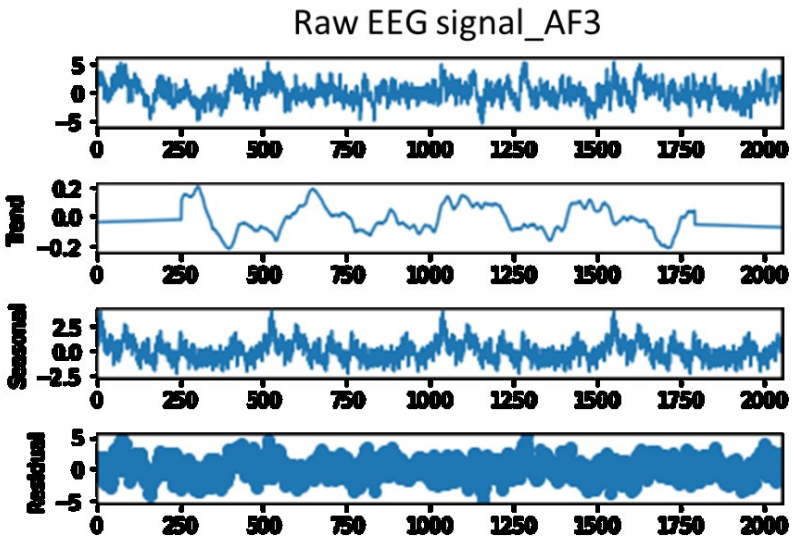

Figure 6.6 Effect of remove trends from EEG signals. This figure depicts an example of channel AF3 in one dataset (one subject, one stimulation waveform, and one pain condition). Each row corresponds to the composition of the signal, which the first row denotes the raw EEG signal. The components of seasonal and residual were used for further analysis, while the trend component was removed.

To indicate how the difference among frequency-related causal interactions (GC measures between channels) during pain response, DTW was used to identify the similarity between two frequency bands of GC measures. According to the DTW algorithm (Chapter 2.4.2.2), the value of DTW close to zero means the high similarity among these two signals, while the higher DTW denotes the distinctive characteristic between these two signals. After detrending and GC analysis, DTW was applied to identify the similarity between GC of two

frequency bands. We hypothesized that some frequency bands might be correlated with others that are ambiguous to classify between nociceptive fibers activations. The results in Figure 6.3 show that detrending and DTW affect GC features. Using GC_DTW features has increased 9.13-25.1% accuracy from GC features. Besides using six channels selected based on Fisher score, we also investigated the effect of GC_DTW features analyzed with different channels (Figure 6.4b). Regardless of trial type (single trial or first n-trial averaging), GC_DTW based on channels from literature still has improved 10.56-37.66% accuracy from GC features.

In conclusion, the average accuracy of classification nociceptive fibers activations were: 38.92% from all GC features (Figure 6.3), 53.33% and 59.27% from GC_DTW based on channels selected by Fisher score with single trial and first n-trial averaging (Figure 6.4a), respectively, 55.64% and 55.74% from GC_DTW based on channels in literature with single trial and first n-trial averaging (Figure 6.4b). Accordingly, it showed that using detrending and DTW could help in improving classifying nociceptive fibers activations.

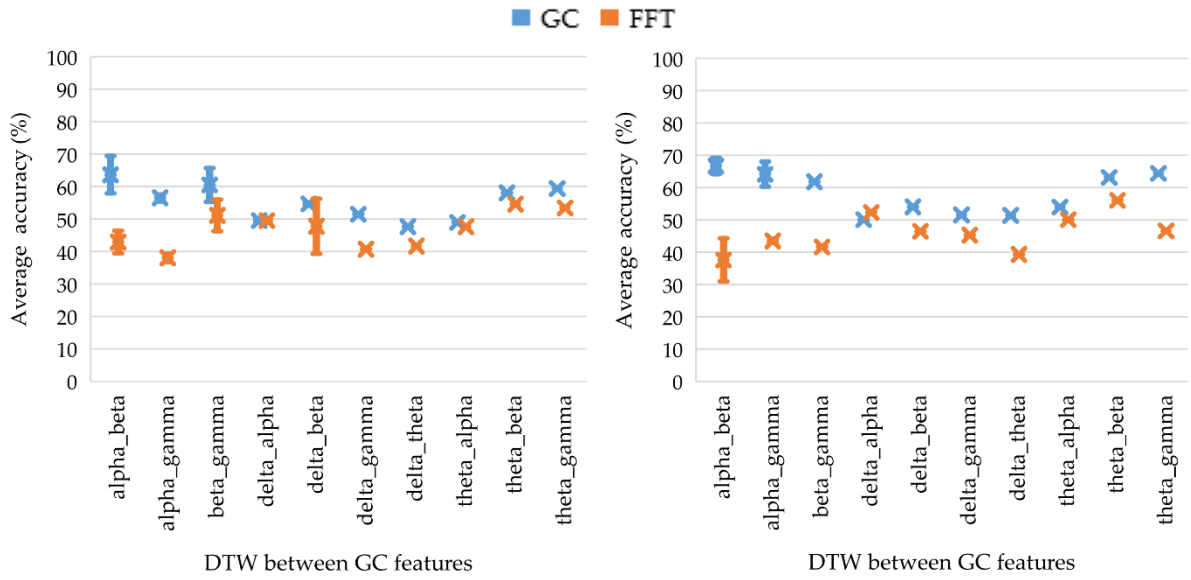

Figure 6.7 Average accuracy of applying DTW to GC features and FFT features at each pair of frequency bands. (a) Selecting EEG channels based on the top six Fisher score; (b) Selecting EEG channels based on literature.

Therefore, DTW contributes to GC measures between channels at each frequency band by detecting which pairs of frequency bands differentiate between them. This can indicate which frequency rhythm of functional connectivity (GC measures) is related to another frequency during pain induced by different nociceptive fibers activations. We applied detrending and DTW to transform data (by fast-Fourier transform, FFT) to prove the contribution of detrending and DTW on other features besides GC features. Figure 6.7 shows the average accuracy of applying detrending and DTW on GC features compared with FFT data. We chose to use transformed data by FFT because it was used before extracting features with nonlinear analysis. The average accuracy of applying detrending and DTW to GC features provides better results than FFT features in channels based on Fisher score (Figure 6.7a) and literature (Figure 6.7b).

Additionally, we classified nociceptive fibers activations by using GC_DTW features with feature selection based on AUC score to investigate the relevance of GC at each frequency

band. All features were ranked by their p-values from the ANOVA test and then selected one by one feature for the feature selection. If the following feature provides a higher AUC score than the previous feature, it will be collected. In contrast, if the following feature has less AUC score than the previous feature, that feature will be excluded. Here, we used only the top two feature inputs derived from this feature selection method. Table 6.2 presents average accuracy and AUC score and Table 6.3 presents the selected top two feature inputs with the corresponding AUC score.

Table 6.2 Classification performances of GC_DTW features using the top two feature inputs. The value after ± is the standard deviation.

Trial type	Number of trial	Average accuracy (%)	AUC
Single	1	50.25 ± 11.31	0.70 ± 0.12
	2	62.92 ± 17.26	0.77 ± 0.16
	3	54.00 ± 10.52	0.73 ± 0.08
	4	55.17 ± 6.83	0.72 ± 0.11
	5	45.08 ± 11.34	0.68 ± 0.11
First n-trial averaging	2	60.42 ± 8.54	0.77 ± 0.06
	3	55.50 ± 12.24	0.75 ± 0.11
	4	64.25 ± 6.88	0.81 ± 0.08
	5	63.08 ± 12.26	0.79 ± 0.07

Table 6.3 The top two feature inputs selected based on AUC score. AUC derives from the classification using the 1st or 2nd selected feature.

Trial type	Number of trial	1st feature				2nd feature			
		Feature *	Minimum AUC	Average AUC	Maximum AUC	Feature *	Minimum AUC	Average AUC	Maximum AUC
Single	1	delta_theta	0.809	0.880	0.934	delta_beta	0.653	0.855	0.982
	2	alpha_beta	0.704	0.820	0.930	delta_beta	0.868	0.922	0.914
	3	alpha_beta	0.727	0.855	0.930	theta_beta	0.691	0.817	0.943
	4	theta_beta	0.726	0.859	0.943	alpha_beta	0.831	0.880	0.930
	5	delta_beta	0.783	0.916	0.982	alpha_beta	0.870	0.890	0.908
First n-trial averaging	2	alpha_beta	0.861	0.900	0.931	delta_beta	0.647	0.842	0.982
	3	delta_beta	0.670	0.867	0.982	beta_gamma	0.789	0.814	0.842
	4	alpha_beta	0.902	0.925	0.938	delta_theta	0.760	0.841	0.934
	5	alpha_beta	0.822	0.887	0.930	delta_theta	0.812	0.859	0.889

* Feature corresponds to DTW between GC at a pair of frequency bands.

It is seen in Table 6.2 that classification with two feature inputs gives better accuracy with a range of 45.08-62.92% with AUC score of 0.68-0.70 for single trial and a range of 55.50-64.25% accuracy with AUC score of 0.77-0.81 for first n-trial averaging. Although using the top two feature inputs does not increase much accuracy, it still improves accuracy compared with using all features. This might lie in the relevant features (frequency bands). That means those relevant frequencies may cause misclassification and degraded accuracy. However, we can obtain a fair AUC score (Table 6.2) to classify nociceptive fibers activations. There might be some classes that are highly capable of differentiation among three stimulations, which we will discuss in the next section.

6.3.4 Differentiation between nociceptive fibers activations

Figure 6.5 shows that the stimulation waveform of 1 Hz (targeting C) achieved efficient distinguishment between Aδ-fibers activation (250 Hz) and another waveform targeting C-fibers activation (5 Hz). On the other hand, 5 Hz stimulation (targeting C) shows vague differentiation from 250 Hz stimulation (targeting Aδ).

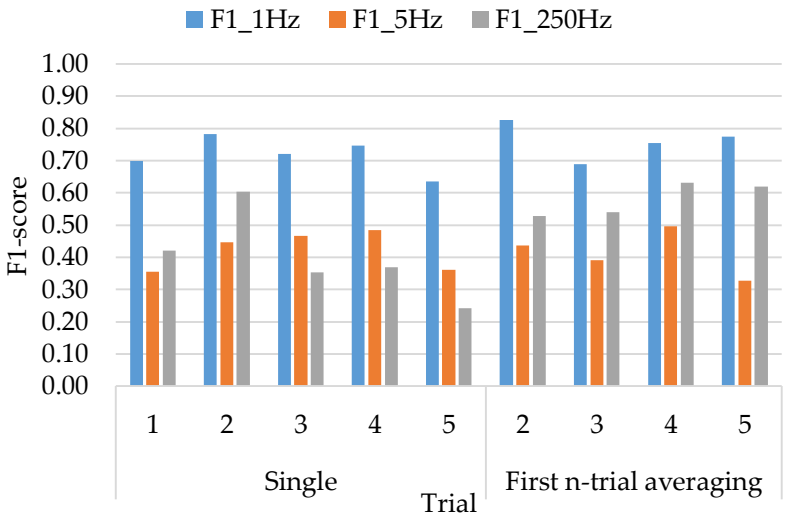

Figure 6.8 F1-score of classification with the top two feature inputs.

Furthermore, as shown in Figure 6.8, which shows the corresponding F1-score of each class (stimulation waveform) for classification with the top two feature inputs, the F1-score of 1 Hz stimulation (F1_1Hz) could differentiate from both 5 Hz (F1_5Hz) and 250 Hz stimulations (F1_250Hz). 1 Hz stimulation achieved the highest F1-score of 0.83 for classification with first 2-trial averaging. In contrast, the highest F1-score of class 5 Hz and 250 Hz stimulations were 0.50 and 0.63, respectively, which is worse than the lowest F1-score of 0.64 in class 1 Hz stimulation. This indicates that there are ambiguous data in 5 Hz and 250 Hz stimulations. Additionally, this F1_1Hz result showed the best differentiation among F1_5Hz and F1_250Hz as the same as results in Figure 5.2 (Chapter 5). Even though the F1-score of 1 Hz stimulation results in this current GC_DTW features (0.721 and 0.764 for GC_DTW features with single trial and first n-trial averaging, respectively) were lower than the previous study (0.989 for GC computed between independent components of each frequency band, GC_CoF), the difference of F1_1Hz between GC features (Chapter 5) and GC_DTW features is reasonable, because the channel numbers, trial numbers, and feature dimensions are completely different.

6.4 Conclusions

A proof of concept for GC features to be used in online classification was performed in this final implementation by testing the corresponding results from features extracted with different channel numbers, trial numbers, and grouped channels. In addition, the nested cross-validation (CV) model was implemented in this study to gain the generalization, and

the results of GC features were compared with the FD features, which achieved high accuracy for classifying pain perception levels in Chapter 4.

The results showed that extracting features from the frequency domain of EEG by only GC analysis is unable to achieve high accuracy, but it needs to do more steps of pre-processing and further extraction with detrending and DTW, respectively. With a modification of the process for the GC_DTW feature, we got better classification accuracy even if we analyzed with a number of trials ≤ 5, which is the crucial issue for analysis in an online manner. Besides, DTW was implemented to indicate the similarity between GC measures at different frequency bands. Furthermore, it revealed that most of the best features for the classification of nociceptive fibers activations are DTW calculated between low frequencies (delta, theta, and alpha) and high frequencies (beta and gamma). Finally, we provided a proof of concept for DTW integration by applying DTW to FFT features besides GC features. Accordingly, the results showed an improvement in classification accuracy too.

In the next chapter, we conclude the thesis and discuss the future work.

Chapter 7

Conclusions and Future Work

7.1 Introduction

In this chapter, to achieve the classification system for pain perception levels and nociceptive fibers activations, we summarize the results throughout the project and state the contributions of our studies to provide a proof of concept.

7.2 Summary of contributions

The novelties and contributions of this Doctoral project were:

1) We developed a fractal dimension (FD) feature, which extracted with nonlinear analysis from the event-related potential (time component of the EEG signals) for classifying multiple pain perception levels (maximum of four-level), as shown in Chapter 4. Furthermore, our findings revealed the number of stimulus repetitions for achieving an acceptable accuracy of classifying three- and four-level with FD features. Thus, this was the first study to explore the characteristic of nonlinear deterministic for pain response.
2) In a big data of time-frequency representations of EEG, we developed the Granger causality (GC) feature, which estimates causal interaction between brain activities in this project, for classifying binary classes of nociceptive fibers activations (Aδ- and C-fibers), as shown in Chapter 5. Due to the association of Aδ- and C-fibers with acute and chronic pain, respectively, it is necessary to differentiate between them. We showed that it is possible to use the frequency-related GC features to predict acute and chronic pain with > 80% accuracy (Chapter 5). This was the first time to use features related to quantifying causal flows between regions, independent components, and frequency bands instead of features related to the activities of a single region, a single independent component, and a single frequency band for classification of nociceptive fibers activations (Chapter 5).
3) We developed the proposed methods for extracting GC features to classify nociceptive fibers activations in simulation for an online scenario. By testing with several channels and trials in GC analysis, sufficient the number of channels and trials for pain classification were discussed (Chapter 6). These gave better information on the EEG data acquisition that will be performed in real-time analysis. Furthermore, we used detrending and dynamic time warping (DTW) to modify the proposed feature. This could be used to evaluate the salient points of the GC feature extracted from a low stationary scenario (a real-time manner), which is the estimate between two nodes in the pain network.

Regarding the classification of multiple pain perception levels, the goal was achieved to some extent. In Chapter 4, we showed how FD could capture pain information from the pain event-related potential of EEG (time domain). However, to gain accuracy for multiple classes

of classification, it requires the combination of FD features to predict three- and four-level of pain intensity. Besides, the number of trials to be used in the online analysis is still unclear since we did not validate the current combined features with other techniques.

Regarding the classification of nociceptive fibers (Aδ and C) activations, which related to the assessment of acute and chronic pain, the results in Chapter 5 showed that the functional connectivity, i.e., GC, measures between independent components of each frequency band could differentiate pain from activations of Aδ- and C-fibers better than GC measures in spatial distribution (between channel areas). Accordingly, we investigated further in terms of the frequency band in the last experiment (Chapter 6) to prove the application of frequency-related GC for online classification. However, the accuracy of GC measures in the frequency domain in Chapter 6 could not achieve a fair accuracy of 80% without adding detrending and DTW in the feature processing. That is, detrending and DTW have a contribution to the GC features for classifying nociceptive fibers activations in an online manner.

All these reasons suggest that the FD obtained from the time domain of EEG can reveal information of pain perception levels, while the frequency-related causal interaction, i.e., GC, analyzed from the time-frequency representations of EEG can differentiate pain between the activations of Aδ- and C-fibers with high accuracy more than 80%. Furthermore, the processing of detrending and DTW affect the improvement of the GC features for classifying multi-class of nociceptive fibers activations in an online manner.

7.3 Limitations

The developed pain classification system was implemented and tested in a controlled environment with healthy people. Accordingly, there were two consequences that we could not be sure about: first, how the classification system would work in real-situation environments; and second, how the system might provide to the pain patient. The former consequence was related to the requirements of applying EEG, which is very sensitive to noise. In contrast, the latter consequence was associated with the individual pain sensitivity that would affect the amplitude of the collecting EEG signal and decrease the system performance. To justify these consequences, recruiting the patients from the hospital that are interested in voluntarily participating in an experiment and arranging the appropriate room like examination room for the first and second consequences, respectively. However, the process for the first consequence is complex and requires the coordination of several groups of people. Besides the laboratory and hospital use, the arrangement of the EEG system in the proper place is difficult to justify for the second consequence because no EEG system is reliable for daily use yet.

Furthermore, a validation in generalizing the current classification systems was not performed in this study, for example, validating by applying the classification system to other pain-related EEG induced from different pain stimuli such as mechanical pressure pain and thermal pain. Thus, the current outcomes were summarized based on only the current stimulation type, electrical stimulation.

7.4 Future work

This project provided the EEG-based feature that achieved high classification performances for multiple pain perception levels and the differentiation between Aδ- and C-fibers activations through offline analysis. In addition, we also provided the investigations of classification with a few channels and trials as a preliminary simulation for online analysis. However, in the perspective of online (real-time) analysis, some factors were not considered in the current project but should be addressed in the future: processing and delay time. Besides, the current features should be validated with other types of pain stimulation such as mechanical pain pressure or other EEG data from open-source.

7.5 Conclusions

We demonstrated that the current features extracted from EEG could capture pain information in terms of pain intensities (low pain and high pain) and pain types (acute pain from Aδ-fibers activation and chronic pain from C-fibers activation). In addition, we can say that this project contributed to the field of pain monitoring by predicting multi-dimension of pain through the classification system. Nevertheless, there are still more steps to take these systems for wide use by real patients, especially for chronic pain cases, and benefit the clinical field and society. Meanwhile, we believe that these systems can be used to open new lines of investigation in the neuroscientific field.

References

[1] R. Melzack , K. L. Casey, "Sensory, motivational, and central control determinants of pain: a new conceptual model," *The skin senses,* vol.1, pp. 423-43, 1968.

[2] A. E. Dubin , A. Patapoutian, "Nociceptors: the sensors of the pain pathway," *The Journal of Clinical Investigation,* vol.120, pp. 3760-3772, 11 2010.

[3] J. Ydrefors, T. Karlsson, U. Wentzel Olausson, B. Ghafouri, A.-C. Johansson, H. Olausson, B. Gerdle , S. S. Nagi, "Automated Nociceptive Withdrawal Reflex Measurements Reveal Normal Reflex Thresholds and Augmented Pain Ratings in Patients with Fibromyalgia," *Journal of Clinical Medicine,* vol.9, 2020.

[4] R. Melzack, P. D. Wall , others, "Pain mechanisms: a new theory," *Science,* vol.150, p. 971–979, 1965.

[5] H. R. Koerber, S. L. McIlwrath, J. J. Lawson, S. A. Malin, C. E. Anderson, M. P. Jankowski , B. M. Davis, "Cutaneous C-polymodal Fibers Lacking TRPV1 are Sensitized to Heat following Inflammation, but Fail to Drive Heat Hyperalgesia in the Absence of TPV1 Containing C-heat Fibers," *Molecular Pain,* vol.6, pp. 1744-8069-6-58, 2010.

[6] J. Serra, A. Collado, R. Solà, F. Antonelli, X. Torres, M. Salgueiro, C. Quiles , H. Bostock, "Hyperexcitable C nociceptors in fibromyalgia," *Annals of Neurology,* vol.75, pp. 196-208, 2014.

[7] I. K. Martikainen, M. Peciña, T. M. Love, E. B. Nuechterlein, C. M. Cummiford, C. R. Green, R. E. Harris, C. S. Stohler , J.-K. Zubieta, "Alterations in Endogenous Opioid Functional Measures in Chronic Back Pain," *Journal of Neuroscience,* vol.33, p. 14729–14737, 2013.

[8] M. Stoeber, D. Jullié, B. T. Lobingier, T. Laeremans, J. Steyaert, P. W. Schiller, A. Manglik , M. von Zastrow, "A Genetically Encoded Biosensor Reveals Location Bias of Opioid Drug Action," *Neuron,* vol.98, pp. 963-976.e5, 2018.

[9] J.-S. Han, "Acupuncture: neuropeptide release produced by electrical stimulation of different frequencies," *Trends in Neurosciences,* vol.26, pp. 17-22, 2003.

[10] X.-H. Chen , J.-S. Han, "Analgesia induced by electroacupuncture of different frequencies is mediated by different types of opioid receptors: another cross-tolerance study," *Behavioural Brain Research,* vol.47, pp. 143-149, 1992.

[11] L. Plaghki , A. Mouraux, "How do we selectively activate skin nociceptors with a high power infrared laser? Physiology and biophysics of laser stimulation," *Neurophysiologie Clinique/Clinical Neurophysiology,* vol.33, pp. 269-277, 2003.

[12] M. Churyukanov, L. Plaghki, V. Legrain , A. Mouraux, "Thermal Detection Thresholds of Aδ- and C-Fibre Afferents Activated by Brief CO2 Laser Pulses Applied onto the Human Hairy Skin," *PLOS ONE,* vol.7, pp. 1-9, 4 2012.

[13] L. Hu, M. M. Cai, P. Xiao, F. Luo , G. D. Iannetti, "Human Brain Responses to Concomitant Stimulation of Aδ and C Nociceptors," *Journal of Neuroscience,* vol.34, p. 11439–11451, 2014.

[14] R. D. Treede, R. A. Meyer, S. N. Raja , J. N. Campbell, "Evidence for two different heat transduction mechanisms in nociceptive primary afferents innervating monkey skin.," *The Journal of Physiology,* vol.483, pp. 747-758, 1995.

[15] S. Omori, S. Isose, S. Misawa, K. Watanabe, Y. Sekiguchi, K. Shibuya, M. Beppu, H. Amino , S. Kuwabara, "Pain-related evoked potentials after intraepidermal electrical stimulation to Aδ and C fibers in patients with neuropathic pain," *Neuroscience Research,* vol.121, pp. 43-48, 2017.

[16] K. Inui , R. Kakigi, "Pain perception in humans: use of intraepidermal electrical stimulation," *Journal of Neurology, Neurosurgery & Psychiatry,* vol.83, p. 551–556, 2012.

[17] B. Bromm , J. Lorenz, "Neurophysiological evaluation of pain," *Electroencephalography and Clinical Neurophysiology,* vol.107, pp. 227-253, 1998.

[18] L. Bai, J. Wang, J. Wang, X. Li, D. Li, X.-L. Li, J.-S. Han , Y. Wan, "Modulation of Brain Electroencephalography Oscillations by Electroacupuncture in a Rat Model of Postincisional Pain," *Evidence-Based Complementary and Alternative Medicine,* vol.2013, p. 160357, 2013.

[19] J. C. T. Fairbank , P. B. Pynsent, "The Oswestry Disability Index," *Spine,* vol.25, 2000.

[20] R. Melzack, "The McGill Pain Questionnaire: Major properties and scoring methods," *PAIN,* vol.1, pp. 277-299, 1975.

[21] K. Koga, H. Furue, M. H. Rashid, A. Takaki, T. Katafuchi , M. Yoshimura, "Selective activation of primary afferent fibers evaluated by sine-wave electrical stimulation," *Molecular Pain,* vol.1, p. 13, 2005.

[22] D. L. Pitei, P. J. Watkins, M. J. Stevens , M. E. Edmonds, "The Value of the Neurometer in Assessing Diabetic Neuropathy by Measurement of the Current Perception Threshold," *Diabetic Medicine,* vol.11, pp. 872-876, 1994.

[23] M. Alkire, N. White, R. Hsieh , R. Haier, "Dissociable Brain Activation Responses to 5-Hz Electrical Pain Stimulation: A High-field Functional Magnetic Resonance Imaging Study," *Anesthesiology,* vol.100, p. 939–946, 4 2004.

[24] C. M. Aasted, M. A. Yücel, S. C. Steele, K. Peng, D. A. Boas, L. Becerra , D. Borsook, "Frontal Lobe Hemodynamic Responses to Painful Stimulation: A Potential Brain Marker of Nociception," *PLOS ONE,* vol.11, pp. 1-12, 11 2016.

[25] A. F. Mills, O. Sakai, S. W. Anderson , H. Jara, "Principles of Quantitative MR Imaging with Illustrated Review of Applicable Modular Pulse Diagrams," *RadioGraphics,* vol.37, pp. 2083-2105, 2017.

[26] C. Cattani, S. Chen , X. Li, "Functional Magnetic Resonance Imaging for Imaging Neural Activity in the Human Brain: The Annual Progress," *Computational and Mathematical Methods in Medicine,* vol.2012, p. 613465, 2012.

[27] M. M. Nickel, E. S. May, L. Tiemann, P. Schmidt, M. Postorino, S. T. Dinh, J. Gross , M. Ploner, "Brain oscillations differentially encode noxious stimulus intensity and pain intensity," *NeuroImage,* vol.148, pp. 141-147, 2017.

[28] L. Tiemann, V. D. Hohn, S. Ta Dinh, E. S. May, M. M. Nickel, J. Gross , M. Ploner, "Distinct patterns of brain activity mediate perceptual and motor and autonomic responses to noxious stimuli," *Nature Communications,* vol.9, p. 4487, 2018.

[29] R.-R. Nir, A. Sinai, E. Raz, E. Sprecher , D. Yarnitsky, "Pain assessment by continuous EEG: Association between subjective perception of tonic pain and peak frequency of alpha oscillations during stimulation and at rest," *Brain Research,* vol.1344, pp. 77-86, 2010.

[30] C. L. Kwan, A. P. Crawley, D. J. Mikulis , K. D. Davis, "An fMRI study of the anterior cingulate cortex and surrounding medial wall activations evoked by noxious cutaneous heat and cold stimuli," *Pain,* vol.85, pp. 359-374, 2000.

[31] A. Mouraux, G. D. Iannetti , L. Plaghki, "Low intensity intra-epidermal electrical stimulation can activate Aδ-nociceptors selectively," *PAIN,* vol.150, pp. 199-207, 2010.

[32] Y. Chu, X. Zhao, J. Han , Y. Su, "Physiological Signal-Based Method for Measurement of Pain Intensity," *Frontiers in Neuroscience,* vol.11, p. 279, 2017.

[33] K. H. Brodersen, K. Wiech, E. I. Lomakina, C.-s. Lin, J. M. Buhmann, U. Bingel, M. Ploner, K. E. Stephan , I. Tracey, "Decoding the perception of pain from fMRI using multivariate pattern analysis," *NeuroImage,* vol.63, pp. 1162-1170, 2012.

[34] J. Lee, I. Mawla, J. Kim, M. L. Loggia, A. Ortiz, C. Jung, S.-T. Chan, J. Gerber, V. J. Schmithorst, R. R. Edwards, A. D. Wasan, C. Berna, J. Kong, T. J. Kaptchuk, R. L. Gollub, B. R. Rosen and V. Napadow, "Machine learning-based prediction of clinical pain using multimodal neuroimaging and autonomic metrics," *Pain,* vol. 160, p. 550–560, 3 2019.

[35] V. Vijayakumar, M. Case, S. Shirinpour , B. He, "Quantifying and Characterizing Tonic Thermal Pain Across Subjects From EEG Data Using Random Forest Models," *IEEE Transactions on Biomedical Engineering,* vol.64, pp. 2988-2996, 2017.

[36] G. Misra, W.-e. Wang, D. B. Archer, A. Roy , S. A. Coombes, "Automated classification of pain perception using high-density electroencephalography data," *Journal of Neurophysiology,* vol.117, pp. 786-795, 2017.

[37] E. Schulz, A. Zherdin, L. Tiemann, C. Plant , M. Ploner, "Decoding an Individual's Sensitivity to Pain from the Multivariate Analysis of EEG Data," *Cereb Cortex,* vol.22, p. 1118–1123, 5 2012.

[38] A. Vuckovic, V. J. F. Gallardo, M. Jarjees, M. Fraser , M. Purcell, "Prediction of central neuropathic pain in spinal cord injury based on EEG classifier," *Clinical Neurophysiology,* vol.129, pp. 1605-1617, 2018.

[39] G. Huang, P. Xiao, Y. S. Hung, G. D. Iannetti, Z. G. Zhang , L. Hu, "A novel approach to predict subjective pain perception from single-trial laser-evoked potentials," *NeuroImage,* vol.81, pp. 283-293, 2013.

[40] Y. Tu, A. Tan, Y. Bai, Y. S. Hung , Z. Zhang, "Decoding Subjective Intensity of Nociceptive Pain from Pre-stimulus and Post-stimulus Brain Activities," *Frontiers in Computational Neuroscience,* vol.10, p. 32, 2016.

[41] H. E. Torebjörk , R. G. Hallin, "Perceptual changes accompanying controlled preferential blocking of A and C fibre responses in intact human skin nerves," *Experimental Brain Research,* vol.16, pp. 321-332, 1973.

[42] J. Ochoa , W. G. P. Mair, "The normal sural nerve in man," *Acta neuropathologica,* vol.13, pp. 217-239, 1969.

[43] A. Mouraux, J. M. Guérit , L. Plaghki, "Non-phase locked electroencephalogram (EEG) responses to CO2 laser skin stimulations may reflect central interactions between Að- and C-fibre afferent volleys," *Clinical Neurophysiology,* vol.114, pp. 710-722, 2003.

[44] Z. Tayeb, R. Bose, A. Dragomir, L. E. Osborn, N. V. Thakor , G. Cheng, "Decoding of Pain Perception using EEG Signals for a Real-Time Reflex System in Prostheses: A Case Study," *Scientific Reports,* vol.10, p. 5606, 2020.

[45] C. Huishi Zhang, A. Sohrabpour, Y. Lu , B. He, "Spectral and spatial changes of brain rhythmic activity in response to the sustained thermal pain stimulation," *Human Brain Mapping,* vol.37, pp. 2976-2991, 2016.

[46] C. W. J. Granger, "Investigating Causal Relations by Econometric Models and Cross-spectral Methods," *Econometrica,* vol.37, p. 424–438, 1969.

[47] N. Karamzadeh, A. Medvedev, A. Azari, A. Gandjbakhche , L. Najafizadeh, "Capturing dynamic patterns of task-based functional connectivity with EEG," *NeuroImage,* vol.66, pp. 311-317, 2013.

[48] A. Delorme , S. Makeig, "EEGLAB: an open source toolbox for analysis of single-trial EEG dynamics including independent component analysis," *Journal of Neuroscience Methods,* vol.134, pp. 9-21, 2004.

[49] N. Bigdely-Shamlo, T. Mullen, C. Kothe, K.-M. Su , K. A. Robbins, "The PREP pipeline: standardized preprocessing for large-scale EEG analysis," *Frontiers in Neuroinformatics,* vol.9, p. 16, 2015.

[50] I. Winkler, S. Debener, K.-R. Müller , M. Tangermann, "On the influence of high-pass filtering on ICA-based artifact reduction in EEG-ERP," *2015 37th Annual International Conference of the IEEE Engineering in Medicine and Biology Society (EMBC)*, 2015.

[51] C.-Y. Chang, S.-H. Hsu, L. Pion-Tonachini , T.-P. Jung, "Evaluation of Artifact Subspace Reconstruction for Automatic EEG Artifact Removal," *2018 40th Annual International Conference of the IEEE Engineering in Medicine and Biology Society (EMBC)*, 2018.

[52] J. A. Palmer, K. Kreutz-Delgado , S. Makeig, "AMICA: An adaptive mixture of independent component analyzers with shared components," *Swartz Center for Computatonal Neursoscience, University of California San Diego, Tech. Rep,* 2012.

[53] S. Wang, C.-L. Liu , L. Zheng, "Feature Selection by Combining Fisher Criterion and Principal Feature Analysis," *2007 International Conference on Machine Learning and Cybernetics*, 2007.

[54] T. Higuchi, "Approach to an irregular time series on the basis of the fractal theory," *Physica D: Nonlinear Phenomena,* vol.31, pp. 277-283, 1988.

[55] A. Accardo, M. Affinito, M. Carrozzi , F. Bouquet, "Use of the fractal dimension for the analysis of electroencephalographic time series," *Biological Cybernetics,* vol.77, p. 339–350, 1997.

[56] C. F. Vega , J. Noel, "Parameters analyzed of Higuchi's fractal dimension for EEG brain signals," *2015 Signal Processing Symposium (SPSympo)*, 2015.

[57] P. Grassberger , I. Procaccia, "Characterization of Strange Attractors," *PRL,* vol.50, p. 346–349, 1 1983.

[58] P. Grassberger , I. Procaccia, "Measuring the Strangeness of Strange Attractors," *The Theory of Chaotic Attractors*, B. R. Hunt, T. Li, J. A. Kennedy , H. E. Nusse, New, York: Springer New York, 2004, p. 170–189.

[59] G. E. P. Box, G. M. Jenkins, G. C. Reinsel , G. M. Ljung, "Time series analysis: forecasting and control John Wiley & Sons," *Hoboken, NJ,* 2008.

[60] T. F. Chan, G. H. Golub , R. J. Leveque, "Algorithms for Computing the Sample Variance: Analysis and Recommendations," *The American Statistician,* vol.37, pp. 242-247, 1983.

[61] Z. Mohamed, M. El Halaby, T. Said, D. Shawky , A. Badawi, "Characterizing Focused Attention and Working Memory Using EEG," *Sensors,* vol.18, 2018.

[62] F. Artoni, C. Fanciullacci, F. Bertolucci, A. Panarese, S. Makeig, S. Micera , C. Chisari, "Unidirectional brain to muscle connectivity reveals motor cortex control of leg muscles during stereotyped walking," *NeuroImage,* vol.159, pp. 403-416, 2017.

[63] E. Florin, J. Gross, J. Pfeifer, G. R. Fink , L. Timmermann, "The effect of filtering on Granger causality based multivariate causality measures," *NeuroImage,* vol.50, pp. 577-588, 2010.

[64] M. Chaumon, D. V. M. Bishop , N. A. Busch, "A practical guide to the selection of independent components of the electroencephalogram for artifact correction," *Journal of Neuroscience Methods,* vol.250, pp. 47-63, 2015.

[65] H. Nolan, R. Whelan , R. B. Reilly, "FASTER: Fully Automated Statistical Thresholding for EEG artifact Rejection," *Journal of Neuroscience Methods,* vol.192, pp. 152-162, 2010.

[66] S. Baillet, A. Delorme, T. Mullen, C. Kothe, Z. Akalin Acar, N. Bigdely-Shamlo, A. Vankov , S. Makeig, "EEGLAB, SIFT, NFT, BCILAB, and ERICA: New Tools for Advanced EEG Processing," *Computational Intelligence and Neuroscience,* vol.2011, p. 130714, 2011.

[67] M. X. Cohen, Analyzing neural time series data: theory and practice, 2014.

[68] P. L. Nunez, R. Srinivasan , others, Electric fields of the brain: the neurophysics of EEG, 2006.

[69] J. Dauwels, F. Vialatte, T. Musha , A. Cichocki, "A comparative study of synchrony measures for the early diagnosis of Alzheimer's disease based on EEG," *NeuroImage,* vol.49, pp. 668-693, 2010.

[70] S. He, Y. Yoshida, K. Tripanpitak, S. Takamatsu, S. Y. Huang , W. Yu, "A Simulation Study on Selective Stimulation of C-Fiber Nerves for Chronic Pain Relief," *IEEE Access,* vol.8, pp. 101648-101661, 2020.

[71] T. Kiso, Y. Nagakura, T. Toya, N. Matsumoto, S. Tamura, H. Ito, M. Okada , T. Yamaguchi, "Neurometer Measurement of Current Stimulus Threshold in Rats," *Journal of Pharmacology and Experimental Therapeutics,* vol.297, p. 352–356, 2001.

[72] H. Sakoe , S. Chiba, "Dynamic programming algorithm optimization for spoken word recognition," *IEEE Transactions on Acoustics, Speech, and Signal Processing,* vol.26, pp. 43-49, 1978.

[73] W. M. Grill , J. T. Mortimer, "Stimulus waveforms for selective neural stimulation," *IEEE Engineering in Medicine and Biology Magazine,* vol.14, pp. 375-385, 1995.

[74] H. Bostock, K. Cikurel , D. Burke, "Threshold tracking techniques in the study of human peripheral nerve," *Muscle & Nerve,* vol.21, pp. 137-158, 1998.

[75] J. Petrofsky, M. Laymon, M. Prowse, S. Gunda , J. Batt, "The transfer of current through skin and muscle during electrical stimulation with sine, square, Russian and interferential waveforms," *Journal of Medical Engineering & Technology,* vol.33, pp. 170-181, 2009.

[76] S. L. H. Notermans, "Measurement of the pain threshold determined by electrical stimulation and its clinical application," *Neurology,* vol.16, p. 1071–1071, 1966.

[77] N. Otsuru Koji Inui, K. Yamashiro, T. Miyazaki, I. Ohsawa, Y. Takeshima , R. Kakigi, "Selective stimulation of C fibers by an intra-epidermal needle electrode in humans," *The Open Pain Journal,* vol.2, 2009.

[78] K. Tripanpitak, W. Viriyavit, S. Y. Huang , W. Yu, "Classification of Pain Event Related Potential for Evaluation of Pain Perception Induced by Electrical Stimulation," *Sensors,* vol.20, 2020.

[79] K. D. Tzimourta, T. Afrantou, P. Ioannidis, M. Karatzikou, A. T. Tzallas, N. Giannakeas, L. G. Astrakas, P. Angelidis, E. Glavas, N. Grigoriadis, D. G. Tsalikakis , M. G. Tsipouras, "Analysis of electroencephalographic signals complexity regarding Alzheimer's Disease," *Computers & Electrical Engineering,* vol.76, pp. 198-212, 2019.

[80] M. Bachmann, L. Päeske, K. Kalev, K. Aarma, A. Lehtmets, P. Ööpik, J. Lass , H. Hinrikus, "Methods for classifying depression in single channel EEG using linear and nonlinear signal analysis," *Computer Methods and Programs in Biomedicine,* vol.155, pp. 11-17, 2018.

[81] S. Kesić , S. Z. Spasić, "Application of Higuchi's fractal dimension from basic to clinical neurophysiology: A review," *Computer Methods and Programs in Biomedicine,* vol.133, pp. 55-70, 2016.

[82] M. F. SHLESINGER, "Fractal Time and 1/f Noise in Complex Systems," *Annals of the New York Academy of Sciences,* vol.504, pp. 214-228, 1987.

[83] K. Tripanpitak, S. He, I. Sönmezışık, T. Morant, S. Y. Huang , W. Yu, "Granger Causality-Based Pain Classification Using EEG Evoked by Electrical Stimulation Targeting Nociceptive Aδ and C Fibers," *IEEE Access,* vol.9, pp. 10089-10106, 2021.

[84] S. Yi , V. Pavlovic, "Sparse Granger causality graphs for human action classification," *Proceedings of the 21st International Conference on Pattern Recognition (ICPR2012)*, 2012.

[85] N. Nicolaou, S. Hourris, P. Alexandrou , J. Georgiou, "EEG-Based Automatic Classification of 'Awake' versus 'Anesthetized' State in General Anesthesia Using Granger Causality," *PLOS ONE,* vol.7, pp. 1-13, 3 2012.

[86] F. Protopapa, C. I. Siettos, I. Evdokimidis , N. Smyrnis, "Granger causality analysis reveals distinct spatio-temporal connectivity patterns in motor and perceptual visuo-spatial working memory," *Frontiers in Computational Neuroscience,* vol.8, p. 146, 2014.

[87] A. B. Barrett, M. Murphy, M.-A. Bruno, Q. Noirhomme, M. Boly, S. Laureys , A. K. Seth, "Granger Causality Analysis of Steady-State Electroencephalographic Signals during Propofol-Induced Anaesthesia," *PLOS ONE,* vol.7, pp. 1-12, 1 2012.

[88] M. Ploner, J.-M. Schoffelen, A. Schnitzler , J. Gross, "Functional integration within the human pain system as revealed by Granger causality," *Human Brain Mapping,* vol.30, pp. 4025-4032, 2009.

[89] D. Chicco , G. Jurman, "The advantages of the Matthews correlation coefficient (MCC) over F1 score and accuracy in binary classification evaluation," *BMC Genomics,* vol.21, p. 6, 2020.

[90] G. Jurman, S. Riccadonna , C. Furlanello, "A Comparison of MCC and CEN Error Measures in Multi-Class Prediction," *PLOS ONE,* vol.7, pp. 1-8, 8 2012.

[91] M. Okamoto, H. Dan, K. Sakamoto, K. Takeo, K. Shimizu, S. Kohno, I. Oda, S. Isobe, T. Suzuki, K. Kohyama , I. Dan, "Three-dimensional probabilistic anatomical cranio-cerebral correlation via the international 10–20 system oriented for transcranial functional brain mapping," *NeuroImage,* vol.21, pp. 99-111, 2004.

[92] J. Gross, A. Schnitzler, L. Timmermann , M. Ploner, "Gamma Oscillations in Human Primary Somatosensory Cortex Reflect Pain Perception," *PLOS Biology,* vol.5, pp. 1-6, 4 2007.

[93] K. Ueda, G. Fujimoto, S. Ubukata , T. Murai, "[Brodmann Areas 11, 46, and 47: Emotion, Memory, and Empathy]," *Brain and nerve = Shinkei kenkyu no shinpo,* vol.69, p. 367—374, 4 2017.

[94] S. Ohara, N. E. Crone, N. Weiss, R.-D. Treede , F. A. Lenz, "Amplitudes of laser evoked potential recorded from primary somatosensory, parasylvian and medial frontal cortex are graded with stimulus intensity," *Pain,* vol.110, pp. 318-328, 2004.

[95] M. Frot, F. Mauguière, M. Magnin , L. Garcia-Larrea, "Parallel Processing of Nociceptive A-δ Inputs in SII and Midcingulate Cortex in Humans," *Journal of Neuroscience,* vol.28, p. 944–952, 2008.

[96] W. Li, W. Qin, H. Liu, L. Fan, J. Wang, T. Jiang , C. Yu, "Subregions of the human superior frontal gyrus and their connections," *NeuroImage,* vol.78, pp. 46-58, 2013.

[97] J. Kong, K. Jensen, R. Loiotile, A. Cheetham, H.-Y. Wey, Y. Tan, B. Rosen, J. W. Smoller, T. J. Kaptchuk , R. L. Gollub, "Functional connectivity of the frontoparietal network predicts cognitive modulation of pain," *PAIN®,* vol.154, pp. 459-467, 2013.

[98] B. T. Gold, D. A. Balota, B. A. Kirchhoff , R. L. Buckner, "Common and Dissociable Activation Patterns Associated with Controlled Semantic and Phonological Processing: Evidence from fMRI Adaptation," *Cereb Cortex,* vol.15, p. 1438–1450, 9 2005.

[99] A. C. N. Chen, "New perspectives in EEG/MEG brain mapping and PET/fMRI neuroimaging of human pain," *International Journal of Psychophysiology,* vol.42, pp. 147-159, 2001.

[100] W. Lutzenberger, H. Flor , N. Birbaumer, "Enhanced dimensional complexity of the EEG during memory for personal pain in chronic pain patients," *Neuroscience Letters,* vol.226, pp. 167-170, 1997.

[101] E. L. Meerwijk, J. M. Ford , S. J. Weiss, "Resting-state EEG delta power is associated with psychological pain in adults with a history of depression," *Biological Psychology,* vol.105, pp. 106-114, 2015.

[102] R. Kakigi, K. Inui , Y. Tamura, "Electrophysiological studies on human pain perception," *Clinical Neurophysiology,* vol.116, pp. 743-763, 2005.

[103] M. Gram, C. Graversen, S. S. Olesen , A. M. Drewes, "Dynamic spectral indices of the electroencephalogram provide new insights into tonic pain," *Clinical Neurophysiology,* vol.126, pp. 763-771, 2015.

Appendix

Table A 1 Average accuracy of classifying nociceptive fibers activations with the different channels, trial numbers, and trial types (single trial and first n-trial averaging). The value after ± is the standard deviation.

Channels	Number of trial	Average accuracy (%)	
		Single trial	First n-trial averaging
Selected based on Fisher score	1	59.42 ± 14.96	
	2	56.58 ± 16.09	58.08 ± 12.66
	3	57.92 ± 9.47	56.75 ± 14.85
	4	43.75 ± 8.18	64.42 ± 12.30
	5	49.00 ± 10.92	57.83 ± 13.06
Selected based on literature			
C3CP1P3C4CP2P4	1	51.84 ± 2.48	
	2	57.21 ± 19.22	53.16 ± 3.89
	3	58.01 ± 2.45	50.74 ± 9.65
	4	58.16 ± 13.32	50.81 ± 11.34
	5	57.87 ± 9.65	56.99 ± 9.16
C3CP1CzC4CP2	1	61.84 ± 8.52	
	2	62.94 ± 7.95	59.41 ± 10.78
	3	53.16 ± 7.88	56.91 ± 7.96
	4	58.16 ± 13.32	65.66 ± 12.44
	5	44.56 ± 7.78	49.49 ± 17.89
C3C4CzP3P4	1	53.01 ± 11.80	
	2	54.41 ± 11.09	49.41 ± 7.99
	3	51.91 ± 8.73	50.51 ± 10.81
	4	59.26 ± 9.27	50.74 ± 6.80
	5	58.01 ± 8.28	50.66 ± 10.14
C3C4Cz	1	51.25 ± 6.39	
	2	51.25 ± 6.39	48.68 ± 6.03
	3	47.65 ± 3.90	56.03 ± 9.93
	4	58.24 ± 6.00	66.84 ± 7.56
	5	53.75 ± 13.70	65.59 ± 11.15
C3CP1Cz	1	54.78 ± 10.79	
	2	52.50 ± 10.06	59.63 ± 6.31
	3	60.81 ± 10.61	54.85 ± 11.80
	4	52.43 ± 4.76	57.43 ± 13.73
	5	51.18 ± 8.65	58.53 ± 9.32
C3CP1P3	1	85.74 ± 7.94	
	2	50.15 ± 7.21	63.01 ± 5.03
	3	54.71 ± 11.10	61.76 ± 8.72
	4	58.46 ± 9.42	48.75 ± 9.08
	5	51.18 ± 13.10	50.15 ± 7.21
C3P3Cz	1	56.03 ± 5.43	
	2	54.85 ± 11.80	53.53 ± 10.26
	3	48.97 ± 8.05	48.82 ± 5.76
	4	59.41 ± 11.82	59.41 ± 9.19
	5	53.68 ± 16.12	63.31 ± 9.71